

**DIURNAL AND SEASONAL ALBEDO TRENDS OF WHEAT
AT THE BRATT'S LAKE OBSERVATORY, SASKATCHEWAN**

by

Reesa Dexter

BES, York University, 1999

THESIS SUBMITTED IN PARTIAL FULFILLMENT OF
THE REQUIREMENTS FOR THE DEGREE OF
MASTER OF SCIENCE

In the Department
of
Geography

© Reesa Dexter 2004

SIMON FRASER UNIVERSITY

July 2004

All rights reserved. This work may not be
reproduced in whole or in part, by photocopy
or other means, without permission of the author.

APPROVAL

Name: **Reesa Heather Dexter**

Degree: Master of Science

Title of Thesis: Diurnal And Seasonal Albedo Trends Of Wheat
At The Bratt's Lake Observatory, Saskatchewan

Examining Committee:
Chair: N.K. Blomley, Professor

Dr. W.G. Bailey, Professor
Senior Supervisor

Dr. L.J.B. McArthur, Head
National Atmospheric Radiation Centre
Meteorological Service of Canada
Committee Member

Dr. A.M. Sawchuk, Instructor
Geography Department, Kwantlen University College

Dr. I. Saunders, Associate Professor
Geography Department, Okanagan University College
External Examiner

Date Approved: July 9, 2004

SIMON FRASER UNIVERSITY



Partial Copyright Licence

The author, whose copyright is declared on the title page of this work, has granted to Simon Fraser University the right to lend this thesis, project or extended essay to users of the Simon Fraser University Library, and to make partial or single copies only for such users or in response to a request from the library of any other university, or other educational institution, on its own behalf or for one of its users.

The author has further agreed that permission for multiple copying of this work for scholarly purposes may be granted by either the author or the Dean of Graduate Studies.

It is understood that copying or publication of this work for financial gain shall not be allowed without the author's written permission.

The original Partial Copyright Licence attesting to these terms, and signed by this author, may be found in the original bound copy of this work, retained in the Simon Fraser University Archive.

Bennett Library
Simon Fraser University
Burnaby, BC, Canada

ABSTRACT

The albedo of two wheat fields was measured throughout the 2001 growing season. In response to the maturing crop, the daily albedo increased by approximately 12 percent from seeding to harvest. Before the fields were seeded, the daily albedo was related to the organic litter that remained on the surface from the previous year's harvest; the average daily albedo was 0.173 and 0.161 for the north and south fields respectively. Following cultivation (May 15), the albedo decreased to 0.093 and 0.109 for the north and south fields. The wheat crop emerged on May 27, but the albedo was not solely that of the vegetation until the extended height of the wheat was 0.12 m on June 7. After this date, the albedo increased daily as the wheat crop matured. The albedo reached a plateau (≈ 0.17) on July 8, and this coincided with the peak of plant fresh weights and the emergence of wheat heads. The albedo began to increase during the week of July 31 and this was related to crop senescence. When the crop was harvested at the end of the growing season, the albedo was approximately 0.22.

Several diurnal albedo trends occurred throughout the growing season. The albedo was symmetrical around solar noon on cloudless and overcast days when the crop canopy dominated the surface condition. The albedo was asymmetrical around solar noon when transmissivity or the surface condition varied during the day. Albedo asymmetry between morning and afternoon regimes was most prominent early in the growing season (up to the end of the emergence stage), and the asymmetry was usually associated with the period following the formation of dew.

Insight into the behaviour of half-hour albedos throughout the growing season permitted an independent test of the use of exponential regression equations to estimate half-hour albedos along with the albedo model employed in the Canadian Land Surface Scheme (CLASS). The regression equations tended to overestimate the albedo at

greater zenith angles. Further, the equations could not reproduce observed asymmetry around solar noon. For bare soil surfaces, the albedo model employed in CLASS did not predict albedo values or diurnal trends satisfactorily. Albedos were generally grossly underestimated and constant throughout the day. However, for vegetated surfaces, the albedo model employed in CLASS estimated the albedo satisfactorily. Although the albedo was underestimated when the zenith angle was $> 60^\circ$, the albedo was accurately estimated when the zenith angle was $\leq 60^\circ$. Diurnal albedo trends were also accurately estimated.

ACKNOWLEDGEMENTS

This project would have not been possible without the support of many people. I cannot thank the Gooding family enough for their interest and patience. The scope of this project was realized because they granted me access to their land. I would also like to thank them for teaching me about their farming practices and the plight of prairie farmers.

Both Ormanda Niebergall and Dr. David Halliwell were instrumental to the success of the measurement program. Ormanda assisted in the set up of the instrumentation and frequently gathered soil samples. Without Ormanda's contribution, the dataset would be less complete. Dave provided great council and assisted me with data quality and troubleshooting. Without Dave's assistance, data quality would have been diminished.

I also owe a lot to my supervisory committee who provided academic and moral support. In terms of data analysis, Dr. Allan Sawchuk bestowed thoughtful incite. Dr. Bruce McArthur provided funding, taught me about field measurement and data quality, and offered important feedback on my research. Dr. Bill Bailey was always available and provided invaluable suggestions, comments and assistance. Indeed, without such a fine supervisory committee this research would not have been possible.

Finally, I want to thank my family who gave me the moral support I needed throughout my Masters. My friends and colleagues also provided me with academic and moral support. In particular, Mungandi Nasitwitwi and François Teste gave me wonderful academic advice and kept me on track.

I cannot thank everyone enough. I will never forget the people, places or pies. . .

TABLE OF CONTENTS

	Page
Approval	ii
Abstract	iii
Acknowledgements	v
Table of Contents	vi
List of Tables	viii
List of Figures	x
Chapter 1 Introduction.....	1
1.1 Study objectives	2
1.2 Thesis organisation	3
1.3 Site description	4
Chapter 2 Albedo trends for wheat throughout a growing season	12
2.1 Introduction	12
2.2 Background	13
2.3 Methods	16
2.3.1 Study site	16
2.3.2 Instrumentation	17
2.3.3 Soil measurements	18
2.3.4 Plant measurements	19
2.3.5 Data analysis	20
2.4 Results and discussion	22
2.4.1 Surface conditions during the growing season	22
a. Soil moisture	22
b. Wheat maturation	24
2.4.2 The seasonal progression of mean daily albedo	30
2.4.3 Albedo differences between the north and south fields	36
2.4.4 Numerical summaries of seasonal albedo controls	39
2.5 Conclusions	41
Chapter 3 The character and modelling of half-hour albedos of wheat	43
3.1 Introduction	43
3.2 Background	45
3.3 Methods	49

3.3.1	Study site and instrumentation	49
3.3.2	Supplemental sampling	50
3.3.3	Data analysis	51
3.4	Results and discussion	56
3.4.1	The diurnal symmetry of albedo throughout the growing season.....	56
3.4.2	Exponential regression equations for estimating albedos	70
3.4.3	The application of the albedo model in the Canadian Land Surface Scheme	77
3.5	Conclusions	85
Chapter 4	Conclusions	90
Appendices	95
A	List of symbols and units	96
B	Missing data	100
C	Dominant weed species	101
D	A comparison of estimated reflected solar radiation from regression equations and observed reflected solar radiation	102
E	Day of year conversion calendar	104
F	Post-season pyranometer intercomparison	105
G	The difference between estimated and observed crop surface albedos	106
H	Error analysis	108
References	110

LIST OF TABLES

Table	Page
2.1 The phenological stages of wheat during the 2001 growing season	21
2.2 The correlation coefficient (r) between the albedo (α), transmissivity (t), the volumetric soil moisture (vsm) of the uppermost 10 mm of soil and the leaf area index (LAI)	33
2.3 Numerical summaries for the 2001 growing season	40
3.1a The α_{CLASS} runs for bare soils	54
3.1b The α_{CLASS} runs for vegetated surfaces	54
3.1c Mean canopy albedos used in α_{CLASS}	54
3.2a Major trends in the percent difference between forenoon and afternoon albedos during the growing season	64
3.2b Major trends in the percent difference between forenoon and afternoon albedos during the growing season and the percentage of days that they represent (out of 116 days)	65
3.3a A comparison of observed and predicted half-hour albedos employing exponential regression equations	71
3.3b A comparison of observed and predicted half-hour albedos employing exponential regression equations	72
3.3c A comparison of observed and predicted half-hour albedos employing exponential regression equations	73
3.4 Comparison of observed and predicted (α_{CLASS}) half-hour albedos and the difference between observed ($K\uparrow_o$) and predicted reflected solar radiation ($K\uparrow_p$)	80
B.1 Missing data from the Kipp and Zonen CM 21 pyranometer measuring global solar radiation at the meteorological compound, and from the inverted Kipp and Zonen CM21 and CM11 pyranometers measuring reflected solar radiation over the north and south fields respectively	100
C.1 Dominant weed species located in the north and south fields during the 2001 growing season	101
D.1 Comparison of estimated reflected solar radiation ($K\uparrow_p$) from regression equations and observed reflected solar radiation ($K\uparrow_o$)	102
F.1 Results of a ten day intercomparison of the pyranometers	105

F.2	The frequency of the absolute difference in global solar radiation between the pyranometers	105
H.1	Error analysis results for global ($K\downarrow$) and reflected solar radiation ($K\uparrow$) for the south field	109
H.2	Error analysis results for the albedo (α)	109

LIST OF FIGURES

Figure	Page
1.1 Map showing the location of the Bratt's Lake Observatory (BLO), Saskatchewan (50° 12' 10" N, 104° 42' 42" W)	5
1.2 A schematic map of the field research site at the Bratt's Lake Observatory...	7
1.3 Inverted pyranometers measuring reflected solar radiation (\approx 2 m above the surface) at several phenological stages throughout the growing season in the north field (left side) and south field (right side)	8
1.4 Inverted pyranometer employed in measuring reflected solar radiation (\approx 2 m above the surface) on May 23	10
2.1 Daily volumetric soil moisture and precipitation from DOY 120 to 237.....	23
2.2 The average standing and extended plant heights throughout the growing season	25
2.3 Wheat fresh and dry weight throughout the growing season for the north and south fields	26
2.4 Fresh and dry weights of leaves, stems and heads as a percent of total weight	27
2.5 The dry to fresh plant weight ratios throughout the growing season	29
2.6 The leaf area index throughout the growing season	29
2.7 The time series of the daily albedo for two wheat fields and the percent difference between them	31
3.1 The diurnal trend of albedo for two wheat fields, transmissivity and vapour pressure deficit (vpd) for seven phenological stages during the 2001 growing season	57
3.2 The albedo, vapour pressure deficit (vpd), vapour pressure (e) and saturation vapour pressure ($e_s(T)$) for DOY 142	62
3.3 The percent difference between the forenoon and afternoon albedo on five selected days	67
3.4 The time series of half-hour albedos on seven selected days	75
3.5 1:1 plots of estimated (α_{CLASS}) and observed albedos	78
3.6 The observed and estimated albedos (A through D) on three selected days representing overcast (DOY 138), cloudless (DOY 142) and partly cloudy (DOY 145) sky conditions	81

3.7	The observed and estimated crop surface albedos on three selected days representing overcast (DOY 193), partly cloudy (DOY 211) and cloudless (DOY 218) sky conditions	83
G.1	The difference ($\Delta\alpha$) between observed and estimated (α_{CLASS}) albedos plotted against the cosine of the zenith angle ($\cos(Z)$)	106
G.2	The difference ($\Delta\alpha$) between observed and estimated (α_{CLASS}) albedos plotted against transmissivity (t)	107

CHAPTER 1

INTRODUCTION

The albedo is an instantaneous, diurnal, seasonal and annual expression of the relationship between solar radiation and the earth-atmosphere interface. It is defined as the ratio between reflected solar radiation and global solar radiation. Some applications, across many temporal scales, use a constant for albedo (Kukla and Robinson, 1980; Morozova, 1994). Dixon (1983) suggests that, although many data sets may give the impression that the albedo is constant, it is actually quite variable. In fact, the albedo varies throughout a day, and for mid-latitudes the albedo varies greatly throughout the year. Graphically, diurnal albedo time series typically show an upward-facing parabolic curve. For mid- and high latitudes, the albedo is greatest in the winter due to snow cover, lowest in the spring before the vegetation emerges, and then increases as vegetation progresses toward maturity (Angle *et al.*, 1992; Kung *et al.*, 1964; Kukla and Robinson, 1980). The complexity in albedo behaviour stems from a multitude of atmospheric and surface controls. These controls include solar position, sky condition, surface type and surface condition. The majority of albedo studies recognise that the albedo is variable over time, and numerous of these have documented diurnal and seasonal albedo trends (Ahmad and Lockwood, 1979; Duchon, 1997; Jacobs and Van Pul, 1990; Kukla and Robinson, 1980; Kung *et al.*, 1964; Piggins and Schwerdtfeger, 1973; Song, 1999; Wanjura and Hatfield, 1986).

The albedo plays an integral role in determining the regional climates of surfaces across both spatial and temporal scales. This has led most designers of general circulation models (GCMs) to include the albedo as a physical parameter (Kondratyev *et al.*, 1982; Randall, 1992). GCMs are sensitive to slight changes in the albedo because it plays a large role in the determination of the net radiation balance at the surface and

hence the surface energy balance and the resulting climatology (Hummel and Reck, 1979; Kondratyev *et al.*, 1982; Myhre and Myhre, 2003). Several papers in the literature conclude that the accuracy of GCMs may be limited by the paucity of seasonal and longer timescale albedo studies over surfaces that are representative of a region (Kondratyev *et al.*, 1982; Myhre and Myhre, 2003). Thus, more long-term albedo studies are merited and required.

This thesis contributes to the growing body of knowledge about albedo and its behaviour. It specifically examines the diurnal and seasonal progression of the albedo of a maturing wheat crop. It is anticipated that a constant value is not representative of the albedo throughout a growing season as the albedo responds to numerous atmospheric and surface controls. It is hypothesised that the diurnal albedo will not always be symmetrical around solar noon because atmospheric and surface conditions are variable throughout daylight periods. This thesis will categorise and examine symmetrical and asymmetrical albedos for a range of atmospheric and surface conditions. Regression analysis has been used in the literature to describe and estimate half-hour albedos (Amfield, 1975; Nkemdirim, 1972). This thesis will estimate half-hour albedos over the growing season using exponential regression equations for the phenological stages of the cropped surface. Finally, the accuracy of the albedo model employed in the Canadian Land Surface Scheme (Versegny, 1991; Versegny *et al.*, 1993) will be assessed by comparing estimated albedos to observed albedos. The broad range of atmospheric and surface conditions during the 2001 growing season provides a suitable test for assessing regression analysis and the albedo model employed in the Canadian Land Surface Scheme.

1.1 Study objectives

The objectives of this study were four-fold:

1. To measure global and reflected solar radiation over two fields at a one minute average, and to compile the fluxes into half-hourly and daily albedos throughout the growing season at the Meteorological Service of Canada's BSRN (Baseline Surface Radiation Network) Observatory, Saskatchewan. A description of the daily progression of albedo throughout the growing season will be provided, and major albedo trends during the season will be identified.
2. Categorise and investigate the diurnal symmetry and asymmetry of the albedo throughout the growing season.
3. Estimate half-hourly albedos by employing regression analysis.
4. Assess the performance of the albedo model in the Canadian Land Surface Scheme throughout the growing season.

Successfully addressing and achieving these objectives will contribute to present knowledge about diurnal and seasonal albedo trends.

1.2 Thesis organisation

This thesis is organized into four chapters. Following the introductory chapter, the daily progress of the albedo for a wheat crop throughout the 2001 growing season will be presented in Chapter 2. In Chapter 3, the diurnal symmetry and asymmetry of the albedo will be examined using half-hourly albedos. Observed atmospheric and surface conditions will be used to examine the diurnal symmetry or asymmetry. The chapter will then compare exponential regression equations to observed half-hour albedos. Chapter 3 will conclude by assessing the performance of the albedo model in the Canadian Land Surface Scheme throughout the growing season. The final chapter will summarise the main findings of this thesis and the potential for future work.

1.3 Site description

This research was conducted at the Meteorological Service of Canada's BSRN Bratt's Lake Observatory (BLO) located in southern Saskatchewan, Canada (50° 12' 10" N, 104° 42' 42" W, at 587m asl) (Figure 1.1). The Observatory is one of 36 long-term BSRN monitoring stations distributed over the globe. The BSRN was developed to ". . . provide continuous, long-term, frequently sampled, state-of-the-art measurements of the surface radiation fluxes adhering to the highest achievable standards of measurement procedures, calibration and accuracy" (McArthur, 1998).

The BLO is located in a semiarid region of the Canadian Prairies where weather systems generally move west to east. Convective storms are common throughout the growing season, where 65 percent of the annual precipitation usually occurs between April and August. Generally, 16 to 18.5 percent of the annual 377 mm of precipitation occurs in June (Fung, 1999; Phillips, 1990). The Westerlies, that are often too dry to yield much precipitation, cause southern Saskatchewan to have an annual moisture deficit between 150 and 250 mm (Phillips, 1990). The mean annual temperature of the Regina Plain is 2.6°C with a range of 35.6°C (Fung, 1999).

The 2001 growing season was considered as a drought year in the Canadian Prairies, but the Observatory did not experience a severe drought season (Wittrock, 2002). The precipitation levels over the region were slightly below average (Wittrock, 2002), where the BLO received 173.1 mm of precipitation from May 30 to August 25. The mean temperature for the growing season was 14.2°C and is 0.4°C above the mean growing season temperature from 1971 to 2000 (Wittrock, 2002).

The Observatory is located in the Regina Plain, and the soil is Regina clay. It is a dark brown chernozemic soil and is well drained with pockets that become saturated for

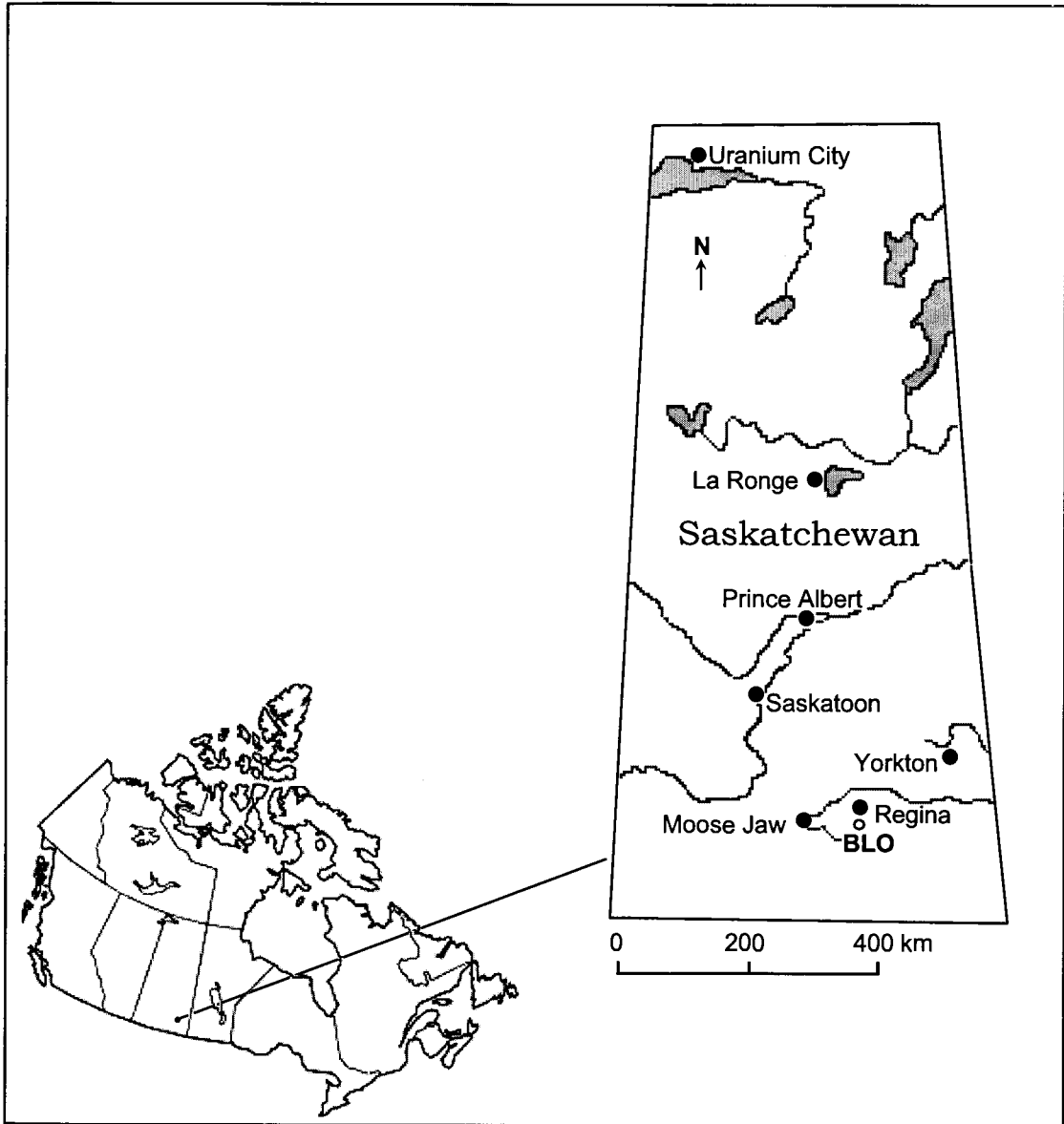


Figure 1.1. Map showing the location of the Bratt's Lake Observatory (BLO), Saskatchewan ($50^{\circ} 12' 10''$ N, $104^{\circ} 42' 42''$ W).

short periods (Fung, 1999; Joel *et al.*, 1936). The primary land use is agricultural with wheat, durum, canola and flax being commonly grown (Policy Branch, 2003).

The wheat yield from the two fields employed in this study was average with approximately 2352 kg ha⁻¹ (J. Gooding, personal communication).

The field site employed at the BLO includes two adjacent fields that share a west-east border (Figure 1.2). The field to the north of the west-east border is referred to as the north field and the other as the south field. The slope for the field site is approximately 1% north-south and approximately 0.5 to 1% east-west. From 1990 to 1994/5, the fields had a two year rotation. They were fallow one year and cultivated the next. Since 1995, the north field has been continuously planted with wheat, lentils and flax (in no particular order). The south field has a three year rotation of fallow, flax and wheat.

When the 2001 growing season commenced, organic litter from the 2000 harvest covered the surface of both fields. The north field was covered by a matted lentil litter and the south field with flax stubble (Figure 1.3). On May 12 (day of year (DOY) 132), the fields were seeded with hard red spring wheat (*Triticum aestivum* L.) (Depauw *et al.*, 1997). The crop was successfully harvested on August 25 (DOY 237).

Albedo measurements for the north and south fields commenced on April 30 (DOY 120) and continued until August 25 (DOY 237). Reflected solar radiation was measured in both fields. Inverted pyranometers were mounted on fixed stands with adjustable arms such that measurement height and surface area was near constant at 2 m (Figures 1.3 and 1.4). A Kipp and Zonen CM21 pyranometer was employed in the north field and a Kipp and Zonen CM11 was employed in the south field. Both sensors were shielded and ventilated. A Campbell Scientific 21X datalogger measured sensor outputs every second with an output of one-minute mean, standard deviation, maximum and minimum values. Incoming solar radiation measurements were made approximately

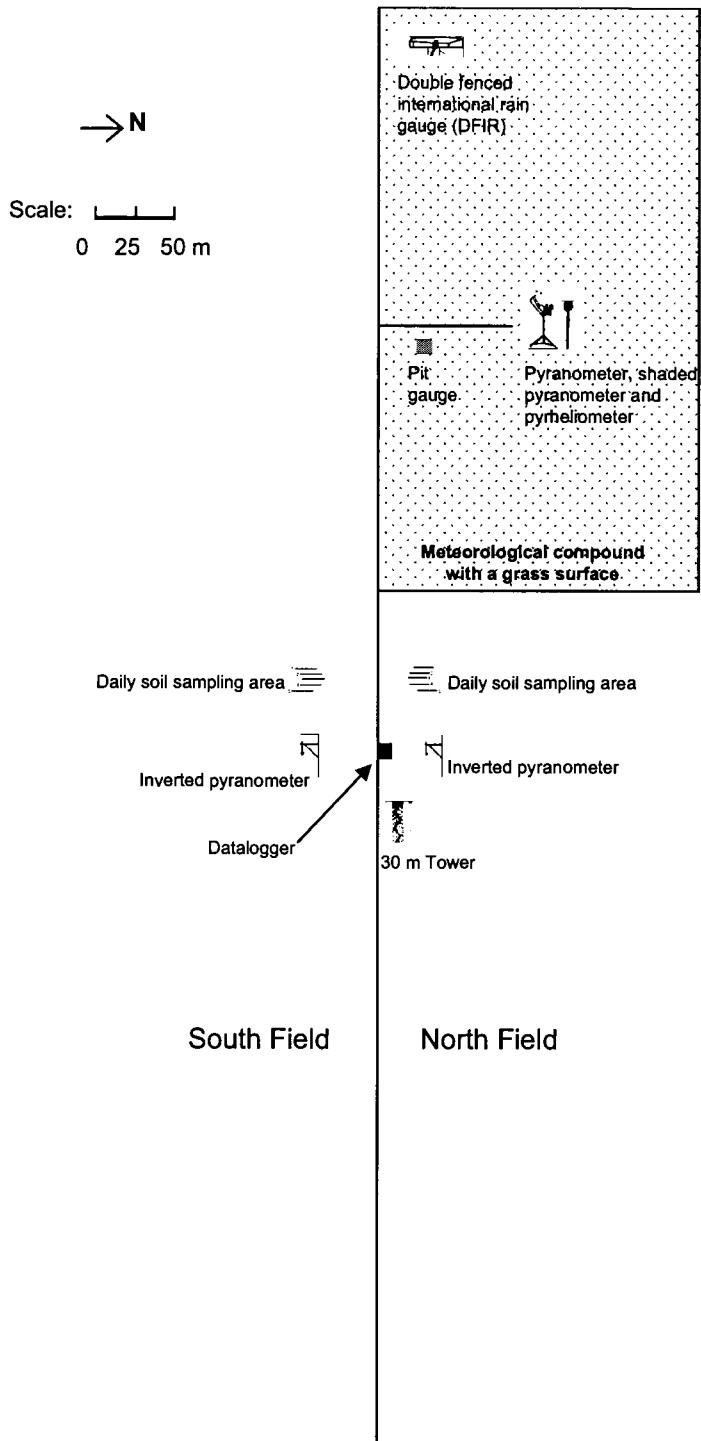


Figure 1.2. A schematic map of the field research site at the Bratt's Lake Observatory.

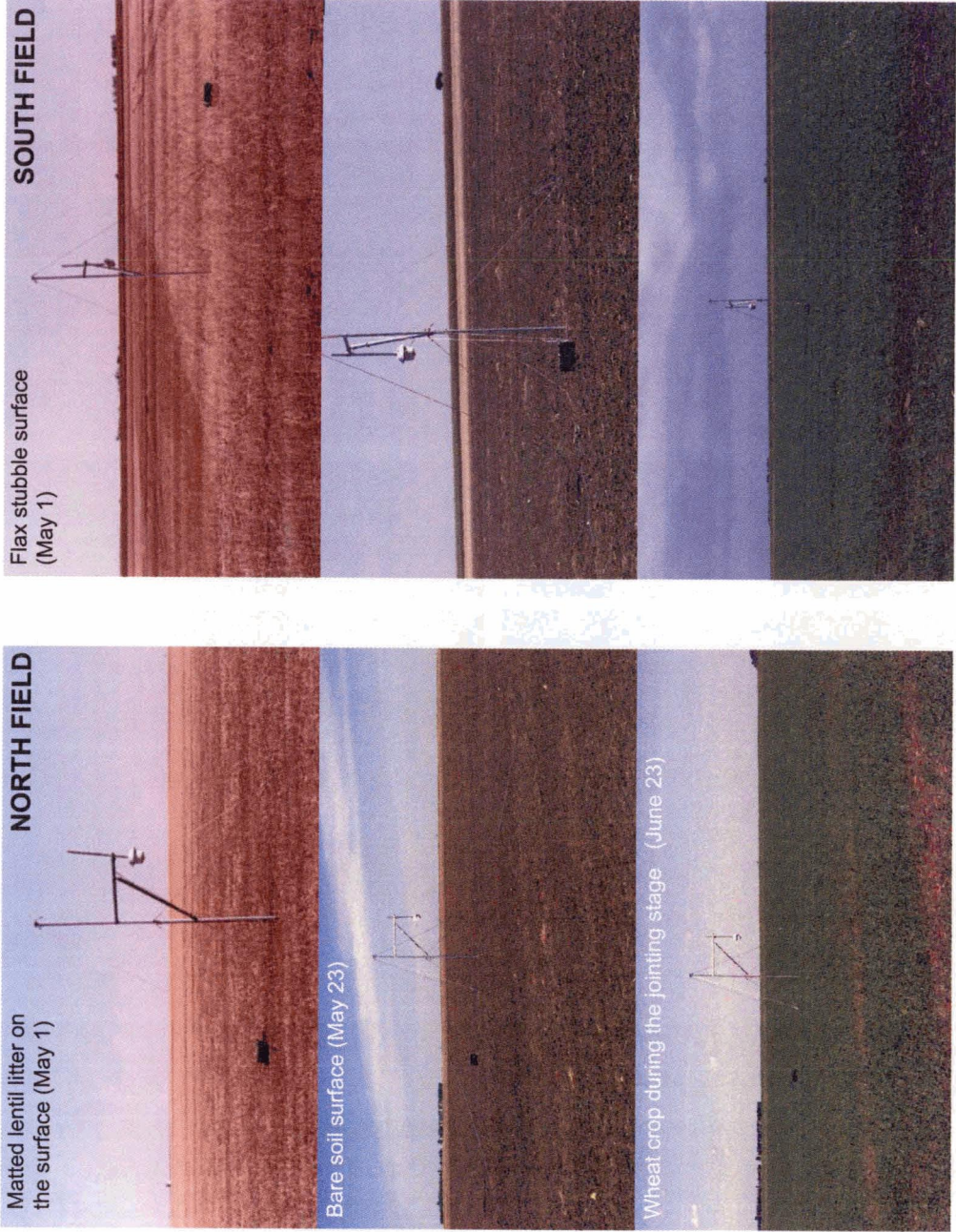
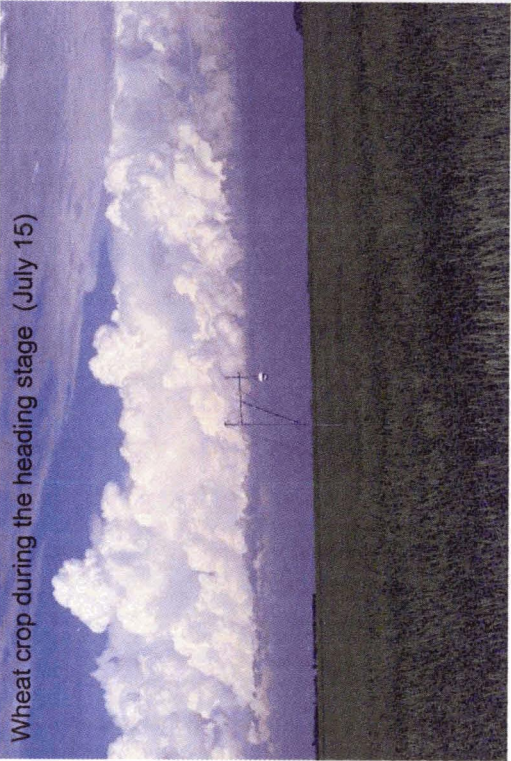


Figure 1.3. Inverted pyranometers measuring reflected solar radiation (≈ 2 m above the surface) at several phenological stages throughout the growing season in the north field (left side) and south field (right side).

Wheat crop during the heading stage (July 15)



Wheat crop during the ripe stage (August 21)

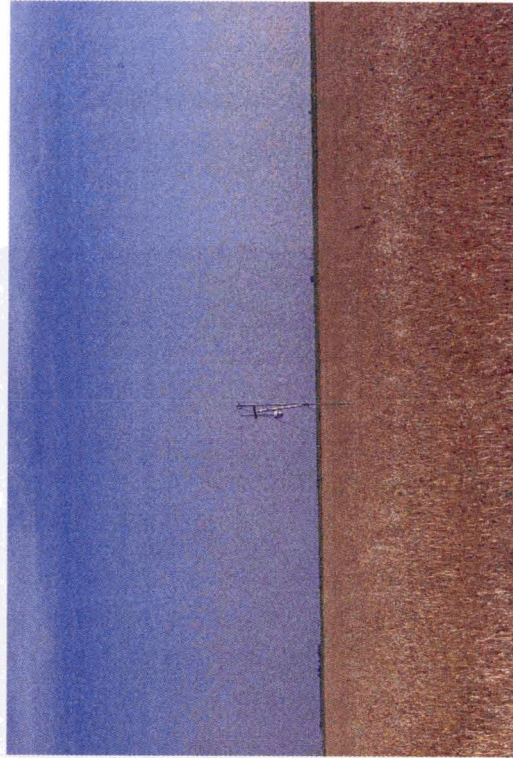
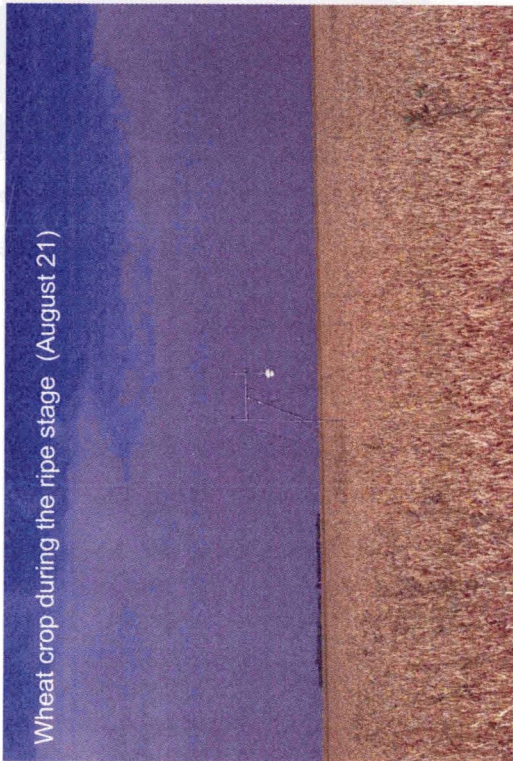


Figure 1.3. Continued

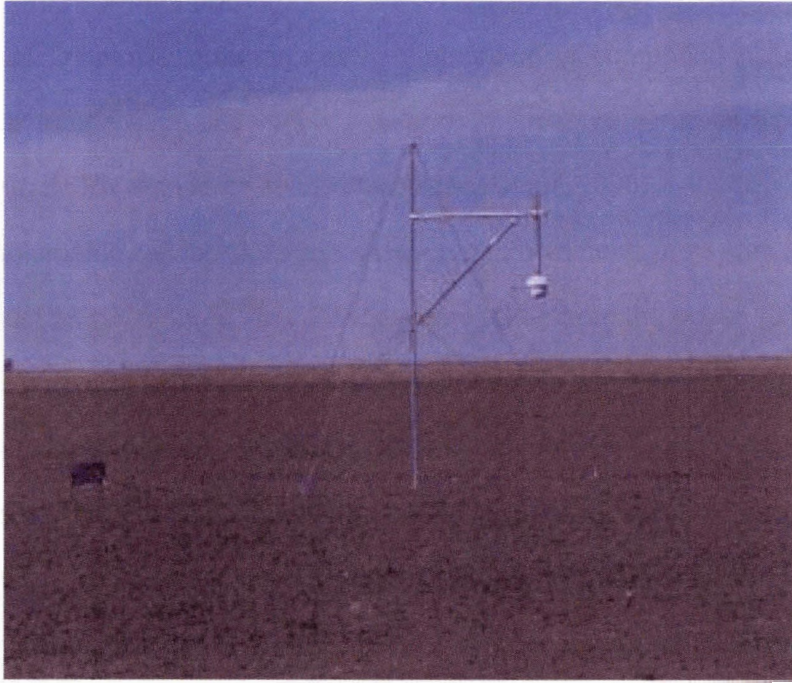


Figure 1.4. Inverted pyranometer employed in measuring solar radiation (≈ 2 m above the surface) on May 23.

3 metres above the surface at an adjacent meteorological compound (approximately 250 m away; Figure 1.2). Global and diffuse solar radiation measurements were made with Kipp and Zonen CM21 pyranometers. Direct beam irradiance was measured with a Kipp and Zonen CH1 pyrhelimeter. Incoming solar irradiance measurements were made every second with an output of one-minute mean, standard deviation, maximum and minimum values. Other measurements at the meteorological compound include precipitation, air temperature and vapour pressure. All measurements were conducted in accordance with BSRN standards and protocols (McArthur, 1998).

Daily volumetric soil moisture was measured in both fields from April 30 (DOY 120) until August 25 (DOY 237). Five samples were taken from the upper 10 mm of soil and five layers from 0 to 250 mm. Volumetric soil moisture was characterized daily by averaging five sample locations for each depth interval from each field.

Plant sampling was conducted throughout the growing season to assess the phenological stage of the wheat, plant height and above ground biomass. Every two or three days, at ten fixed locations in each field, the standing and extended heights of the crop were recorded. The standing height is the height of the plant from the ground to its highest point. The extended height is the height of the plant from the ground to the highest standing point when all parts of the plant are manually extended upwards.

Above ground biomass was determined by manually harvesting the crop from ten randomly selected quadrants (250 x 500 mm) in each field. At each location, the surface was first photographed and five plant heights recorded (one in each corner of the quadrant and one in the center). The vegetation was then harvested at ground level. Fresh and dry weights for nine of the ten sample locations in each field were obtained by weighing the samples and then drying the samples for 72 hours at 70°C. The remaining sample had its plant components (leaves, stems and heads) separated and weighed. From this sample, the leaf area index was also determined.

CHAPTER 2

ALBEDO TRENDS FOR WHEAT THROUGHOUT A GROWING SEASON

2.1 Introduction

As it is important to recognise and understand seasonal and annual albedo trends, this chapter investigates the daily albedo of wheat throughout a growing season. Albedo trends affect the surface energy balance and hence local and regional climates throughout the year (Hummel and Reck, 1979; Kung *et al.*, 1964; Kukla and Robinson, 1980). For mid- and high latitudes, the albedo will experience great annual variation (Hummel and Reck, 1979; Kung *et al.*, 1964; Kukla and Robinson, 1980). For example, in Wisconsin, Kung *et al.* (1964) reported that the albedo was greatest in the winter as a consequence of snow cover and in the spring, the albedo decreased abruptly with spring melt. In early to mid-summer, the albedo increased as the vegetation matured, and in autumn, the albedo then decreased to its lowest annual value as the deciduous trees lost their leaves, and vegetation died or senesced. Within an individual season, the albedo is strongly related to the surface type and its state. A number of studies have documented albedo trends throughout a growing season (Al-Yemeni and Grace, 1995; Jacobs and Van Pul, 1990; Kung *et al.*, 1964; Song, 1999). For example, the albedo of a crop will often initially increase as plant height, leaf area and canopy cover increase. After maturation, the albedo will again increase as the crop senesces (Al-Yemeni and Grace, 1995; Duchon, 1997; Jacobs and Van Pul, 1990; Kung *et al.*, 1964; Meek and Hatfield, 2001; Song, 1999).

Based on current literature and understanding, it was hypothesized that the daily progression of albedo throughout the 2001 growing season would generally increase as the crop matured and that the albedo would increase when either surface soil moisture decreased or atmospheric transmissivity increased. Hence, albedo measurements were

made and related to changes in atmospheric transmissivity (mainly influenced by cloud cover), surface soil moisture availability and crop phenology. Daily albedo, plant and soil measurements were then used to produce numerical summaries of seasonal albedo trends.

2.2 Background

The solar electromagnetic spectrum range includes the ultraviolet (0.12 to 0.38 μm), visible (0.39 to 0.77 μm) and near infrared (0.78 μm and beyond) wavelengths. Climates, across a range of timescales, are fundamentally created and controlled by solar radiation. The relationship between solar radiation and the earth-atmosphere interface is expressed by the albedo. The albedo is the ratio of broadband reflected solar radiation to broadband global solar radiation, and is controlled by a number of factors: surface type, moisture content, surface roughness, etc.

Bare soil albedos are predominantly controlled by soil moisture content, the surface organic matter content and surface roughness. The albedo is inversely related to surface soil moisture because as soil moisture increases, soil particles are enveloped by a thin film of water that results in increased solar radiation absorption and reduced reflected solar radiation in predominantly the visible and near infrared regions of the solar spectrum (Baumgardner *et al.*, 1985; Idso *et al.*, 1975; Post *et al.*, 2000; Potter *et al.*, 1987; Proctor and Blackburn, 1983; Twomey *et al.*, 1986). During a rain event with overcast conditions, the albedo will decrease for an additional reason. Under such conditions, solar radiation will be predominately diffuse as the radiation that is scattered by the clouds is near isotropic, and this will cause global solar radiation to strike the surface from overhead (Dixon, 1983; Piggin and Schwerdtfeger, 1973). As a result, more radiation will be absorbed by the surface.

The albedo of a bare soil will also be influenced by the organic matter content of the surface layer. The more organic matter a soil has, the lower the albedo, since organic matter will generally absorb more solar radiation across the electromagnetic spectrum than bare soil (Baumgardner *et al.*, 1985). A study by Major *et al.* (1992) examined several soils in southern Alberta and attributed a 32 percent change in reflected solar radiation to differences in the organic carbon content of the soil.

The albedo of a bare soil is also controlled by its surface roughness. Several studies have examined the relationship between albedo and surface roughness, and have observed that the albedo decreased as surface roughness increased (Idso *et al.*, 1975; Matthias *et al.*, 2000; Potter *et al.*, 1987; Proctor and Blackburn, 1983). As soils are not Lambertian in character, any irradiance that strikes a bare soil surface will experience multiple reflections between the soil particles. Therefore, as surface roughness increases, the probability that reflected solar radiation will be absorbed by the surface increases. A soil may be relatively smooth because of its fine texture (e.g. clay soil) or because a thin crust has developed on the surface. These relatively smooth soils have a higher albedo than coarser soils (e.g. sand) or tilled soils. For example, Matthias *et al.* (2000) reported that once a relatively smooth brown fine sandy loam was ploughed, the albedo decreased by 25 percent. Conversely, after a rain event, Potter *et al.* (1987) observed an unexpected ≤ 25 percent increase in the albedo of a bare soil for some wavelengths between 0.40 μm to 1.35 μm . This unexpected finding led them to suggest that the albedo increased because the impact of the rain droplets caused soil pores to infill, which reduced surface roughness. A small number of studies have also observed that the albedo will increase when a wet soil dries because a thin crust develops on the surface, which reduces surface roughness (Baumgardner *et al.*, 1985; Proctor and Blackburn, 1983).

A principal factor that affects the albedo of a crop is the phenological stage of the vegetation. As a crop matures, the albedo will respond to changes in surface cover, crop height, leaf area, greenness (i.e. the amount of chlorophyll contained in the plant tissue) and plant water content. In the spring, the surface is composed of two components, bare soil and newly emerged plants. The albedo throughout the day will exhibit the combined influence of controls exerted by both surface components. A crop with less than 15 percent vegetation cover will have a similar albedo to a bare soil (Baumgardner *et al.*, 1985). Until the crop covers 40 percent of the surface, the albedo is controlled by both the vegetation and soil (Baumgardner *et al.*, 1985). As plants mature, the canopy will increase in height and foliage volume. Weiss (1982) reported an 8 percent increase in the albedo as the height of alfalfa increased from 0.15 to 0.60 m.

Foliage density for crops such as grasses and cereals do not vary greatly with height, but for crops like maize and potatoes, there is a canopy layer above the stem (Oke, 1987). The architecture in the later case leads to a decrease in the albedo with increased canopy depth because as the canopy increases in height and complexity (i.e. leaf area and angular orientation of the leaves), the number of multiple reflections in the canopy also increase. Hence, the potential for global solar radiation to be absorbed will increase. The amount of solar radiation that is reflected from a canopy will decline exponentially as canopy depth increases (Oke, 1987).

Throughout a growing season, the albedo will respond to changes in leaf area, plant turgidity and greenness (Jacobs and Van Pul, 1990; Kung *et al.*, 1964; Song, 1999). Numerous studies have reported that the albedo is predominately controlled by the leaf area index (LAI) (Jacobs and Van Pul, 1990; Song, 1999; Walter-Shea *et al.*, 1992; Yin, 1998). If the albedo of the vegetation is greater than the albedo of the soil, which is generally the case, the albedo will increase as LAI increases because more of the surface is covered with vegetation and less soil is exposed. For example, the LAI for

wheat will generally increase until peak greenness, when the crop has completed growth. Thereafter, the LAI will decrease until harvest (Al-Yemeni and Grace, 1995; Song, 1999). In response to the change in LAI, the albedo will increase from emergence to peak greenness, and decrease slightly before crop senescence (Al-Yemeni and Grace, 1995; Jacobs and Van Pul, 1990; Song, 1999). Additionally, Song (1999) suggested that the albedo will decrease before senescence because plants are wilting. This results in decreased reflected solar radiation in the infrared region of the solar spectrum. Once a crop commences senescence, the albedo will increase again as plants lose chlorophyll and internal water. Song (1999) reported that the increase in albedo during senescence is greater than during the growth stage.

In summary, the albedo of wheat generally increases as the crop matures. Initially the albedo will be that of the underlying soil until the wheat covers approximately 15 percent of the surface. The albedo will then increase as the vegetation increases in plant height and leaf area. After peak greenness, the albedo will decrease slightly as the wheat wilts before senescence. Once the wheat senesces, the albedo will increase until harvest.

2.3 Methods

2.3.1 Study site

Research was conducted at the Meteorological Service of Canada's Bratt's Lake Observatory (BLO) (50° 12' 10" N, 104° 42' 42" W). The Observatory is located in the grain belt of Saskatchewan where crops such as wheat, barley, flax and canola are commonly grown. The study site employed two adjacent fields that are referred to as the north field and south field (Figure 1.2). During the 2001 growing season, AC Barrie, a hard red spring wheat (*Triticum aestivum* L.) (Depauw *et al.*, 1997) was seeded in both fields.

Observations commenced on April 30 (day of year (DOY) 120). At this time, the surface of the north field was covered by a matted lentil litter and the south field by flax stubble. Observations were halted on May 12 through May 14 (DOY 132 through 134), when the fields were seeded and harrowed. The observations began again on May 15 (DOY 135), and continued until harvest on August 25 (DOY 237).

2.3.2 Instrumentation

In the north and south fields, reflected solar radiation was measured with inverted pyranometers that were mounted on fixed stands with adjustable arms. The inverted pyranometers were maintained at a height of approximately 2 m above the surface (Figure 1.4). A Kipp and Zonen CM21 pyranometer was employed in the north field and a Kipp and Zonen CM11 pyranometer in the south field. Both sensors were shielded and ventilated. Pre- and post-season calibrations of the pyranometers were conducted at the National Atmospheric Radiation Centre, and sensor performance did not change over the growing season. A post-season intercomparison also confirmed the agreement between the two pyranometers (Appendix F). A Campbell Scientific 21X datalogger measured sensor outputs every second with an output of one-minute mean, standard deviation, maximum and minimum values.

Global, direct and diffuse solar radiation was measured at an adjacent meteorological compound (Figure 1.2). On DOY 120, 121, 123, 167 and 177, the pyranometer measuring global solar radiation failed for several hours and a pyranometer at an adjacent observation tower (30 m above the surface) was used for global solar radiation data (Figure 1.2). Again, incoming solar irradiance measurements were made every second with an output of one-minute mean, standard deviation, maximum and minimum values.

All sensor outputs were converted from millivolts to radiation flux densities

($W m^{-2}$). The zero offset of the sensors (McArthur, 1998) was corrected by averaging a nightly sensor output between zenith angles of 102° to 106° , and applying the average to the daily values. Half-hour averages were computed from the minute data for both global and reflected solar radiation. The half-hour radiation fluxes were then summed over the day for the period when the zenith angle was $\leq 80^{\circ}$. On many occasions, the small solar radiation values at zenith angles $> 80^{\circ}$ led to erroneous albedos because instrument sensitivity is less exact at low voltages, thus increasing sensor error, and at larger zenith angles the error in cosine response increases. Thus, the daily albedo was created from fluxes with a zenith angle $\leq 80^{\circ}$ by dividing the daily reflected solar radiation by the daily global solar radiation.

2.3.3 Soil measurements

Daily volumetric soil moisture measurements were made throughout the growing season. Soil sampling (between 7:00 and 9:00 CST) commenced on DOY 120 and continued until DOY 237. At five locations in each field, soil samples were taken from the upper 10 mm of soil and from 0 to 250 mm (Figure 1.2). The soil cores from 0-250 mm were sectioned into five depth intervals (0-50, 50-100, 100-150, 150-200 and 200-250 mm). The soil moisture content of each sample was determined by weighing the soil sample, drying the soil at $107^{\circ}C$ for twenty-four hours, and then weighing the sample again (Bailey and Dexter, 2003). All gravimetric soil moisture measurements were converted to volumetric soil moisture values by multiplying the gravimetric soil moisture by the bulk density (Bailey and Dexter, 2003) of the soil layers. The soil moisture was characterized each day by averaging the five sample locations for each depth interval.

2.3.4 Plant measurements

AC Barrie, a hard red spring wheat, was planted in both fields on DOY 132. Plant emergence occurred on DOY 144 in the south field and DOY 147 in the north field. Crop senescence began on DOY 213, and the crop was harvested on DOY 237. Plant sampling was conducted over the growing season to assess the phenological stage of the wheat, plant height and above ground biomass. Every two or three days, at ten fixed locations in each field, the standing and extended heights of the crop was recorded. The standing height is the height of the plant from the ground to its highest point. The extended height is the height of the plant from the ground to the highest standing point when all parts of the plant are manually extended upwards.

In both the north and south fields, ten quadrants (250 x 500 mm) were randomly selected for manual harvesting to determine above ground biomass. At each location, the surface was first photographed and five plant heights were recorded before harvesting. The height of a plant in each corner of the quadrant and the plant closest to the centre of the quadrant were measured. The surface vegetation was then removed at ground level with a utility knife. In the laboratory, nine of the ten sample locations in each field had the vegetation transferred to a paper bag, weighed and placed in an oven for 72 hours at 70°C (Bailey and Dexter, 2003). After drying, the dry weight of each sample was recorded. The remaining sample had its plant components (leaves, stems and heads) separated and weighed.

The sample that had its plant components separated was also used to determine the leaf area (LA) and leaf area index (LAI). The fresh leaves were laid flat on a white bristol board, covered with plexiglas and photographed (Bailey and Stewart, 1982). The leaf area was determined from the photographs with a density slice function (Scion Image). A representative leaf area throughout the growing season was produced by

expressing the leaf areas as a function of the average leaf dry weights. A relationship between leaf area (m²) and leaf dry weight (l_{dw}) (kg m⁻²) was developed

$$LA = 0.0166 l_{dw} + 0.0135, r^2 = 0.85. \quad (2.1)$$

A leaf area for each sample date was then produced by applying equation 2.1 to the average leaf dry weight at each sample period. The leaf area was then divided by the sampling area (i.e. 250 x 500 mm) to produce LAI.

The growing season was divided into seven stages based on surface and crop conditions (Table 2.1). These divisions, except pre-seeding, are based on the phenological stages of wheat as outlined by Robertson (1968) and the Agrometeorological Centre of Excellence (ACE, 2002).

2.3.5 Data Analysis



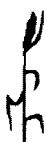
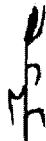

The albedo and all supplemental measurements were analysed over the duration of the growing season. The albedo was plotted against transmissivity (direct beam solar radiation/extraterrestrial solar radiation) and the surface controls during pre-seeding and for each crop phenological stage. The albedo was also correlated against potential surface controls for pre-seeding and each crop stage using Pearson product-moment coefficient of correlation (r) because it estimates the degree of closeness of the linear relationship between two variables.

The difference between the albedos in the north and south fields was examined. The percent difference between the north and south field albedos (α_{diff}) was expressed by

$$\alpha_{diff} = \frac{(\alpha_S - \alpha_N)}{\alpha_N} * 100 \quad (2.2)$$

where α_N is the north field albedo and α_S is the south field albedo. Pearson product-

Table 2.1 The phenological stages of wheat during the 2001 growing season.

Stage	DOY	Description
Pre-seeding	120-131	The surface is covered with litter from the 2000 growing season.
Bare soil	135-146	Period from seeding to plant emergence.
Emergence 	147-160	Period begins when more than fifty percent of plants are visible and ends once jointing occurs. The wheat emerged on DOY 144 in the south field and DOY 147 in the north field.
Jointing  Tillers	161-188	Period begins when the elongation of the first internode occurs on the fifth leaf and ends with heading. Jointing was determined by observing changes in the plant structure, such as advanced tillering, that normally happens at this time.
Heading 	189-210	Period begins when wheat heads emerge from the boot and have reached the base of the short blade.
Soft Dough 	211-222	Period when kernels are easily deformed when pressed between two fingers and no milky substance is extruded.
Ripe 	223-236	Period when kernels cannot be deformed when pressed between two fingers.

moment coefficient of correlation was used to relate the α_{diff} to surface soil moisture and plant measurements.

A numerical summary was then developed to describe the albedo for pre-seeding and each crop stage. The expressions employed the relationship between the albedo and the dominant surface control. When the albedo for a phenological stage was constant, the albedo was expressed in terms of a bare soil albedo. Further details on this are provided in Section 2.4.4.

2.4 Results and Discussion

2.4.1 Surface conditions during the growing season

As the albedo is primarily a function of surface conditions, the results and discussion section of this chapter will focus on the albedo and observations of surface soil moisture and plant phenology. Section 2.4.1 will provide an overview of the surface conditions observed throughout the growing season. Daily albedo trends will then be discussed in Sections 2.4.2 through 2.4.4.

a. Soil moisture

Throughout the season, the uppermost 10 mm and 250 mm soil layers had numerous drying trends (Figure 2.1). Throughout the season, the uppermost layer of soil (0-10 mm) demonstrated the greatest variation in volumetric soil moisture. For this layer, volumetric soil moisture decreased from DOY 120 to DOY 134 as precipitation inputs on DOY 121, 122 and 127 provided subtle recharge to the soil (Figure 2.1). On DOY 135, a rain event (2.3 mm) increased soil moisture from $0.11 \text{ mm}^3 \text{ H}_2\text{O}/\text{mm}^3$ soil in the north field and $0.05 \text{ mm}^3 \text{ H}_2\text{O}/\text{mm}^3$ soil in the south field to $0.19 \text{ mm}^3 \text{ H}_2\text{O}/\text{mm}^3$ soil in the north field and $0.22 \text{ mm}^3 \text{ H}_2\text{O}/\text{mm}^3$ soil in the south field. The difference in increased

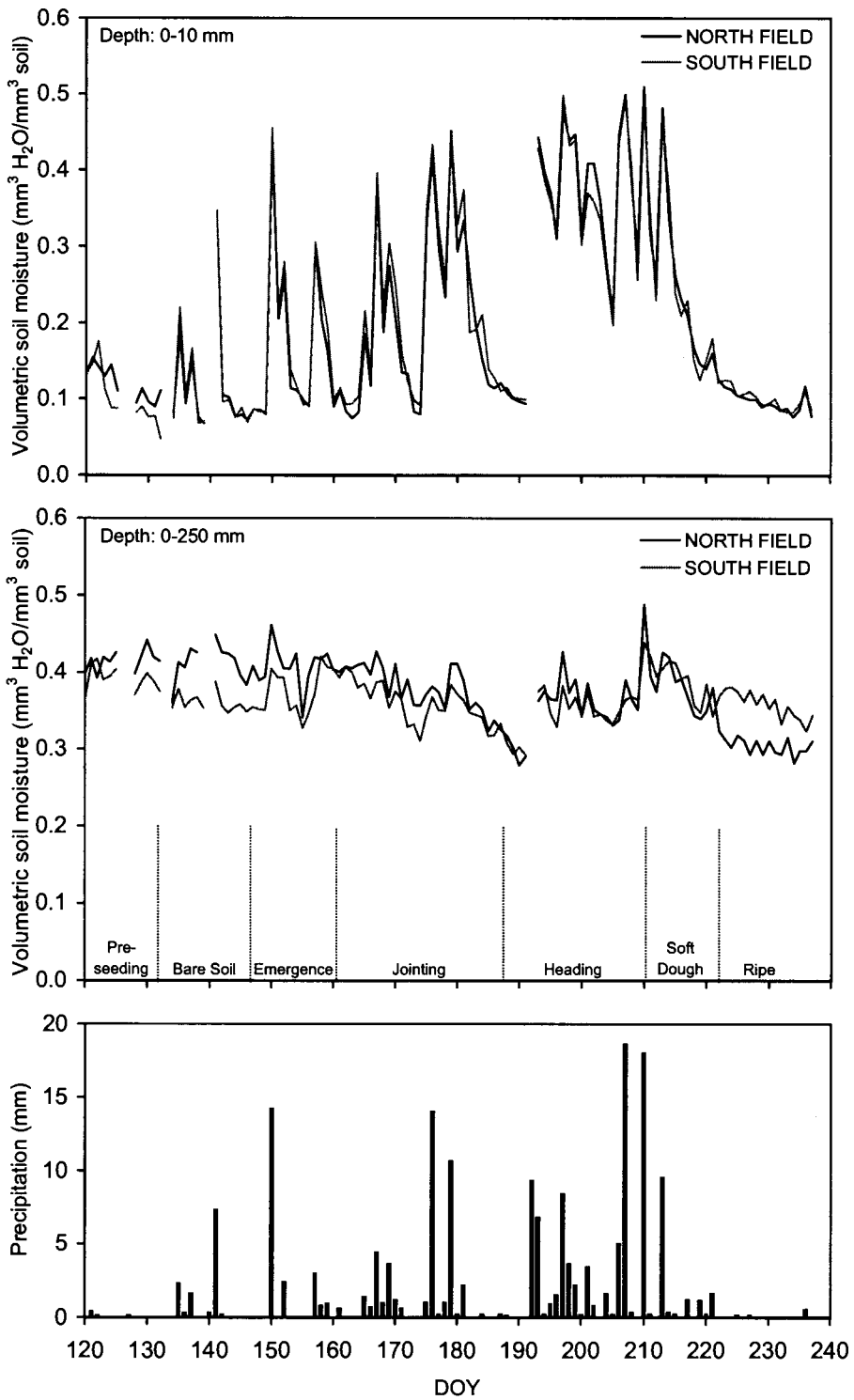


Figure 2.1. Daily volumetric soil moisture and precipitation from DOY 120 to 237. Soil moisture is presented for two depths (0 - 10 mm and 0 - 250 mm).

soil moisture maybe caused by the difference in soil composition, but it is more likely due to the inherent spatial variability of soil moisture over the surfaces. After DOY 135, the uppermost layer of soil began to dry, but there was another rain event on DOY 137. The soil moisture for the uppermost layer increased again to $0.15 \text{ mm}^3 \text{ H}_2\text{O}/\text{mm}^3$ soil in the north field and $0.17 \text{ mm}^3 \text{ H}_2\text{O}/\text{mm}^3$ soil in the south field, and then decreased until DOY 140. The soil moisture of the uppermost layer always sharply increased when there was a rain event and then gradual drying followed. The longest drying trends in the uppermost soil layer were from DOY 181 to DOY 191 and DOY 214 to DOY 237.

The soil moisture in the 0-250 mm layer demonstrated less variation than the upper 10 mm of soil. From DOY 120 until jointing (DOY 161), the volumetric soil moisture was approximately $0.40 \text{ mm}^3 \text{ H}_2\text{O}/\text{mm}^3$ soil (Figure 2.1). During the jointing stage (DOY 161 to DOY 188), the wheat utilized significant amounts of soil water. Even with precipitation inputs, a decline in soil moisture in the 0-250 mm layer occurred as a consequence of soil water uptake by the crop. The wheat crop began to show signs of moisture stress during the jointing stage. The drying trend continued until a series of 5 rain events ($\geq 9 \text{ mm}$), from DOY 192 to DOY 213, slightly increased soil moisture. This maintained the soil moisture for several days. However, after DOY 221, precipitation inputs were limited and a slight drying trend resulted.

b. Wheat maturation

The wheat emerged on DOY 144 in the south field and DOY 147 in the north field. As a result, until the wheat had fully matured, the plant height and mean dry plant weights were greater in the south field than in the north field (Figures 2.2 to 2.4). The plant heights, fresh weights, dry weights, dry to fresh weight ratio and LAI are all related to plant phenology and thus several interrelated trends are evident during the growing season.

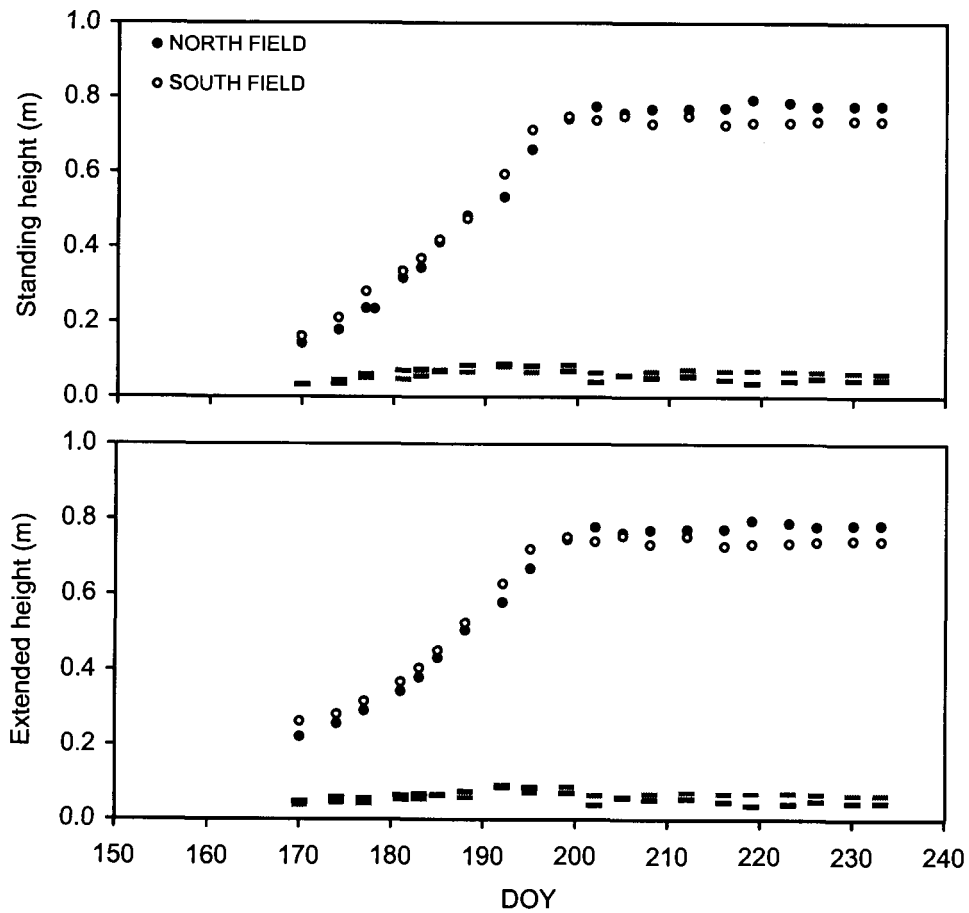


Figure 2.2. The average standing and extended plant heights throughout the growing season. The black and grey bars are the standard deviations of the ten plant heights in the north and south field, respectively.

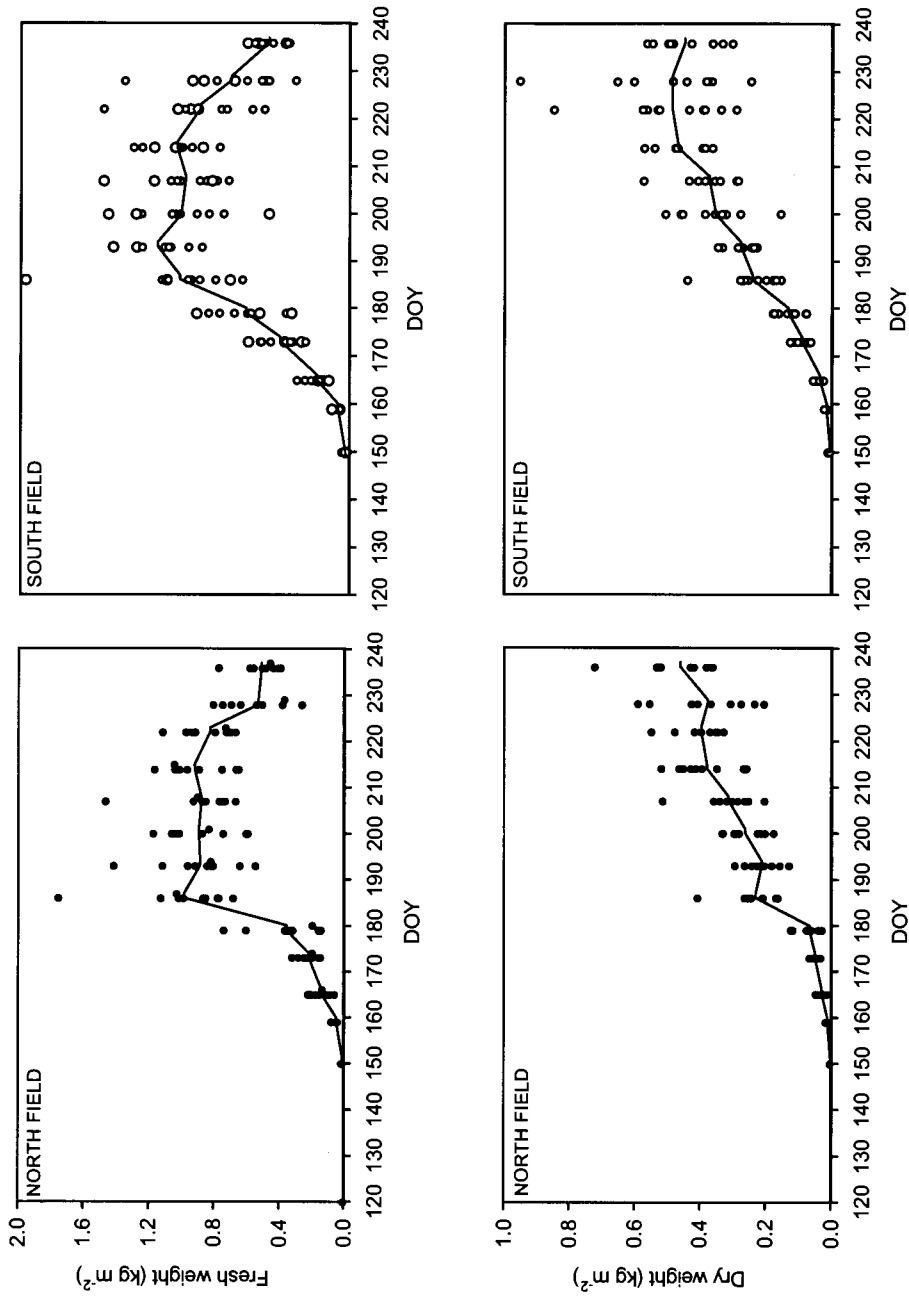


Figure 2.3. Wheat fresh and dry weight throughout the growing season for the north and south fields. For each sampling date, 10 samples are displayed. A linear trend line through the average at each sampling date is also denoted.

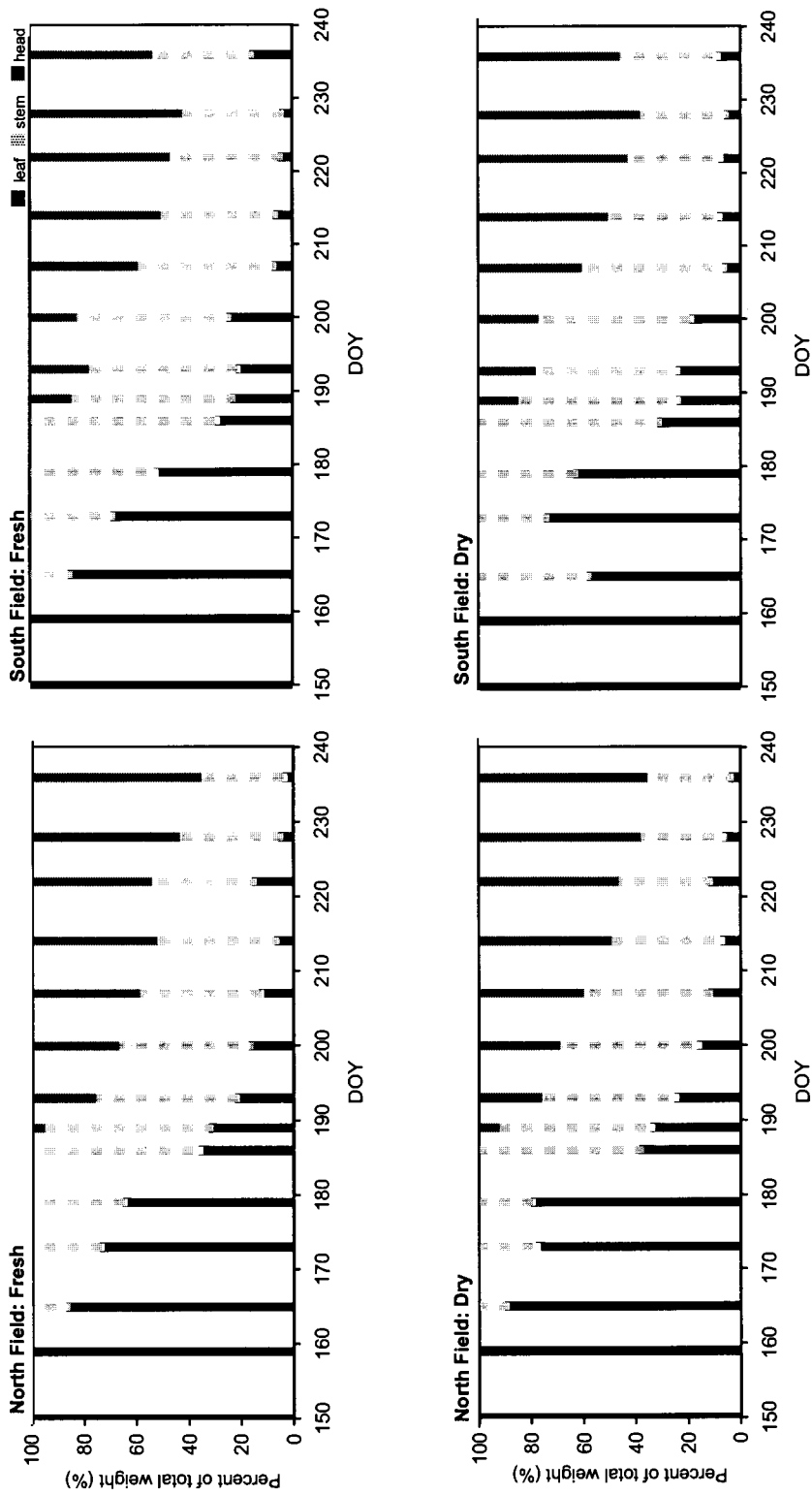


Figure 2.4. Fresh and dry weights of leaves, stems and heads as a percent of total weight.

The plant heights increased until approximately DOY 199 (Figure 2.2). During the emergence stage, plant height increased because leaf length increased. Throughout the jointing stage, the plant heights rapidly increased as both leaves and stems grew. This increase was primarily due to the production of stems (Figure 2.4). The stems reached their maximum height just after the jointing stage, and during the heading stage, stem height and mass increased minimally. During the first half of the heading stage, the plant heights continued to increase because the wheat heads were increasing in length. Once the heads stopped growing, plant height reached a plateau.

In both fields, the fresh plant weight and absolute water content increased from emergence (DOY 147) to heading (DOY 189) (Figure 2.3). Once the heading stage began, the primary plant production was seed development, and this coincided with no significant increase in the internal water content of the plants. As a result, the fresh plant weights reached their peak during the heading stage. After DOY 212, the fresh plant weights declined as the internal water content of the plants decreased.

The plant dry weights increased until the soft dough stage (Figure 2.3). At the beginning of the soft dough stage, the dry plant weights began to slowly plateau, until approximately DOY 212 when a plateau was reached. The plateau coincided with the leaves and tips of the wheat heads turning golden brown in colour. The above trend in plant dry weight occurred for both the north and south fields. Throughout the growing season, the mean dry weights between the two fields, as expected, were very well correlated ($r^2 = 0.96$). However, the plant dry weights from week to week were consistently greater in the south field and acknowledge that the wheat emerged three days earlier in that field.

The dry to fresh plant weight ratio was essentially constant until heading (DOY 189), and after that, the ratio began to increase (Figure 2.5). From plant emergence until heading, the dry to fresh weight ratio was approximately 22 percent, and indicated

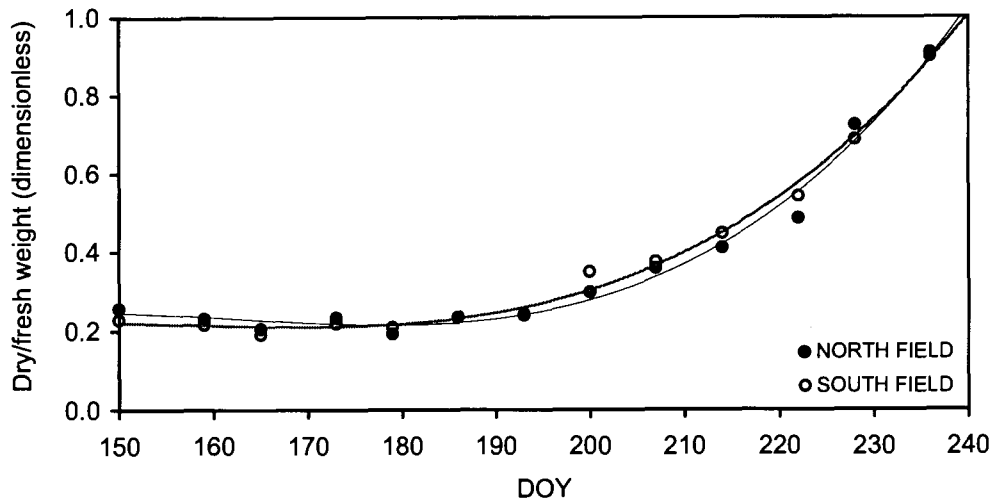


Figure 2.5. The dry to fresh plant weight ratios throughout the growing season. The black line is a fitted polynomial for the north field and the grey line is the fitted polynomial for the south field.

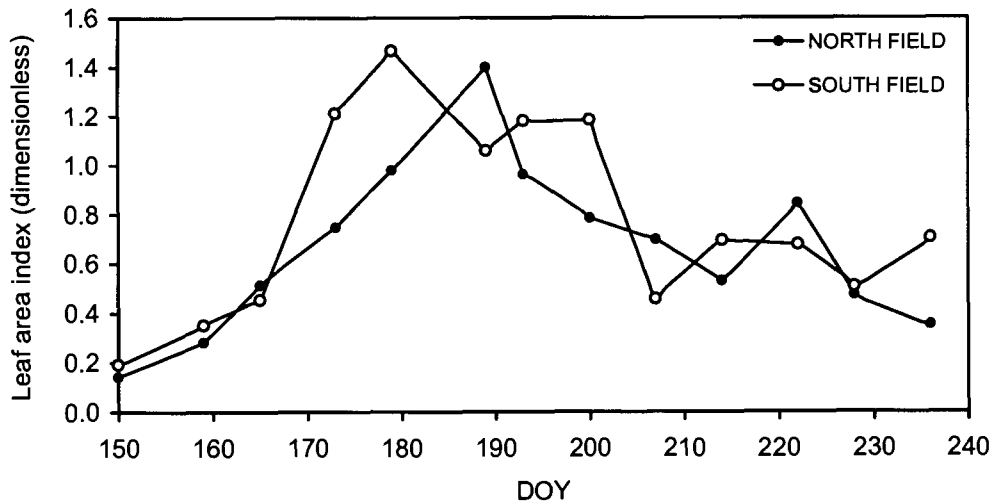


Figure 2.6. The leaf area index throughout the growing season.

that the amount of water and tissue being gained by the crop were proportional to one another. Throughout the heading stage, the ratio increased slowly because there was reduced plant growth and the internal plant water content was decreasing. During the soft dough stage, the seeds began to harden, and the dry to fresh weight ratio rapidly increased as the fresh plant weights began to decline. The ratio continued to increase during the ripe stage, as the wheat began to desiccate, and the rate of increase was at its maximum.

The leaf area increased until the heading stage (LAI = 1.5), and then decreased until the soft dough stage as numerous leaves on the plants died (Figure 2.6). The variation in LAI between sample dates, such as the drop in the LAI on DOY 189 in the south field, is due to errors that arise from a small sample size. However, previous studies have reported a similar overall LAI trend (Ahmad and Lockwood, 1979; Song, 1999). Hucl (1995) reported similar LAI for hard red spring wheat in Saskatoon for the 1990 growing season, but most studies observed a peak LAI approximately four times greater than this study (Bauer *et al.*, 1987; Maas, 1993; Piggin and Schwerdtfeger, 1973; Song, 1999). The observed difference in LAI in this and Hucl's (1995) study suggests that the lower LAI is likely linked to crop moisture stress associated with periods of moisture deficit.

2.4.2 The seasonal progression of mean daily albedo

The daily albedo demonstrated a distinct seasonal trend (Figure 2.7). Initially, the surface was covered with organic litter and stubble from the 2000 growing season. The matted lentil litter in the north field had a higher albedo ($\bar{\alpha} = 0.173$, $\sigma = 0.003$) than the flax stubble in the south field ($\bar{\alpha} = 0.161$, $\sigma = 0.006$). The higher albedo in the north field arose because the surface had more organic litter coverage. Even though the volumetric soil moisture was on average 21 percent higher in the north field, the greater

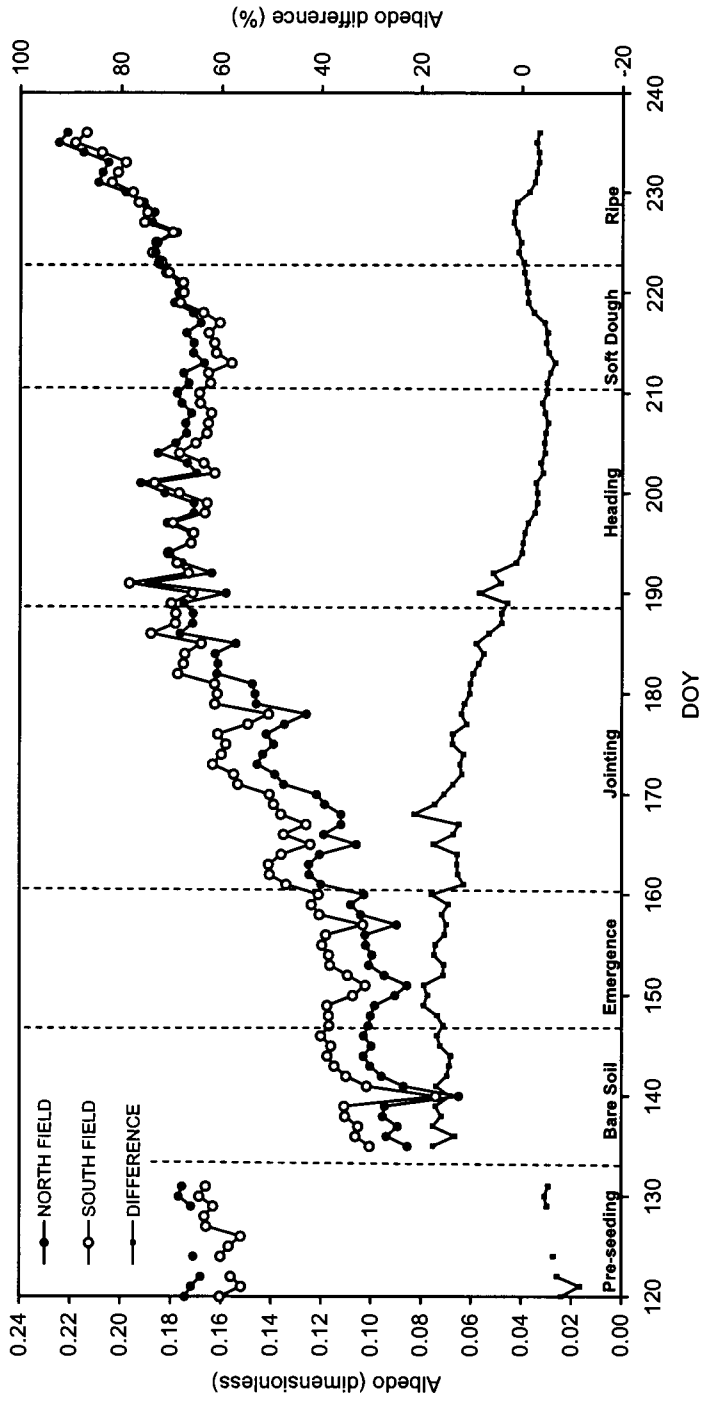


Figure 2.7. The time series of the daily albedo for two wheat fields and the percent difference between them. The difference is $(\alpha_S - \alpha_N) / \alpha_N$ expressed as percentage, where α_S is the south field albedo and α_N is the north field albedo. The phenological periods are denoted throughout the growing season.

litter coverage had a larger affect on surface reflectance than surface moisture. Aase and Tanaka (1991) observed that reflected solar radiation increased as the amount of litter on the surface increased from no cover to 33, 66 and 100 percent. The albedo may have also been influenced by the orientation of the litter on the surface. The majority of the litter in the north field rested flat on the surface, while the majority of litter in the south field was vertical. The greater surface roughness in the south field may have contributed to more solar radiation absorption. Thus, the albedo during pre-seeding was influenced by the type, quantity and orientation of the organic litter.

During pre-seeding, the albedo was negatively correlated with surface soil moisture (depth of 0 - 10 mm) (Table 2.2). On the second day of observations (DOY 121), a small rain event occurred early in the morning. This caused an increase in surface moisture and, in response, the albedo decreased. In the north field, the albedo decreased by 0.002, and in the south field the albedo decreased by 0.008. The reason the albedo decreased more in the south field was because the soil and straw retained water better than the lentil mat in the north field, as evident by the volumetric soil moisture (measured on DOY 122) of $0.14 \text{ mm}^3 \text{ H}_2\text{O}/\text{mm}^3 \text{ soil}$ for the north field and $0.18 \text{ mm}^3 \text{ H}_2\text{O}/\text{mm}^3 \text{ soil}$ for the south field. It must also be noted that the probable absolute error in the albedo is approximately 0.008, and thus this difference is within the range of measurement errors (Appendix H). The following day, a very light and brief shower (trace $\approx 0.1 \text{ mm}$) in the morning added moisture to the surface and decreased the albedo in the north field. However, the albedo in the south field did not decrease from surface rewetting. The uppermost layer of soil was dryer on DOY 123 and, as a result, the albedo increased. On DOY 126, the albedo decreased in response to increased soil moisture and, after DOY 126, the albedo increased as the surface to dried (Figures 2.1 and 2.7).

Table 2.2 The correlation coefficient (r) between the daily albedo (α), transmissivity (t), the volumetric soil moisture (vsm) of the uppermost 10 mm of soil and the leaf area index (LAI).

Phenological Stage	North		South		North		South		North		South	
	n	$r_{t,\alpha}$	n	$r_{t,\alpha}$	n	$r_{vsm,\alpha}$	n	$r_{vsm,\alpha}$	n	$r_{LAI,\alpha}$	n	$r_{LAI,\alpha}$
Pre-seeding	7	-0.05	11	0.03	7	-0.74	9	-0.74	2	1.00	2	1.00
Bare Soil	11	0.77	11	0.73	11	-0.72	11	-0.75	3	0.87	3	0.97
Emergence	14	0.23	14	0.20	14	-0.63	14	-0.63	4	-0.34	4	0.93
Jointing	28	0.61	28	0.58	28	-0.07	28	-0.09	2	1.00	2	-1.00
Heading	21	-0.42	21	-0.63	21	0.04	21	-0.42	2	-1.00	2	-1.00
Soft Dough	12	-0.41	12	-0.20	12	-0.72	12	-0.80	2	-1.00	2	-1.00
Ripe	13	-0.41	13	-0.43	14	-0.44	14	-0.49	2	-1.00	2	1.00

By DOY 135, the fields had been harrowed and seeded. Throughout the bare soil stage, the albedo fluctuated (Figure 2.7) in response to changing transmissivity, surface soil moisture (0-10 mm) (Figure 2.1) and surface roughness. The albedo was strongly correlated to both transmissivity and surface soil moisture during the bare soil stage (Table 2.2). During the bare soil stage, the transmissivity was an important factor during overcast days with rain events. On rainy days, the albedo decreased in response to the combined effects of increased diffuse solar radiation and higher surface soil moisture. The greatest decrease in the daily albedo was on DOY 140 when the albedo reached its lowest level of the study. At this time, the surface soil moisture increased and there was very thick cloud cover. A study by Duchon (1997) supports this observation as the albedo was observed to decrease to its lowest levels during large rain events when the soil was saturated and global solar radiation decreased. Under all other sky conditions, there is no clear relationship between the albedo and transmissivity.

Similar to the pre-seeding stage, the albedo during the bare soil stage was inversely related to surface soil moisture (Table 2.2). After the fields had been seeded, the albedo began to increase as surface soil moisture declined. The albedo continued to increase until a rainstorm (7.3 mm) on DOY 140 (note: precipitation collected on DOY 141). On DOY 140, the albedo reached its lowest level for reasons previously stated. After DOY 140, the soil surface dried quickly, and the albedo rose sharply. By DOY 143, the albedo was higher than before the rain event, but the surface soil moisture was also slightly higher. The higher albedo arose because a thin crust (< 10 mm) developed on the soil surface and resulted in reduced surface roughness. Several authors have also reported that a thin crust on the soil surface will reduce surface roughness and thereby increase the albedo (Baumgardner *et al.*, 1985; Proctor and Blackburn, 1983).

The next phenological stage was emergence, and the albedo was influenced by surface soil moisture and the vegetation cover. For most of the emergence stage, the

albedo was similar to the bare soil albedo. Throughout the emergence stage, the albedo responded to three rain events on DOY 149 (at night), DOY 151 and DOY 157. Initially, the albedo decreased in response to surface soil moisture increasing. The albedo may have also decreased on DOY 151 because transmissivity declined to 0.058 even though there is a no correlation between transmissivity and soil moisture for this phenological stage. Following each of these rain events, the albedo increased as surface soil moisture declined.

The albedo increased slightly at the end of the emergence stage. This coincided with the crop reaching an extended height of 0.12 m (on approximately DOY 158). Before the extended crop height reached 0.12 m, the albedo seemed unaffected by the presence of the wheat crop. However, once the crop reached 0.12 m, the crop had covered enough of the surface (LAI = 0.3) to become a dominant control on the albedo.

After the emergence stage, the albedo increased as the canopy matured. This maturation is evident from the increased plant height, plant biomass and LAI (Figures 2.2, 2.3, 2.6 and 2.7). Several studies have reported that the albedo is essentially controlled by LAI during jointing (Jacobs and Van Pul, 1990; Song, 1999; Walter-Shea *et al.*, 1992), and during this stage, the albedo was well correlated to LAI (Table 2.2). During the jointing stage the albedo was also strongly correlated to plant height (h) ($r_{h,\alpha} = 0.933$ for the north field and $r_{h,\alpha} = 0.893$ for the south field).

The albedo reached a plateau when the heads reached their maximum length. The albedo did not change when plant biomass slightly increased as the seed heads filled. The albedo also did not respond to the small decrease in LAI from DOY 189 to 210.

Throughout the soft dough stage that albedo was controlled by the wheat's internal water content coupled with LAI and chlorophyll content. During the first half of

the soft dough stage (DOY 211 to approximately 216), the albedo exhibited a slight decrease as the dry to fresh weight ratio increased and the LAI decreased. A few studies have also observed a decrease in the albedo after peak greenness as both plant turgidity and LAI decreases (Jacobs and Van Pul, 1990; Song, 1999; Walter-Shea *et al.*, 1992). The albedo may have also decreased when LAI decreased, as soil conditions once again became important. This assumption is substantiated by the stronger relationship between the albedo and soil moisture (Table 2.2). During the latter part of the soft dough stage, the albedo sharply increased and continued in this way until harvest (DOY 216 to 236). The albedo increased during the soft dough stage when the wheat lost 40 percent of its water content and the chlorophyll content declined. The rate of increase in the albedo was greater than the jointing stage, and is quite similar to the trend observed by Song (1999).

2.4.3 Albedo differences between the north and south fields

Throughout the growing season, the albedo trend was similar for the north and south fields. However, the daily albedo values were not identical (Figure 2.7). During pre-seeding, the fields had differing surface types and amounts of organic litter. As a result, α_{diff} was -6.9 percent ($\sigma = 2.4$ percent). During the bare soil and emergence stages, α_{diff} was related to the characteristics of the soil and surface soil moisture. The soil was visually darker in the north field and for the bare soil stage, this translated into an approximate 16 percent difference between the two fields (Figure 2.7). The α_{diff} also increased after surface soil moisture increased (Figure 2.7). For example, on DOY 149 to 151, the α_{diff} increased to 19.5 percent as surface soil moisture increased. The α_{diff} then decreased as surface of the north field dried faster than the south field. This

difference suggests that surface the south field retained more water. However, α_{diff} was weakly and inversely related to surface soil moisture ($r_{vsm, \alpha_{diff}} = -0.23$).

The α_{diff} decreased throughout the jointing stage, but from DOY 161 to 178 it is quite variable. The α_{diff} declined as both fields became similar in height and architecture. From DOY 179 to 188, the rate of decrease in α_{diff} is larger as the mean height of the wheat increased at a greater rate in the north field (Figure 2.2). It is suggested that the wheat height increased at a greater rate in the north field than the wheat in the south field because the crop in the south field was subject to more water stress. This is substantiated by Figure 2.1, where soil moisture from 0 to 250 mm was decreasing throughout the jointing state, and the rate of decline was greatest after DOY 179.

During the jointing stage, several small increases or peaks occurred in α_{diff} and the largest peaks occurred on DOY 165 and 168 (Figure 2.7). These peaks surround clusters of rain events (Figure 2.1). For example precipitation fell daily from DOY 165 to 171. In terms of DOY 165 and 168, the peaks occurred when the additions in soil moisture were enough to make the soil moisture in the south field approximately 14 percent greater than the north field. Following the peaks, α_{diff} decreased over several days because the south field retained more surface soil moisture and dried more slowly than the north field (Figure 2.1). The above explanation is complicated by days such as DOY 179, which have large precipitation inputs, but no increase in α_{diff} . This maybe because the surface soil moisture was relatively high before the rain event, and the surface was much drier before precipitation inputs on DOY 165 and 168.

The difference in the albedos continued to decrease through the heading stage. However, α_{diff} sharply increased from 2.8 percent on DOY 189 to 8.4 percent on DOY

190, and remained above 2.8 percent until DOY 193 (Figure 2.7). The difference from DOY 190 to 192 corresponded to the production of the heads. It was visually observed that the heads emerged from the boots and began to mature approximately 12 to 24 hours earlier in the south field. The slight dissimilarity in wheat head morphology between the fields increased α_{diff} . After this peak, the difference between the albedos almost disappeared as both wheat crops reached maturation.

On DOY 194, α_{diff} decreased to -0.03 percent. A small cluster of perennial sow thistles (*Sonchus arvensis* L.) bloomed above the canopy in the north field, southwest of the inverted pyranometer. These yellow flowers caused the albedo to be slightly greater in the north field. The α_{diff} continued to decrease as the number of sow thistles increased. By DOY 213, the crop in the south field began to senesce, and once again the α_{diff} increased. The difference in the albedo from DOY 194 to 213 highlights the variable nature of crop surfaces as weeds heterogeneously distributed over space and time. Even though a wheat crop is quite homogenous, there are slight variations with space that influences the albedo.

After DOY 213, α_{diff} began to increase because the wheat in the south field began to senesce first as the crop emerged three days before the crop in the north field. The wheat in the south field also senesced more rapidly as its greater biomass contributed to the crop being under more water stress. The north and south field albedos were essentially identical once both fields had turned golden brown in colour, and the sow thistles in the north field had stopped flowering. After DOY 219, the α_{diff} cannot be simply accounted for by the observed soil and plant characteristics. It is likely that α_{diff} was caused by subtle differences in the surface character, such as the type and amount of weeds under each sensor (Appendix C).

2.4.4 Numerical summaries of seasonal albedo controls

Throughout the growing season, the daily albedo can be related to a number of surface controls and can be summarized numerically (Table 2.3). During the pre-seeding stage, the albedo was strongly influenced by the organic litter layer on the surface. The albedo was nearly constant throughout this stage and was inversely related to surface soil moisture levels. The albedo during the emergence stage was similar to the bare soil albedo and was also inversely related to surface soil moisture levels. Thus, the albedo of the pre-seeding stage (the albedo of a bare soil with an organic litter layer) and emergence stage can be expressed in terms of the albedo of the average bare soil condition (Table 2.3).

After the emergence stage, the albedo began to increase, and this was well related to increasing plant height, plant weight and LAI. Throughout the jointing stage, the albedo was related to these factors, and the albedo was most successfully expressed in terms of the extended plant height ($r_{h,\alpha} = 0.93$ for the north field; $r_{h,\alpha} = 0.89$ for the south field). Separate expressions for the north and south fields were necessary as the albedos and crop heights are somewhat distinct (Table 2.3).

Once the heads emerged, the albedo reached a plateau and remained fairly constant until the midpoint of the soft dough stage (DOY 215). The albedo from DOY 189 to DOY 215 was thus expressed in terms of the albedo of the average bare soil condition. However, describing DOY 189 to 215 this way will cause the modelled albedo to vary more day-to-day than the observed values because the albedo of a bare soil is more sensitive to surface soil moisture than the albedo of a wheat crop.

The albedo increased throughout the senescence period (from the midpoint of the soft dough stage (DOY 216) until harvest), and was most strongly correlated with the dry to fresh weight ratio ($r_{dfw,\alpha} = 0.975$ for the north field; $r_{dfw,\alpha} = 0.998$ for the south field).

Table 2.3. Numerical summaries for the growing season.

Phenological stage or period	North Field				South Field					
	Expression*	$\bar{\alpha}$	σ	$\Delta\bar{\alpha}_{ps}$	r^2	Expression	$\bar{\alpha}$	σ	$\Delta\bar{\alpha}_{ps}$	r^2
Pre-seeding	$\alpha_p = \alpha_b + \Delta\bar{\alpha}_{ps}$	0.093	0.009	0.080		$\alpha_p = \alpha_b + \Delta\bar{\alpha}_{ps}$	0.109	0.011	0.052	
Emergence	$\alpha_e = \alpha_b + \Delta\bar{\alpha}_{ps}$	0.099	0.007	0.006		$\alpha_e = \alpha_b + \Delta\bar{\alpha}_{ps}$	0.115	0.006	0.006	
Jointing	$\alpha_j = 0.1297 h + 0.1075$				0.87	$\alpha_j = 0.1332 h + 0.1177$				0.80
DOY 189 - 215	$\alpha_h = \alpha_b + \Delta\bar{\alpha}_{ps}$	0.171	0.007	0.082		$\alpha_h = \alpha_b + \Delta\bar{\alpha}_{ps}$	0.175	0.009	0.062	
DOY 216 - 236	$\alpha_s = 0.1122 dfw + 0.1176$				0.95	$\alpha_s = 0.0926 dfw + 0.1289$				0.99

* Where α_p is the estimated albedo for the pre-seeding stage, α_b is the bare soil albedo, α_j is the estimated albedo for the jointing stage, h is the extended height (m), α_h is the estimated albedo from DOY 189 to 215, α_s is the estimated albedo for the senescence period and dfw is the dry to fresh weight ratio. $\Delta\bar{\alpha}_{ps}$ is the difference between the average albedo for the phenological stage or period (e.g. pre-seeding, emergence and DOY 189 to 215) and the average bare soil albedo.

Separate expressions for the north and south fields were necessary as the albedos and dry to fresh weight ratios are slightly distinct ($dfw_S = 0.8343dfw_N + 0.1198$, $r^2 = 0.94$) for each field (Table 3.2).

2.5 Conclusions

This chapter has contributed to the body of knowledge about albedo trends throughout a growing season. The albedo was characterized in terms of the changes in surface type and conditions. The growing season was divided into seven distinct intervals based on soil and crop conditions. Initially, the albedo was influenced by the organic litter that remained on the surface from the previous year's harvest. The albedo was greater for the north field during the pre-seeding stage because more organic litter covered the surface. Throughout the pre-seeding stage, the albedo increased as soil moisture decreased. Following seeding, the albedo decreased by approximately 0.07. This confirms other studies that observed: (1) a higher albedo for surfaces with greater amounts of crop residue; (2) the albedo increases as surface moisture decreases; and (3) a bare soil with an organic litter layer has a higher albedo than a bare soil. Approximately three weeks following the emergence stage, the above-ground biomass increased dramatically, and the surface vegetation became the dominant albedo control. This observation is in agreement with other studies, which have reported that the albedo of a newly emerged crop will have the properties of both vegetation and soil (Baumgardner *et al.*, 1985). When the albedo was approximately 0.17, it reached a plateau, and this was related to the peak in plant fresh weights and the emergence of the heads (DOY 189). Song (1999) observed that the albedo will increase until the wheat crop reaches peak greenness, which occurs during the heading stage. The wheat began to senesce during the week of DOY 213 and, in response, the albedo increased to 0.22. Song (1999) also found that the albedo increases throughout the senescence period.

It was anticipated that the albedo of the north and south fields would be identical after seeding. However, slight differences in north and south fields were documented. For the most part, the day to day albedo trend was similar for both fields, but the actual daily albedo values were different because the reflective properties of the soils were dissimilar and the crops matured at slightly different rates.

The daily albedo was predominately controlled by surface conditions. However, atmospheric conditions played a small role in determining the albedo. This was statistically significant during the bare soil and jointing stage, where the albedo was positively correlated to atmospheric transmissivity (Table 2.2). During all other phenological stages the albedo was not correlated to transmissivity. However, throughout the growing season, it was observed that the albedo was influenced by the combined effects of heavy cloud cover (when solar is predominately diffuse) and increased surface moisture. It is unclear why the albedo was only correlated with transmissivity during the bare soil and jointing stages, and why the signs are negative for the pre-seeding, heading, soft dough and ripe stages (Table 2.2). This maybe due to the small sample sizes (i.e. $n < 30$).

The albedos of the wheat fields investigated are primarily functions of surface soil moisture and the phenological stage of the crop. Up to the end of the emergence stage, the albedo was influenced by surface soil moisture. During the jointing stage, the albedo was well related to plant height. The albedo reached a plateau at the heading stage, as the crop reached its peak plant height. The albedo during the soft dough stage was related to the LAI until the crop began to senesce, after which the albedo was related to the dry to fresh plant weight ratio.

CHAPTER 3

THE CHARACTER AND MODELLING OF HALF-HOUR ALBEDOS OF WHEAT

3.1 Introduction

This chapter examines the diurnal character of albedo and its modelling. Many studies have found that albedos are symmetrical around solar noon, and a few have indicated that albedo trends can be asymmetrical around solar noon as atmospheric and surface conditions change. The first section of this chapter will examine what controls half-hour albedos of two wheat fields, and will characterize the diurnal symmetry or asymmetry of albedos throughout the growing season. The sections that follow will determine if regression analysis and the albedo model employed in the Canadian Land Surface Scheme (CLASS) (Verseghy, 1991; Verseghy *et al.*, 1993) can be successfully used to estimate diurnal albedo regimes.

During the past several years, the number of studies reporting and characterising asymmetrical albedos has grown (Al-Yemeni and Grace, 1995; Arnfield, 1975; Grant *et al.*, 2000; Minnis *et al.*, 1997; Nkemdirim, 1972; Prata *et al.*, 1998; Song, 1998). Minnis *et al.* (1997) suggest that, for regions like the southern Great Plains in North America, the albedo tends to be asymmetrical over prairie and pasture surfaces because of variations in sky condition and surface moisture throughout the day. They and other researchers point out that morning dew caused an asymmetrical albedo for bare soil, grass and crop surfaces (Grant *et al.*, 2000; Minnis *et al.*, 1997; Song, 1998). Other studies observed an asymmetrical albedo from a reclined canopy in moderate to strong wind, from leaf tracking or from changes in leaf wetness (Al-Yemeni and Grace, 1995; Song, 1998). The studies over grass and crop surfaces observed that forenoon and afternoon albedos were asymmetrical by 2 to 20 percent. As most of these studies

discuss the symmetry or asymmetry of the albedo on cloudless days, there is a paucity of published information about the symmetry or asymmetry of the albedo on partly cloudy and overcast days. This chapter will provide a detailed description of the character of the albedo throughout the day by characterising the symmetry or asymmetry of the albedo for cloudless, partly cloudy and overcast conditions.

Not only is it important to characterize the albedo, but for many climate models and studies it is important to accurately estimate albedos. Several approaches can be employed to estimate diurnal albedo trends. A simple approach is the application of regression equations (Arnfield, 1975; Hasson, 1990; Morozova, 1994; Nkemdirim, 1972; Post *et al.*, 2000). Although regression equations may appear to estimate albedos satisfactory, they are often restricted in their use because they are site specific. This chapter will use the Arnfield (1975) and Nkemdirim (1972) approaches to estimate half-hour albedos.

Often, albedo models are more complex than regression equations because they estimate albedos as a function of controlling factors like sky condition and surface type (Post *et al.*, 2000; Versegby, 1991; Versegby *et al.*, 1993; Yin, 1998). These models range in complexity, and strive to be suitable for application in a variety of locations, and for a variety of surface types.

The albedo model in the Canadian Land Surface Scheme (CLASS) includes both atmospheric and surface controls. CLASS is a second-generation land surface model developed in 1983 for use within the Canadian General Circulation Model (GCM). CLASS was developed to represent the many surface conditions and types found in Canada and throughout the world. It simulates the surface energy balance for bare soil, vegetated surfaces, snow covered surfaces and surfaces consisting of both vegetation and snow. The soil, vegetation and snow algorithms are presented by Versegby (1991) and Versegby *et al.* (1993). Several additions to CLASS were made throughout the

1990s, but the basic structure of CLASS remains unchanged (Verseghy, 2000). Micrometeorological datasets across Canada were compared to modelled data to examine its accuracy and to find ways of enhancing model performance (Verseghy, 2000). Hence, additional testing of the albedo model in CLASS will contribute to the development of CLASS and any GCM that incorporates similar approaches. In this chapter, the albedo models for bare soil and crop surfaces in CLASS were compared to observed albedos at the Bratt's Lake Observatory throughout the 2001 growing season.

3.2 Background

One of the keys in understanding how a surface or region utilizes solar radiation is to understand the relationship between reflected and global solar radiation. The ratio between reflected ($K\uparrow$) and global ($K\downarrow$) solar radiation is expressed as the albedo (α)

$$\alpha = \frac{K\uparrow}{K\downarrow} . \quad (3.1)$$

Although the albedo is a simple ratio, it is complex in behaviour as it is influenced by both atmospheric and surface controls: solar position, atmospheric transmissivity, surface type and surface condition.

One of the most important albedo controls is the zenith angle as it denotes the angle between the position of the sun and the zenith. The zenith angle is an important atmospheric control during cloudless and partly cloudy conditions, where albedos are found to increase as the zenith increases. Generally, as cloud cover increases and diffuse radiation increases, the role of the zenith angle diminishes. The zenith angle (Z) is calculated from

$$\cos(Z) = \sin(\phi) \sin(\delta) + \cos(\phi) \cos(\delta) \cos(h) \quad (3.2)$$

where ϕ is the latitude, δ is the solar declination and h is the solar hour angle. The solar hour angle is given by

$$h = 15 |12 - \text{LAT}| \quad (3.3)$$

where LAT is the local apparent time (in hours).

In general, during cloudless days, the albedo is symmetrical around solar noon when the surface condition remains constant. In contrast, during overcast days, the albedo is nearly constant (Ahmad and Lockwood, 1979) because most global solar radiation received at the surface is diffuse. On partly cloudy days, cloud cover may result in varying albedos that can be asymmetrical around solar noon. The albedo will decrease as cloud cover increases, and this is related to decreasing direct beam and enhanced diffuse solar radiation (Ahmad and Lockwood, 1979; Duchon, 1997; Iqbal, 1983; Nkemdirim, 1972). The influence of cloud cover can be expressed in terms of atmospheric transmissivity (t)

$$t = \frac{S}{K_{\text{ex}}} \quad (3.4)$$

where S is the direct beam irradiance and K_{ex} is the extraterrestrial radiation. K_{ex} is given by

$$K_{\text{ex}} = \frac{I_0 \cos(Z)}{RV^2} \quad (3.5)$$

where I_0 is the solar constant and RV is the radius vector.

As discussed in Chapter 2, the surface type and conditions significantly affect the albedo. For example, as a bare soil becomes wetter, the albedo will decrease because the film of water on individual soil particles readily absorbs solar irradiance in the near infrared spectrum. Several authors have observed a decrease in the albedo after a rainstorm (Idso *et al.*, 1975; Post *et al.*, 2000; Twomey *et al.*, 1986). This is followed by an increase in the albedo as the soil dries (Idso *et al.*, 1975; Post *et al.*, 2000; Twomey *et al.*, 1986). Post *et al.* (2000) observed a 45 percent mean change in the albedo for twenty-eight different soil types as conditions changed from wet to dry.

Diurnal albedo trends for a crop may be controlled by plant water content and leaf orientation (Ahmad and Lockwood, 1979; Jacobs and Van Pul, 1990; Song, 1999). For example, a water stressed crop may go from turgid to wilting throughout the day, and, in response, reflection from the canopy may increase over the day. Thus, the albedo will be asymmetrical about the midday period (Ahmad and Lockwood, 1979; Nkemdirim, 1972). Al-Yemeni and Grace (1995) have also observed that leaf tracking can also cause morning and afternoon albedos to be different.

The diurnal progression of the albedo can be modelled using explicit atmospheric and surface controls. The albedo model in the Canadian Land Surface Scheme (α_{CLASS}) estimates the albedo using zenith angle, global solar radiation, volumetric soil moisture for bare soil and the mean canopy albedo for crop surfaces.

For bare soils, α_{CLASS} estimates the albedo from surface soil moisture. Atmospheric controls, such as the zenith angle control, are not considered because the zenith angle influence is assumed small when it is $< 80^\circ$ (Verseghy, 1991). The bare soil albedo (α_b) for α_{CLASS} is estimated from

$$\alpha_b = \frac{\theta(\alpha_{\text{sat}} - \alpha_{\text{dry}})}{0.20 + \alpha_{\text{dry}}} \quad \theta < 0.20 \quad (3.6a)$$

and

$$\alpha_b = \alpha_{\text{sat}} \quad \theta \geq 0.20 \quad (3.6b)$$

where θ is the observed volumetric soil moisture ($\text{mm}^3 \text{H}_2\text{O}/\text{mm}^3 \text{soil}$), α_{sat} is the limiting wet soil albedo and α_{dry} is the limiting dry soil albedo. The limiting wet and dry soil albedos are determined from Wilson and Henderson-Sellers (1985).

Mailhot *et al.* (1998) presented a modified version of Verseghy's (1991) bare soil algorithm that should be more sensitive to changes in volumetric soil moisture. The modified bare soil algorithm is

$$\alpha_b = \alpha_{dry} \quad \theta \leq 0.04 \quad (3.7a)$$

$$\alpha_b = \theta \frac{(\alpha_{sat} - \alpha_{dry})}{0.16} + \alpha_{dry} - \frac{(\alpha_{sat} - \alpha_{dry})}{4} \quad 0.04 < \theta < 0.20 \quad (3.7b)$$

and

$$\alpha_b = \alpha_{sat} \quad \theta \geq 0.20 \quad (3.7c)$$

For crop surfaces, α_{CLASS} includes both explicit atmospheric and surface controls. The albedo model in CLASS for crop surfaces has separate algorithms for cloudless, partly cloudy and overcast conditions. These three sky conditions are determined by a cloud function (FCloud)

$$FCloud = \frac{ED}{K_{vis} + K_{NIR}} \quad (3.8)$$

where ED is estimated diffuse solar radiation, K_{vis} is estimated visible solar radiation and K_{NIR} is estimated near infrared solar radiation. The estimated K_{vis} and K_{NIR} are each one-half of the global solar radiation value. Employing α_{CLASS} version (2.6), diffuse radiation was estimated from

$$ED = K\downarrow \times \text{xdiffuse} \quad (3.9)$$

where

$$\text{xdiffuse} = 1 - 0.9 \cos(Z). \quad (3.10)$$

When FCloud is 1, it is overcast; when FCloud is >0 but <1, it is partly cloudy; and when FCloud is 0, it is cloudless.

During cloudless conditions, atmospheric and surface controls are incorporated into α_{CLASS} by including both the mean canopy albedo ($\bar{\alpha}_c$) and the zenith angle. The albedo for cloudless conditions (α_{cc}) is estimated from

$$\alpha_{cc} = \frac{\bar{\alpha}_c}{0.5 + \cos(Z)} \quad \cos(Z) < 0.5 \quad (3.11a)$$

and

$$\alpha_{oc} = \bar{\alpha}_c \left[\frac{1}{1 + 2 \cos(Z)} \right] \quad \cos(Z) \geq 0.5. \quad (3.11b)$$

During overcast conditions, only a surface control is included in α_{CLASS} as the albedo is equal to the mean canopy albedo. For partly cloudy conditions (α_{pc}), both atmospheric and surface controls are again included in α_{CLASS} . The controls include direct beam radiation, diffuse radiation and the albedo for cloudless and overcast conditions

$$\alpha_{pc} = \frac{\alpha_{oc}ES + \alpha_{oc}ED}{ES + ED} \quad (3.12)$$

where ES is estimated direct beam solar radiation and α_{oc} is the albedo for overcast conditions.

3.3 Methods

3.3.1 Study site and instrumentation

Research was conducted at the Bratt's Lake Observatory (BLO), Saskatchewan (50° 12' 10" N, 104° 42' 42" W) where the albedo was measured over two adjacent fields. Observations commenced before the crops were planted on April 30 (day of year (DOY) 120) when the north field was covered with a matted lentil material and the south field was cover with flax stubble (Figure 1.2). Observations were halted from May 12 through May 14 (DOY 132 through 134) so that the field could be harrowed and seeded with hard red spring wheat (*Triticum aestivum* L.). The observations commenced again on May 15 (DOY 135), and continued until harvest on August 25 (DOY 237). Further details on the site were previously provided in Chapters 1 and 2.

Throughout the 2001 growing season, measurements of global solar, reflected solar, direct beam and diffuse radiation were undertaken. An adjustable stand was

employed to measure reflected solar radiation at 2 m above the surface with a ventilated Kipp and Zonen CM11 pyranometer in the north field and a ventilated Kipp and Zonen CM21 pyranometer in the south field. Pre- and post-season calibrations of these pyranometers were conducted at the National Atmospheric Radiation Centre and confirmed that their performance did not change over the growing season. Data were collected and stored by a Campbell Scientific 21X datalogger that measured sensor outputs every second and, every minute, a mean, standard deviation, maximum and minimum value was recorded.

Global solar radiation, direct beam radiation, diffuse solar radiation, vapour pressure and air temperature were measured at the BLO's meteorological compound (Figure 1.2). Measurements were made every second and, every minute, a mean, standard deviation, maximum and minimum value was recorded. Precipitation was also measured daily at the meteorological compound.

3.3.2 Supplemental sampling

Daily volumetric soil moisture measurements were made throughout the growing season. Soil sampling (between 7:00 and 9:00 CST) commenced on DOY 120 and continued until DOY 237. At five locations in each field, soil samples were taken from the upper 10 mm of soil and five layers from 0 to 250 mm. The volumetric soil moisture was characterized each day by averaging the five sample locations for each depth interval.

Plant sampling was conducted throughout the growing season to assess the phenological stage of the wheat, plant height and above ground biomass. Every two or three days, at ten fixed locations in each field, the standing and extended heights of the crop was recorded. The standing height is the height of the plant from the ground to its highest point. The extended height is the height of the plant from the ground to the highest standing point when all parts of the plant are manually extended upwards.

In both of the north and south fields, ten quadrants (250 x 500 mm) were randomly selected for manual harvesting to determine above ground biomass. At each location, the surface was first photographed and five plant heights were recorded before harvesting (in each corner of the quadrant and in the center of the quadrant). The surface vegetation was then removed at ground level. For nine of the ten sample locations in each field, vegetation was transferred to a paper bag, weighed and placed in an oven for 72 hours at 70°C. After drying, the dry weight of each sample was recorded. The remaining sample had its plant components (leaves, stems and heads) separated and weighed.

The sample that had its plant components separated was also used to determine the leaf area and leaf area index (LAI). The fresh leaves were laid flat on a white bristol board, covered with plexiglas and photographed (Bailey and Stewart, 1982). The leaf area was determined from the photographs with a density slice function. The relationship between leaf area (LA) to leaf dry weight (l_{dw}) is given by

$$LA = 0.0166 l_{dw} + 0.0135, r^2 = 0.85. \quad (3.13)$$

A leaf area for each sample date was then determined by applying equation 3.13 to the average leaf dry weight at each sample period. The leaf area was then divided by the sampling area to produce LAI.

The growing season was divided into seven stages based on surface and crop conditions. These divisions, except pre-seeding, are based on the phenological stages of wheat as outlined by Robertson (1968) and the Agrometeorological Centre of Excellence (ACE, 2002).

3.3.3 Data analysis

To examine the diurnal symmetry of the albedo, half-hour forenoon and afternoon albedos, at the same zenith angle, were compared

$$\Delta\alpha_z = \frac{\alpha_{am,z} - \alpha_{pm,z}}{0.5(\alpha_{am,z} + \alpha_{pm,z})} * 100 \quad (3.14)$$

where $\Delta\alpha_z$ is the percent difference of the forenoon and afternoon albedo, $\alpha_{am,z}$ is the forenoon albedo at a particular zenith angle, and $\alpha_{pm,z}$ is the afternoon albedo at a particular zenith angle. Initially, the $\Delta\alpha_z$ data was graphed for each day against the zenith angle, and thereafter re-occurring trends were grouped for analysis.

Both atmospheric and surface conditions were employed to investigate $\Delta\alpha_z$ behaviour. Differences in forenoon and afternoon sky conditions, at the same zenith angle, were compared by examining the difference in transmissivity. Differences in the available surface moisture condition were examined through a consideration of the vapour pressure deficit. The vapour pressure deficit (vpd) was calculated for each half-hour using the observed half-hour average vapour pressure (e) and air temperature

$$vpd = e_s(T) - e \quad (3.15)$$

where $e_s(T)$ is the half-hour average of the saturation vapour pressure at the average air temperature.

The diurnal progression of the albedo was further examined using exponential regression equations. In the mid-1970s, exponential regression equations were found to describe diurnal albedo trends adequately. This technique was based on the relationship between the albedo and zenith angle

$$\alpha = \alpha_0 e^{bz} \quad (3.16)$$

where α_0 is the coefficient that is an estimate of the albedo at $Z = 0^\circ$, and b is the coefficient that describes the rate of change in the albedo with respect to the zenith angle (Arnfield, 1975; Nkemdirim, 1972).

Exponential regression equations were produced for three cases. In the first case, a single exponential regression equation for each phenological stage was

produced. This case assumes that the albedo is symmetrical about solar noon. However, as albedos are not always symmetrical, the second case produced exponential regression equations for forenoon and afternoon periods to create a diurnal albedo trend that would acknowledge any asymmetry. This was done for each phenological stage. The first and second cases are limited, as they do not explicitly represent changes in sky conditions, particularly the role of cloud on the direct and diffuse components of global solar radiation. The third case combines the second case with sky conditions through a stratification of the data into three categories based on transmissivity:

Category I	$1.0 \leq t < 0.667$
Category II	$0.333 < t \leq 0.667$
Category III	$0 < t \leq 0.333$

For each case, exponential regression equations were produced from 70 percent of the observed half-hour albedos from the south field during the 2001 growing season. These equations are referred to hereafter as BLO 2001. The BLO 2001 curves were then compared to the remaining 30 percent of the data. In addition, exponential regression equations produced by Nkemdirim (1972) and Arnfield (1975) were considered for comparison purposes. The accuracy and precision of each exponential regression equation was assessed by difference measures (mean bias error (MBE), root mean square error (RMSE) and index of agreement (d); Willmott, 1982).

The albedo model in CLASS was tested for the duration of the growing season (from bare soil to harvest). Four runs were applied to the bare soil algorithm (equations 3.6 and 3.7). Three of these runs (A, B and C) used different limiting wet and dry soil albedos (Table 3.1a). Run A used the limiting wet and dry soil albedo for a dark brown chernozemic soil from Wilson and Henderson-Sellers (1985). Run B used the observed maximum and minimum volumetric soil moisture from the 2001 season for the limiting

Table 3.1a. The α_{CLASS} runs for bare soils. Run A through C uses the version created by Versegby (1991) and run D uses a modified version from Mailhot *et al.* (1998).

Run	Limiting wet and dry soil albedo source
A	Wilson and Henderson-Sellers (1985) for dark brown chernozemic soil
B	Observed maximum and minimum albedo
C	Maximum and minimum from Wilson and Henderson-Sellers (1985)
D	Wilson and Henderson-Sellers (1985)

Table 3.1b. The α_{CLASS} runs for vegetated surfaces.

Run	Mean canopy albedo
ED*	observed fluxes - 5 phenological stage
OD†	observed fluxes - 5 phenological stages
Oke ED	constant
Oke OD	constant
lqbal ED	4 phenological stages
lqbal OD	4 phenological stages

*ED is estimated diffuse solar radiation

†OD is observed diffuse solar radiation

Table 3.1c. Mean canopy albedos used in α_{CLASS} .

Phenological stage	From the present study	From Oke (1987)	From lqbal (1983)
Emergence (initial growth)	0.116	0.180	0.100
Jointing (initial growth)	0.157	0.180	0.100
Heading (milky light green)	0.172	0.180	0.130
Soft Dough (yellow ripeness)	0.167	0.180	0.170
Ripe (fully ripe)	0.195	0.180	0.210

wet and dry soil albedo. Run C used the minimum limiting wet soil albedo and maximum limiting dry soil albedo for all soil types from Wilson and Henderson-Sellers (1985). Runs A, B and C were created to examine if the limiting wet and dry soil albedos from Wilson and Henderson-Sellers (1985) could estimate the albedo accurately. The fourth run, D, is the application of the bare soil modification of α_{CLASS} by Mailhot *et al.* (1998) (equation 3.7). It employed the Wilson and Henderson-Sellers (1985) limiting wet and dry soil albedos.

When the surface was vegetated, several runs of α_{CLASS} were performed that included two diffuse radiation values and three ways of obtaining the mean canopy albedo (Table 3.1b). The albedo model in CLASS was run once using estimated diffuse radiation (equations 3.9 and 3.10) and once using observed diffuse radiation. Observed diffuse radiation was used in α_{CLASS} to test the accuracy of estimated diffuse radiation (equation 3.10).

The mean canopy albedo was determined from observed fluxes and also from Oke (1987) and Iqbal (1983) (Table 3.1c). Observed fluxes were also used to determine the mean canopy albedo for each phenological stage. A constant mean canopy albedo was obtained from Oke (1987) and was used to determine if a single value would provide a reasonable estimate of the albedo throughout the growing season. Values from Iqbal (1983) provided albedo values for wheat at different growth stages. These stages are initial growth, milky light green, yellow ripeness and fully ripe. Again, the four values from Iqbal (1983) were used to see if they could adequately estimate the albedo.

Once all the α_{CLASS} runs were completed, the observed and estimated albedos were examined and evaluated by difference measures (MBE, RMSE, d; Willmott, 1982). Additionally the difference between observed and estimated reflected solar radiation for each half-hour and for each day (for $Z \leq 80^\circ$) was assessed. For each phenological

stage, the sum, maximum, minimum and standard deviation of the difference between observed and estimated reflected solar radiation values were determined.

3.4 Results and Discussion

3.4.1 The diurnal symmetry of albedo throughout the growing season

Diurnal albedo trends were influenced by both atmospheric and surface conditions. Throughout the season, the diurnal albedo trend was often an upward facing parabolic curve or a near horizontal line (Figure 3.1). On cloudless days, the albedo exhibited an upward facing parabolic curve because the zenith angle was the dominant control. On overcast days, the albedo was a near horizontal line as the zenith angle was an inconsequential albedo control. During partly cloudy conditions, the albedo curve was more complex because the albedo was influenced by both the zenith angle and cloud properties (amount, type, etc.). The diurnal symmetry or asymmetry of the above albedo curves depended on the variability of both the sky and surface conditions. The following will more fully consider these aspects of the study.

The diurnal symmetry of the albedo was predominately related to transmissivity. During cloudless or nearly cloudless conditions, the albedo was inversely related to transmissivity (Figure 3.1), and other authors have observed this relationship (Arnfield, 1975; Nkemdirim, 1972). For example, the albedo was inversely related to transmissivity on DOY 187 to 190, as both are influenced by the zenith angle. When the zenith angle increases, global solar radiation will travel further through the atmospheric column to reach the surface. This will result in less direct beam radiation reaching the surface due to atmospheric absorption and scattering. Hence, transmissivity will decrease as the zenith angle increases. In terms of reflected solar radiation, as the zenith angle increases, less solar radiation is back-scattered and absorbed by the surface because

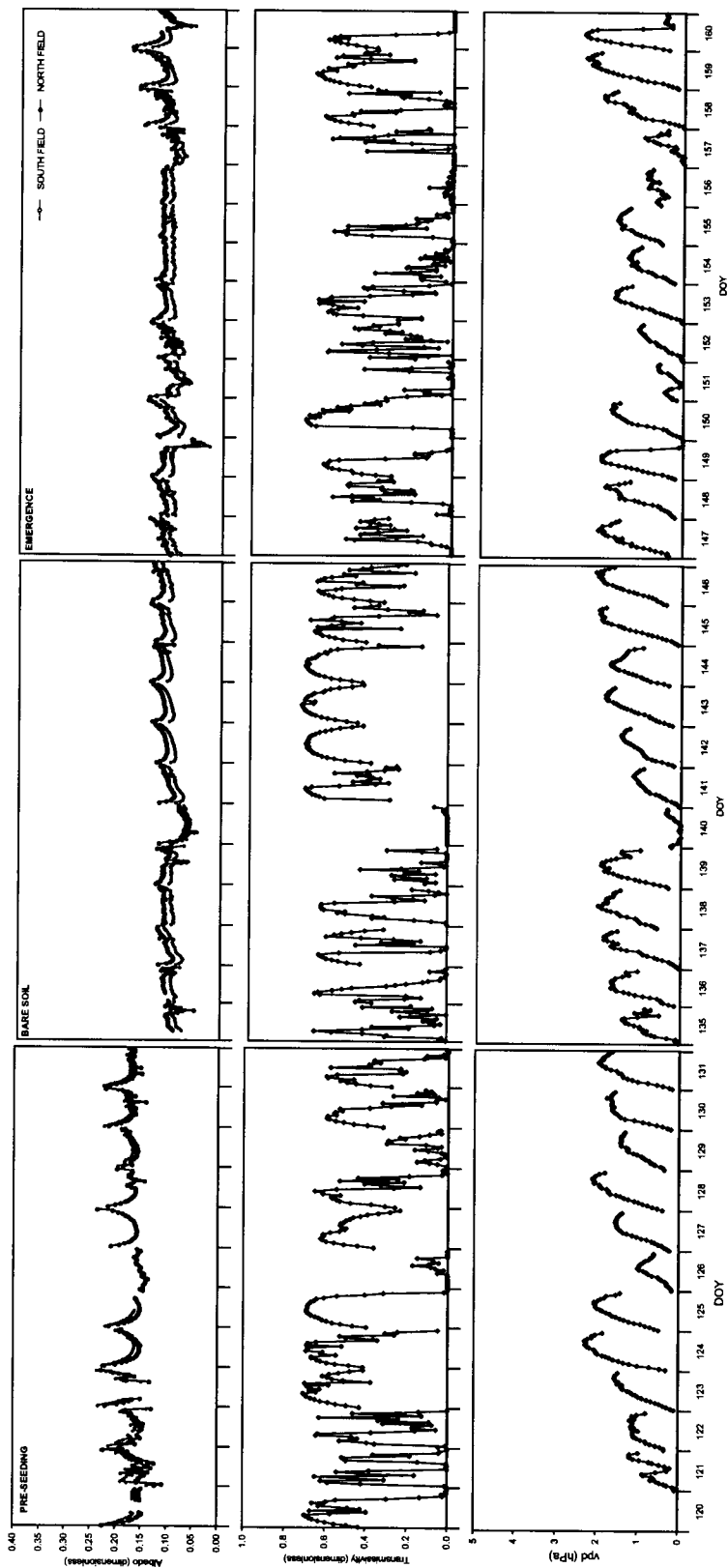


Figure 3.1. The diurnal trend of albedo for two wheat fields, transmissivity and vapour pressure deficit (vpd) for seven phenological stages during the 2001 growing season.

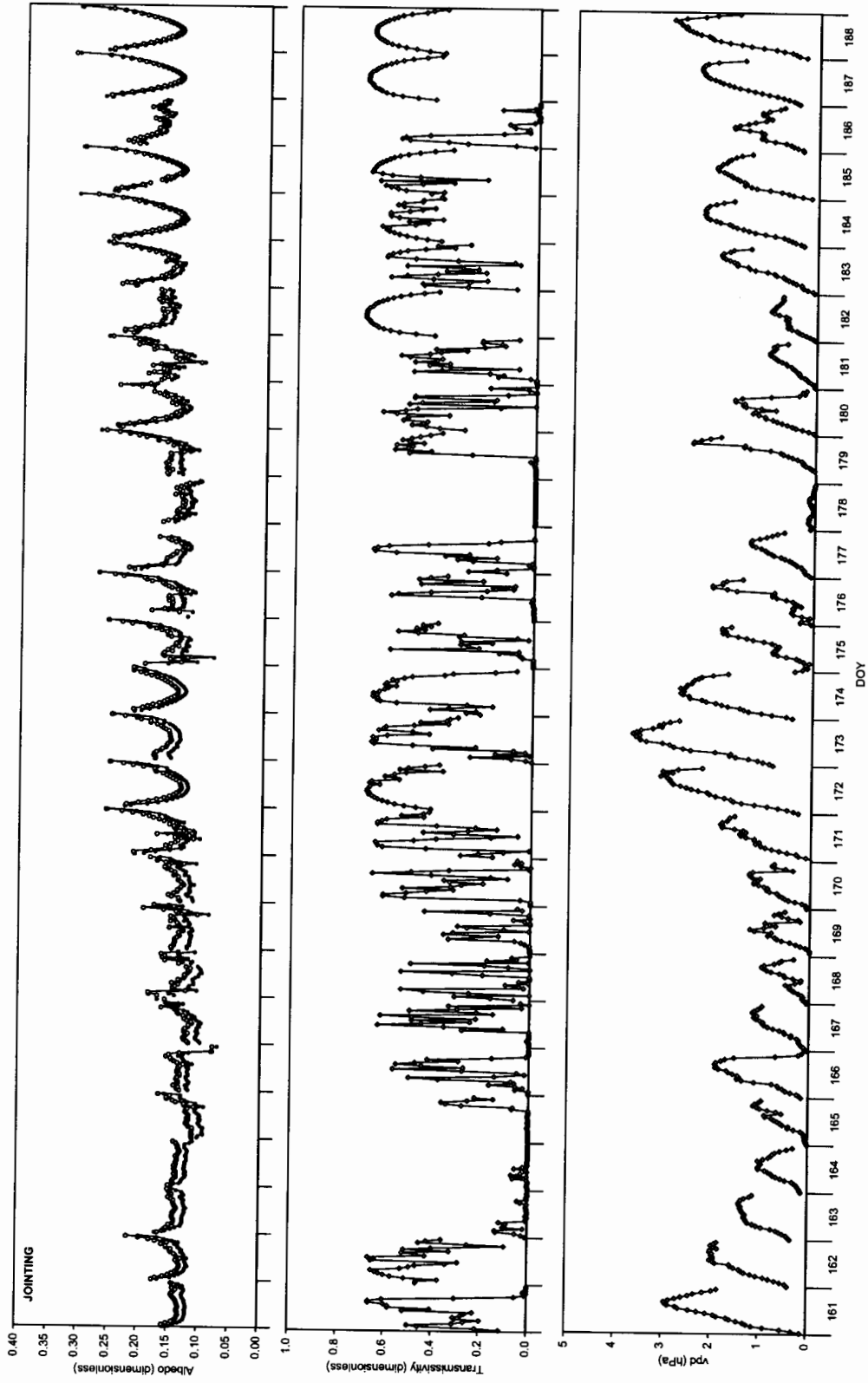


Figure 3.1. Continued

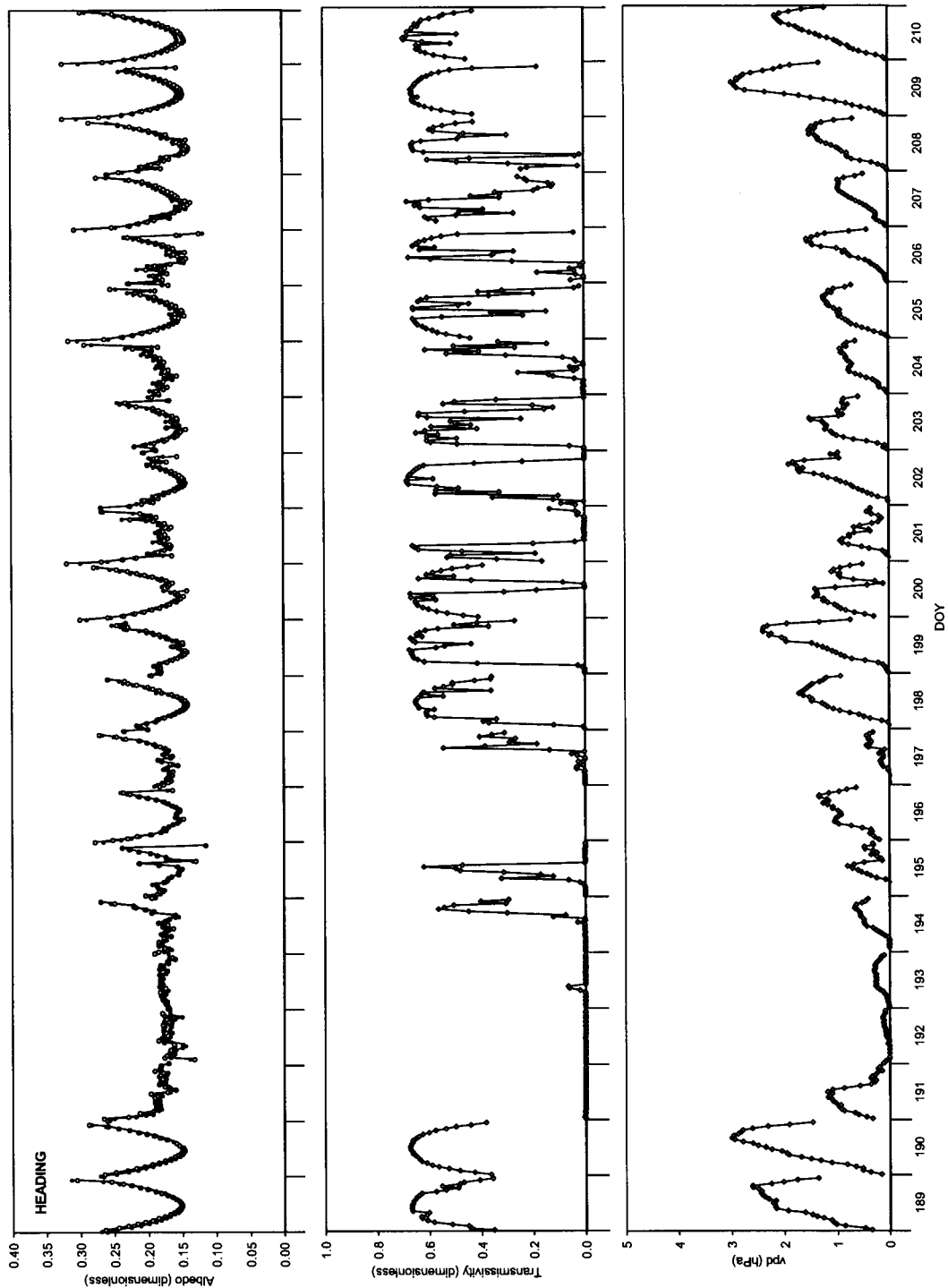


Figure 3.1. Continued

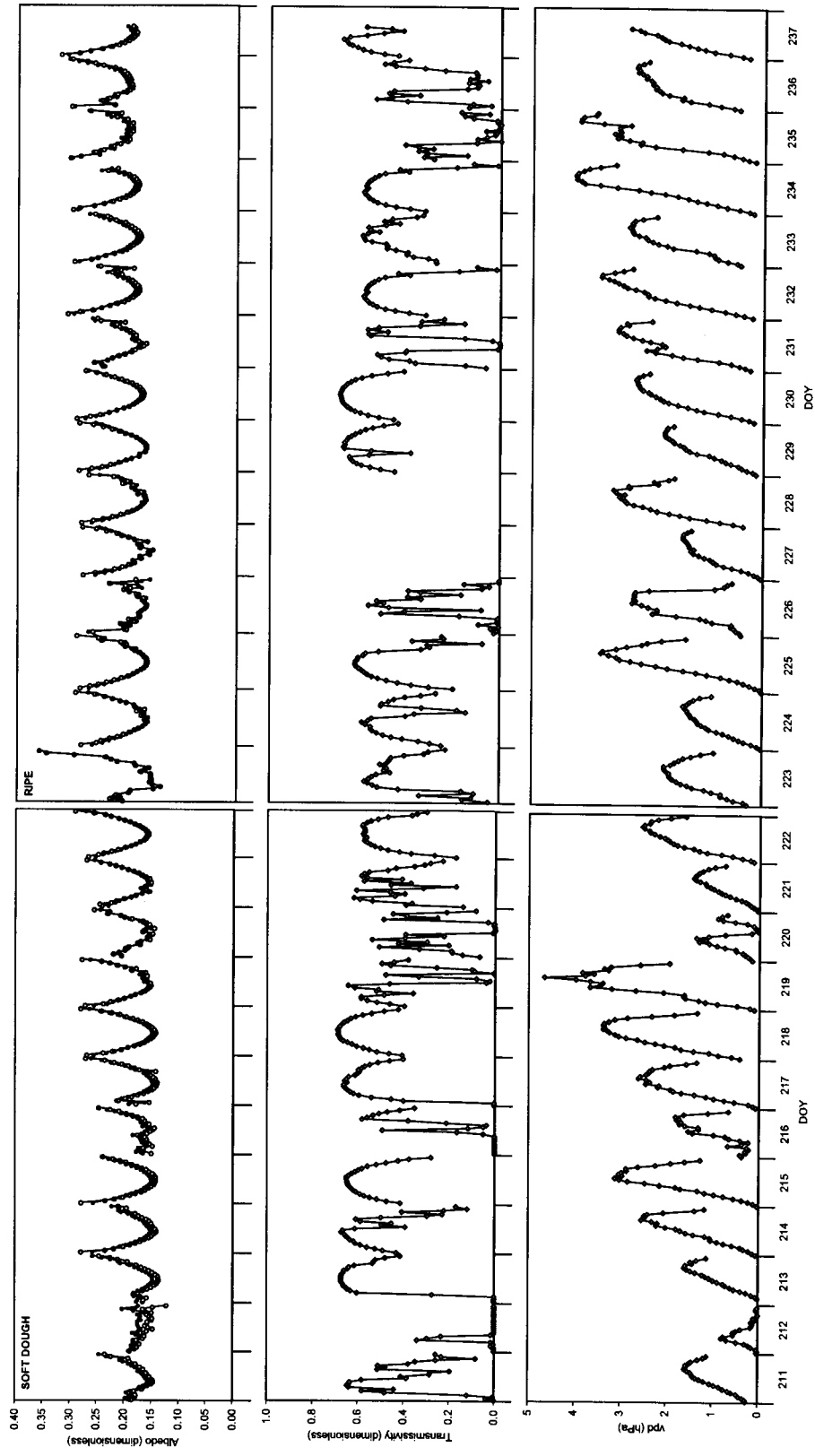


Figure 3.1. Continued

the ground is more characteristic of a smooth surface. As a result, the albedo increases as the zenith angle increases.

Clouds dampen the zenith angle control and, when cloud cover increases, both transmissivity and the albedo decrease. This was most apparent during overcast conditions which produced a nearly constant albedo throughout the day since global solar radiation was diffuse. The small variations in the albedo during overcast days can be attributed to changes in cloud type and thickness. For example, on DOY 163, the albedo decreased slightly over the day as the cloud cover changed from altostratus and altocumulus in the morning, to altostratus and cumulus in the afternoon. On DOY 163, the albedo also varied slightly from one half-hour to the next in response to changes in cloud thickness. During partly cloudy conditions, the albedo also increased or decreased from one half-hour period to the next in response to transmissivity increasing or decreasing.

The diurnal variation in albedo was also controlled by changes in the surface condition. During the pre-seeding, bare soil and emergence stages, surface soil moisture decreased during the morning on cloudless and partly cloudless days and this resulted in the albedo being asymmetrical. During these stages, the minimum albedo was observed between 7:30 and 10:30 LAT. The relationship between the albedo and surface moisture availability was evidenced through a comparison of the albedo to the vapour pressure deficit (vpd) (Figure 3.1). As surface soil moisture increases, more moisture is available for evaporation, and the vpd will have lower values. DOY 142 is a good example of the early morning drying trend that occurred up to the end of the emergence stage (Figure 3.2). The vapour pressure and the vpd increased from dawn until 7:30 LAT. This suggests that dew, which provided water for ready evaporation, was decreasing. The surface soil moisture evaporated as the morning progressed because there was more potential energy for the vaporization of surface dew. After 7:30 LAT, the

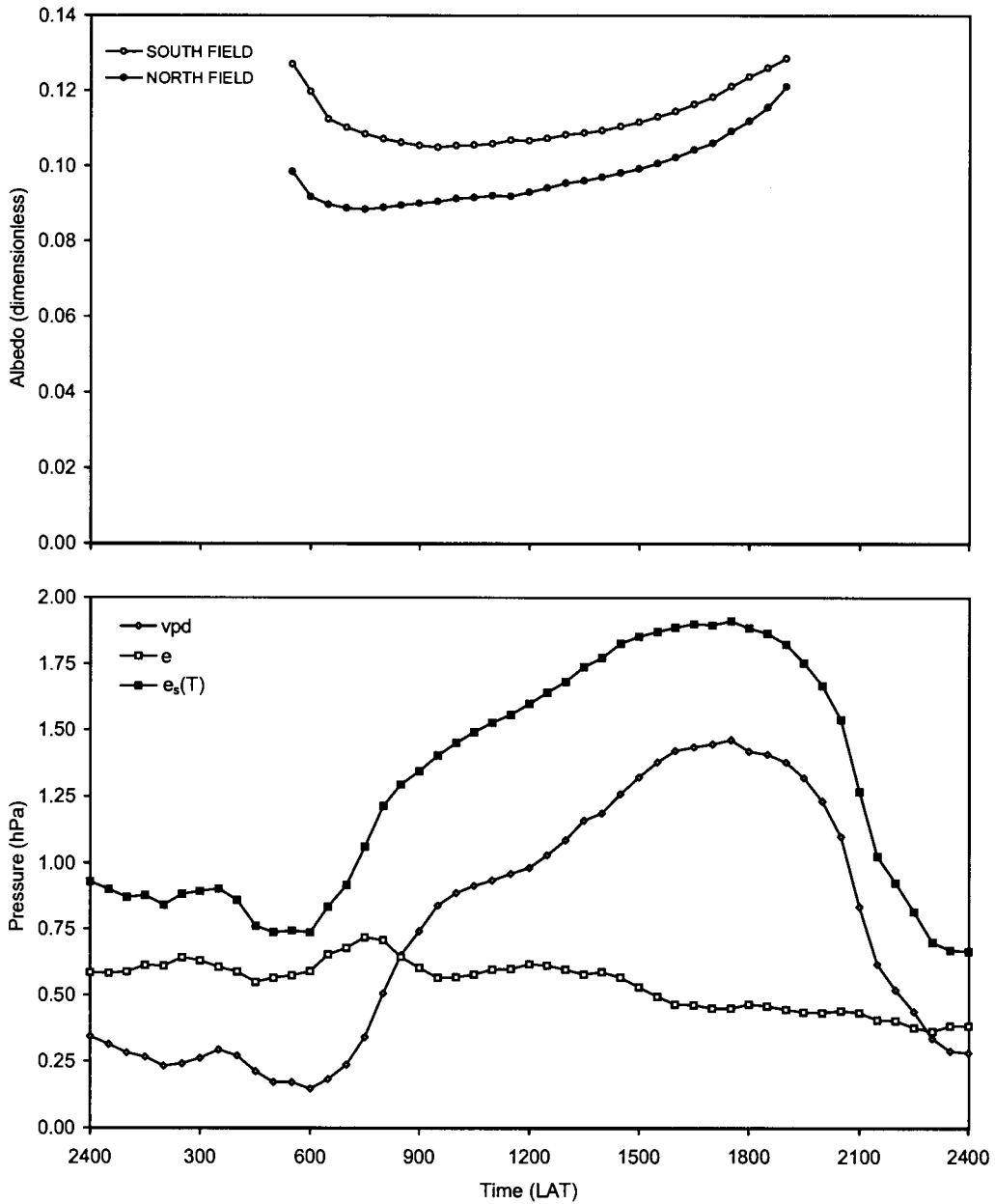


Figure 3.2. The albedo, vapour pressure deficit (vpd), vapour pressure (e) and saturation vapour pressure ($e_s(T)$) for DOY 142.

vapour pressure declined and the vpd increased sharply because the dew was now fully evaporated. Initially, the albedo decreased on DOY 142 as the zenith angle decreased, but once the dew had fully evaporated, the albedo was predominately controlled by the drier surface and in response, the albedo increased. After solar noon, the albedo continued to increase as the zenith angle increased.

Following the emergence stage, during cloudless and most partly cloudy conditions, the albedo did not demonstrate a relationship with vpd or soil moisture. During nearly overcast and overcast conditions with a period of precipitation, the albedo was related to the vpd (but to a lesser extent than during pre-seeding, bare soil and emergence stages) because the albedo decreased as surface moisture increased. Therefore, during nearly overcast and overcast conditions with a period of precipitation, the albedo decreased as both vpd and transmissivity decreased.

Several patterns emerged when the symmetry of the daily albedo was described by the percent difference between the forenoon and afternoon albedos (equation 3.15 and Table 3.2a and b). Each day $\Delta\alpha_z$ was plotted against the zenith angle and trends were grouped. The difference between the forenoon and afternoon albedos was considered symmetrical when $\Delta\alpha_z < \pm 10\%$. Approximately 23 percent of the days were considered symmetrical. The remaining days were considered asymmetrical around solar noon and five main trends were observed (Table 3.2a). When $\Delta\alpha_z$ was mostly asymmetrical and sloped negatively, it was considered to have a negative slope over the day. When $\Delta\alpha_z$ was symmetrical ($\pm 10\%$) for $Z < 60^\circ$, but became asymmetrical when $Z \geq 60^\circ$, then $\Delta\alpha_z$ was either increasing positively or decreasing negatively at the end of the day.

For most days during the growing season, the albedo was asymmetrical. Commonly, the asymmetry was in response to changes in transmissivity. The albedo

Table 3.2a. Major trends in the percent difference between forenoon and afternoon albedos during the growing season. When only one field conforms to the trend described, an N or S will follow the DOY for the north and south field respectively.

Description of the trend	Phenological stage and DOY
Symmetrical:	
Symmetrical \pm 10%	Pre-seeding - 124, 125, 127, 129 Bare soil - 145 S, 138 S Emergence - 154 N, 155, 156 Jointing - 161 N, 164 N, 163 S, 174 Heading - 190, 193, 210 Soft Dough - 215 N, 218, 219, 222 Ripe - 224, 229, 230
The south field illustrates symmetry, but the percent difference for the north field is 5 to 10% for most of the day. When $Z = 80^\circ$, the percent difference for both fields is greater than 10%.	Jointing - 183, 184, 185, 187, 188 Heading - 189, 190
Asymmetrical:	
A concave curve that is skewed to the right. The percent difference is mostly negative.	Pre-seeding - 126 Bare soil - 137, 141, 142, 143, 146 Emergence - 148, 150, 153, 158, 159
Negative slope over the day	Bare soil - 145 N Emergence - 147 Jointing - 165, 167, 170, 171, 176, 179, 181 Heading - 197 Soft Dough - 216 Ripe - 223
Increasing positively at the end of the day	Pre-seeding - 120 Emergence - 149 Jointing - 163 and 166 N, 178, 182, 186 Heading - 196, 202, 205, 207, 209 Soft Dough - 211, 214, 215 S Ripe - 228, 232, 233, 228
Increasing negatively at the end of the day	Bare soil - 138 N Jointing - 173, 175 Heading - 194, 198 Soft Dough - 213, 217 Ripe - 231
Does not conform to the above groupings	e.g. 139 (remaining days - 39 N and 44 S)

Table 3.2b. Major trends in the percent difference between forenoon and afternoon albedos during the growing season and the percentage of days that they represent (out of 116 days)

Description of the trend	North field (%)	South field (%)
Symmetrical:	24.1	22.4
Symmetrical \pm 10%	18.1	16.4
The south field illustrates symmetry, but the percent difference for the north field is 5 to 10% for most of the day. When $Z = 80^\circ$, the percent difference for both fields is greater than 10%.	6	6
Asymmetrical:	42.2	39.7
A concave curve that is skewed to the right. The percent difference is mostly negative.	9.5	9.5
Negative slope over the day	10.3	9.5
Increasing positively at the end of the day	15.5	14.7
Increasing negatively at the end of the day	6.9	6
Does not conform to the above groupings	33.7	37.9

was symmetrical ($\pm 10\%$) for overcast, nearly overcast, cloudless and nearly cloudless days when the surface condition was unvarying.

Throughout the pre-seeding, bare soil and emergence stages, the $\Delta\alpha_z$ curves were skewed to the right because the surface soil moisture was greater at the beginning of the day (Figure 3.3a). This trend was only present for the pre-seeding, bare soil and emergence stages because this is when changes in surface moisture most strongly affected the albedo.

On numerous occasions, $\Delta\alpha_z$ had a negative slope and this was most prevalent during the jointing stage (Table 3.2a and Figure 3.3b). In most cases, the asymmetry occurred because the transmissivity increased throughout the day. On several occasions, the slope was negative when it rained in the morning and the skies cleared in the afternoon. On other days, such as DOY 179, $\Delta\alpha_z$ was positive around midday and dropped to negative values at the end of the day, as transmissivity was greater in the afternoon. DOY 179 provides an interesting example where the morning was foggy until approximately 8:30 LAT ($Z = 51^\circ$), and overcast until 12:00 LAT ($Z = 27^\circ$). Thereafter, cloud cover began to decrease until 13:00 LAT ($Z = 28^\circ$), when approximately half the sky was covered with cumulus clouds. The sky remained this way for the rest of the day. In response, $\Delta\alpha_z$ was negative because transmissivity was lower in the morning than the afternoon, and as difference transmissivity decreases $\Delta\alpha_z$ decreased. After the fog lifted, $\Delta\alpha_z$ was ± 1 percent ($Z = 46^\circ$) and, after which, $\Delta\alpha_z$ increased as the zenith angle decreased. The $\Delta\alpha_z$ increased because transmissivity was low in the morning and the afternoon albedo was influenced by the zenith angle and clearer sky conditions. When all solar radiation is diffuse, the albedo is equivalent to a cloudless sky albedo with a

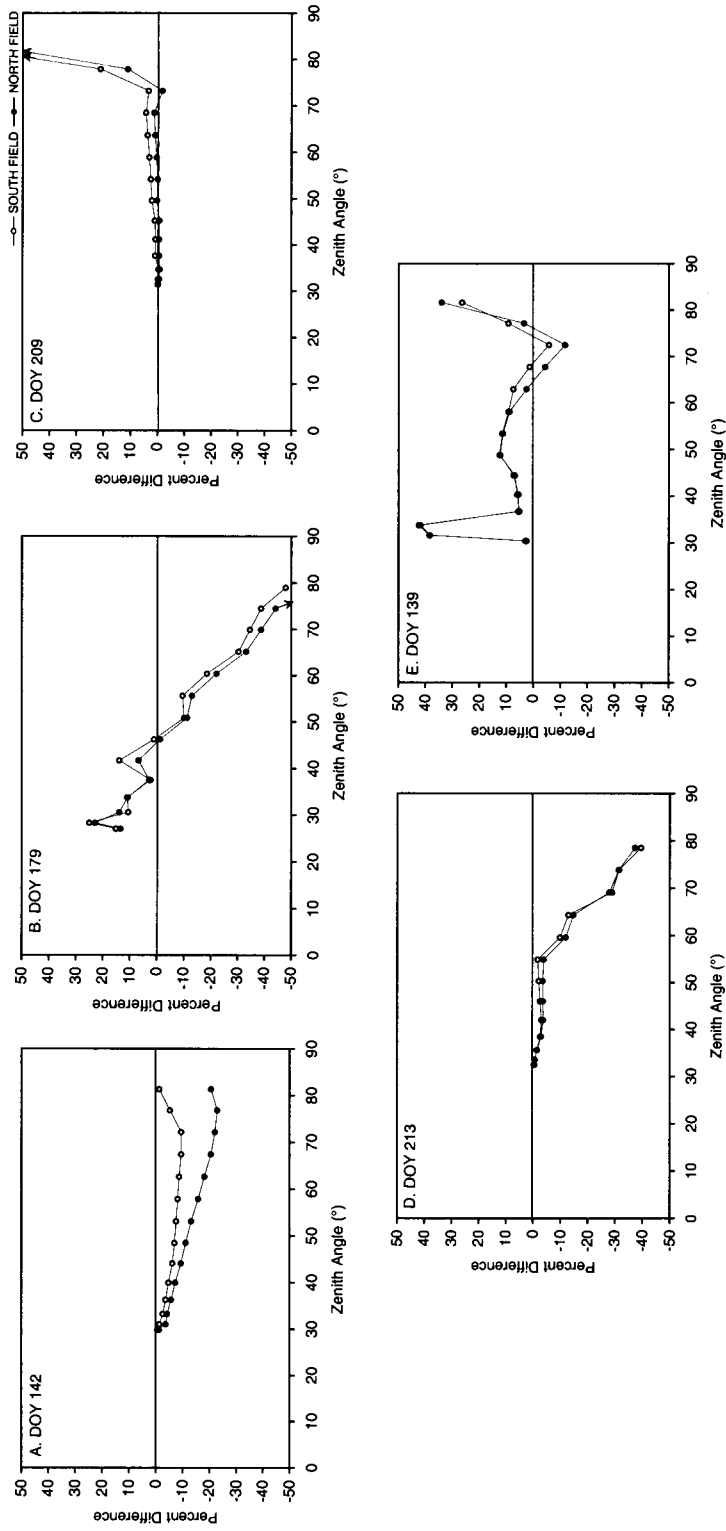


Figure 3.3. The percent difference between the forenoon and afternoon albedo on five selected days. The percent difference is the forenoon albedo subtracted from the afternoon albedo and divided by the average of the forenoon and afternoon albedo.

zenith angle of approximately 45° (Piggin and Schwerdtfeger, 1973). Thus, the forenoon albedo was greater than the afternoon albedo when $Z < 46^\circ$.

As the zenith angle increased, $\Delta\alpha_z$ generally increased either negatively or positively. This was a function of the sky condition where forenoon and afternoon transmissivities were more alike at lower zenith angles than larger zenith angles. This trend is not a surprise because as the zenith angle increases, the time between the morning and corresponding afternoon albedo is greater, and the sky condition may be very different. In contrast, $\Delta\alpha_z$ at small zenith angles are closer in time, and therefore there is a greater likelihood that the sky condition remained the same.

Several days were symmetrical ($\pm 10\%$) at lower zenith angles, but became asymmetrical at higher zenith angles as the sky and surface conditions changed (Figure 3.3c and 3.3d). Again, changes in transmissivity are often related to these differences. However, on a few occasions, the albedo decreased from the combined effect of lower transmissivity and increased soil moisture from a rain event at the beginning or end of the day. DOY 209 is an example of how a change in transmissivity can influence the symmetry of the albedo (Figure 3.3c). The day was nearly cloudless ($\leq 0.5\%$ cloud cover) until approximately 18:00 LAT when the transmissivity decreased as cloud cover increased, and in response the albedo was greater in the morning than the afternoon for $Z > 73^\circ$. On DOY 213, the opposite was true (Figure 3.3d). The morning was nearly overcast until $Z \approx 55^\circ$, and was partly cloudy for the rest of the day. The sky condition did not vary greatly after $Z \approx 55^\circ$, and thus the albedo was symmetrical for most of the day. On DOY 213, the asymmetry increased negatively at higher zenith angles because the morning had a lower transmissivity.

This discussion of $\Delta\alpha_z$ has primarily focused on how $\Delta\alpha_z$ changed as the zenith angle increased, and how the albedo is often symmetrical around solar noon. However,

for several days, the middle of the day had differing forenoon and afternoon sky conditions. For example, on DOY 139, the highest $\Delta\alpha_z$ occurred at $Z = 34^\circ$ because cloud cover was lower in the morning than the afternoon counterpart (Figure 3.3e). When $Z > 34^\circ$, the cloud cover was more alike and in response, $\Delta\alpha_z$ decreased to previous levels. The $\Delta\alpha_z$ was negative when $Z = 72^\circ$ because the cloud cover in the morning was higher than the cloud cover in the afternoon. The $\Delta\alpha_z$ increased after $Z = 72^\circ$ because the cloud cover in the morning was lower than the afternoon.

The days that do not conform to the above $\Delta\alpha_z$ trends have irregular shaped trends throughout the day (Table 3.2a and b). In all of these instances, the asymmetry was related to changes in transmissivity over the day, or from changes in both transmissivity and surface soil moisture brought about by one or more rain events.

The asymmetry of the albedo was similar for the north and south fields, except when the surface was predominately a bare soil and for the period of DOY 183-190. The difference in the asymmetry was a consequence of the difference between the two surfaces. Throughout the pre-seeding, bare soil and emergence stages, $\Delta\alpha_z$ was different for each field because the soil dried at slightly different rates (refer to section 2.3.2 and 2.3.3). When both fields were vegetated, the two surfaces were almost identical, and the differences in $\Delta\alpha_z$ between the two fields were negligible. However, from DOY 183 to 190, $\Delta\alpha_z$ was slightly different in each field (Table 3.2), and was because the wheat in the south field was three days more mature than the north field. During this period, the boots were forming (\approx DOY 183 to 186) and heads were emerging from the boot (\approx DOY 186 to 190) at different rates.

3.4.2 Exponential regression equations for estimating albedos

Exponential regression equations were created to describe the diurnal variation in the albedo (Table 3.3a to 3.3c). Even though it was predicted that Arnfield (1975) and Nkemdirim's (1972) regression equations would inaccurately estimate the albedo at the BLO, they were compared to observed data to find the sensitivity of the albedo to the zenith angle, and to find the implications of using their results at another location.

When the BLO 2001 regression curves were compared to observed albedos, several shortcomings were identified. Two major shortcomings were that the amplitude and symmetry of the albedo were not correctly represented (Figure 3.4). The pre-seeding BLO 2001 equations underestimated the albedo at the end of day, and the asymmetry caused by changes in surface soil moisture were not emulated, as surface soil moisture was excluded from the regression analysis. Additionally, on overcast days, such as DOY 126, the exponential regression equations exhibited a zenith angle control when there was none, and this resulted in erroneous results.

The regression curves had the weakest performance during the bare soil and emergence stages. During these stages, Arnfield's (1975) exponential regression equations poorly represented the observed albedo (Table 3.3a). Arnfield's (1975) equations grossly overestimated the albedo because his regression equations were derived from a much different soil at Simcoe, Ontario, than the soil at BLO. The amplitude of the estimated albedo curve was also greater than the observed albedo curve because 35 percent of Arnfield's (1975) data were in cloud category I ($0.667 < t \leq 1.000$), whereas during the bare soil and emergence stages, only 5 percent of the data was in cloud category I. As a result, the amplitude in the observed albedo curve was less than Arnfield's (1975) albedo curve (Figure 3.4). The BLO 2001 exponential regression equations for the bare soil and emergence stages also had the weakest performance (for the bare soil stage $RMSE = 0.022$ and $d = 0.189$, and for the emergence stage

Table 3.3a. A comparison of observed and predicted half-hour albedos employing exponential regression equations. For each phenological stage, one exponential regression curve was created to represent the albedo when $Z \leq 80^\circ$. The units of the mean bias error (MBE), the root mean square error (RMSE) and the index of agreement (d) are dimensionless.

Phenological stage	From BLO 2001					From Arnfield (1975)				
	equation	n	MBE	RMSE	d	equation	n	MBE	RMSE	d
Pre-seeding	$\alpha = 0.1336e^{0.0038Z}$	78	0.000	0.015	0.662	$\alpha = 0.227e^{0.0076Z}$	320	0.231	0.234	0.092
Bare Soil	$\alpha = 0.1014e^{0.0016Z}$	84	0.008	0.022	0.189	$\alpha = 0.194e^{0.00844Z}$	391	0.222	0.225	0.098
Emergence	$\alpha = 0.1017e^{0.0021Z}$	112	-0.006	0.015	0.355	$\alpha = 0.194e^{0.00844Z}$	765	0.136	0.141	0.332
Jointing	$\alpha = 0.1159e^{0.0068Z}$	221	0.012	0.029	0.654	$\alpha = 0.194e^{0.00844Z}$	613	0.121	0.125	0.361
Heading	$\alpha = 0.1196e^{0.0079Z}$	168	-0.003	0.024	0.787	$\alpha = 0.194e^{0.00844Z}$	312	0.128	0.130	0.361
Soft Dough	$\alpha = 0.1048e^{0.0099Z}$	78	0.009	0.021	0.861	$\alpha = 0.194e^{0.00844Z}$	355	0.101	0.103	0.457
Ripe	$\alpha = 0.1127e^{0.0108Z}$	96	-0.006	0.013	0.958					

Table 3.3b. A comparison of observed and predicted half-hour albedos employing exponential regression equations. For each phenological stage, forenoon (am) and afternoon (pm) exponential regression curves were produced to estimate the albedo when $0^\circ \leq Z \leq 80^\circ$. The results were compared to observed albedos and the combined result of the forenoon and afternoon albedo curves (all) were also assessed. The units of the mean bias error (MBE), the root mean square error (RMSE) and the index of agreement (d) are dimensionless.

Phenological stage	From BLO 2001				From Arnfield (1975)				From Nkemdirim (1972)							
	Equation	n	MBE	RMSE	d	Equation	n	MBE	RMSE	d	Equation	n	MBE	RMSE	d	
Pre-seeding	all		0.000	0.015	0.671											
	am	$\alpha = 0.1290e^{0.0044Z}$	39	0.001	0.017	0.671										
	pm	$\alpha = 0.1384e^{0.0032Z}$	39	-0.001	0.013	0.675										
Bare Soil	all		0.008	0.023	0.415			0.223	0.227	0.095			0.058	0.089	0.198	
	am	$\alpha = 0.1011e^{0.0015Z}$	42	0.009	0.021	0.432	$\alpha = 0.244e^{0.00526Z}$	153	0.214	0.215	0.094	$\alpha = 0.1247e^{-0.0003Z}$	153	0.015	0.021	0.409
	pm	$\alpha = 0.1017e^{0.0016Z}$	42	0.007	0.022	0.387	$\alpha = 0.212e^{0.00891Z}$	166	0.232	0.237	0.095	$\alpha = 0.0626e^{0.0216Z}$	166	0.096	0.122	0.178
Emergence	all		-0.006	0.017	0.370			0.213	0.217	0.100			0.046	0.080	0.210	
	am	$\alpha = 0.0964e^{0.0035Z}$	56	0.003	0.013	0.526	$\alpha = 0.244e^{0.00526Z}$	195	0.205	0.207	0.102	$\alpha = 0.1247e^{-0.0003Z}$	195	0.008	0.017	0.327
	pm	$\alpha = 0.1072e^{0.0006Z}$	56	-0.015	0.020	0.451	$\alpha = 0.212e^{0.00891Z}$	196	0.221	0.228	0.098	$\alpha = 0.0626e^{0.0216Z}$	196	0.085	0.112	0.203
Jointing	all		0.012	0.029	0.676			0.137	0.141	0.332			0.053	0.107	0.463	
	am	$\alpha = 0.1172e^{0.0062Z}$	112	0.013	0.027	0.649	$\alpha = 0.198e^{0.00804Z}$	388	0.140	0.145	0.417	$\alpha = 0.0842e^{0.0134Z}$	388	0.010	0.037	0.712
	pm	$\alpha = 0.1145e^{0.0074Z}$	109	0.011	0.030	0.705	$\alpha = 0.190e^{0.00887Z}$	377	0.133	0.138	0.359	$\alpha = 0.0559e^{0.0287Z}$	377	0.096	0.148	0.304
Heading	all		-0.003	0.025	0.782			0.121	0.125	0.361			0.044	0.111	0.440	
	am	$\alpha = 0.1165e^{0.0084Z}$	84	-0.002	0.024	0.787	$\alpha = 0.198e^{0.00804Z}$	307	0.120	0.123	0.364	$\alpha = 0.0842e^{0.0134Z}$	307	-0.010	0.029	0.839
	pm	$\alpha = 0.1227e^{0.0073Z}$	84	-0.004	0.025	0.777	$\alpha = 0.190e^{0.00887Z}$	306	0.122	0.126	0.357	$\alpha = 0.0559e^{0.0287Z}$	306	0.099	0.155	0.389
Soft Dough	all		0.009	0.020	0.804			0.129	0.130	0.361			0.051	0.101	0.511	
	am	$\alpha = 0.1061e^{0.0096Z}$	39	0.013	0.027	0.721	$\alpha = 0.198e^{0.00804Z}$	156	0.130	0.132	0.331	$\alpha = 0.0842e^{0.0134Z}$	156	-0.001	0.022	0.879
	pm	$\alpha = 0.1035e^{0.0102Z}$	39	0.005	0.009	0.976	$\alpha = 0.190e^{0.00887Z}$	156	0.127	0.129	0.387	$\alpha = 0.0559e^{0.0287Z}$	156	0.103	0.142	0.459
Ripe	all		-0.007	0.014	0.955			0.102	0.103	0.456			0.022	0.088	0.539	
	am	$\alpha = 0.1087e^{0.0117Z}$	48	-0.004	0.012	0.968	$\alpha = 0.198e^{0.00804Z}$	184	0.099	0.098	0.480	$\alpha = 0.0842e^{0.0134Z}$	184	-0.032	0.037	0.778
	pm	$\alpha = 0.1180e^{0.0097Z}$	48	-0.009	0.015	0.938	$\alpha = 0.190e^{0.00887Z}$	171	0.105	0.107	0.427	$\alpha = 0.0559e^{0.0287Z}$	171	0.081	0.121	0.501

Table 3.3c. A comparison of observed and predicted half-hour albedos employing exponential regression equations. For each phenological stage, forenoon (am) and afternoon (pm) exponential regression curves, for each transmissivity category,* were produced to estimate the albedo when $0^\circ \leq Z \leq 80^\circ$. The units of the mean bias error (MBE), the root mean square error (RMSE) and the index of agreement (d) are dimensionless.

Phenological stage	From BLO 2001						From Arnfield (1975)					
	Equation	n	MBE	RMSE	d	Equation	n	MBE	RMSE	d		
Pre-seeding	all [®]		-0.001	0.014	0.701							
	am I	$\alpha = 0.1524e^{-0.0003Z}$	2	0.000	0.000	0.999						
	am II	$\alpha = 0.1208e^{-0.0057Z}$	23	-0.007	0.010	0.880						
	am III	$\alpha = 0.1420e^{-0.0022Z}$	14	0.012	0.021	0.459						
	pm I	$\alpha = 0.2303e^{-0.0118Z}$	3	-0.005	0.008	0.014						
	pm II	$\alpha = 0.1293e^{-0.0054Z}$	7	-0.004	0.010	0.594						
	pm III	$\alpha = 0.1376e^{-0.0029Z}$	29	-0.005	0.015	0.576						
Bare Soil	all		0.009	0.020	0.540			0.223	0.227	0.179		
	am I	$\alpha = 0.1185e^{-0.0025Z}$	9	0.001	0.003	0.168	$\alpha = 0.2420e^{-0.00608Z}$	34	0.203	0.203	0.055	
	am II	$\alpha = 0.1000e^{-0.0018Z}$	18	-0.004	0.007	0.515	$\alpha = 0.2220e^{-0.00639Z}$	70	0.206	0.209	0.162	
	am III	$\alpha = 0.1008e^{-0.0017Z}$	15	0.031	0.005	0.423	$\alpha = 0.2580e^{-0.00631Z}$	44	0.257	0.260	0.112	
	pm I	$\alpha = 0.1100e^{-0.0013Z}$	9	0.004	0.005	0.483	$\alpha = 0.1900e^{-0.0111Z}$	21	0.176	0.178	0.031	
	pm II	$\alpha = 0.1007e^{-0.0029Z}$	14	-0.003	0.005	0.848	$\alpha = 0.2150e^{-0.00898Z}$	59	0.233	0.237	0.065	
	pm III	$\alpha = 0.0952e^{-0.0019Z}$	19	0.019	0.003	0.481	$\alpha = 0.2340e^{-0.0065Z}$	82	0.231	0.234	0.111	
Emergence	all		-0.004	0.011	0.788			0.215	0.221	0.061		
	am I							$\alpha = 0.2420e^{-0.00608Z}$	8	0.198	0.199	0.070
	am II	$\alpha = 0.0881e^{-0.0063Z}$	17	-0.005	0.010	0.873	$\alpha = 0.2220e^{-0.00639Z}$	76	0.184	0.185	0.135	
	am III	$\alpha = 0.0988e^{-0.0023Z}$	31	0.003	0.009	0.419	$\alpha = 0.2580e^{-0.00631Z}$	112	0.252	0.225	0.071	
	pm I							$\alpha = 0.1900e^{-0.0111Z}$	3	0.154	0.154	0.026
	pm II	$\alpha = 0.0888e^{-0.0059Z}$	38	-0.005	0.011	0.793	$\alpha = 0.2150e^{-0.00898Z}$	59	0.220	0.223	0.101	
	pm III	$\alpha = 0.0888e^{-0.0045Z}$	15	-0.012	0.015	0.674	$\alpha = 0.2340e^{-0.0065Z}$	128	0.213	0.216	0.077	
Jointing	all		0.009	0.022	0.831			0.132	0.315	0.894		
	am I	$\alpha = 0.1156e^{-0.009Z}$	6	0.021	0.022	0.244	$\alpha = 0.1810e^{-0.01013Z}$	33	0.104	0.105	0.236	
	am II	$\alpha = 0.0949e^{-0.0116Z}$	24	0.011	0.021	0.874	$\alpha = 0.2050e^{-0.00711Z}$	137	0.123	0.125	0.420	
	am III	$\alpha = 0.1276e^{-0.0034Z}$	81	0.008	0.089	0.511	$\alpha = 0.2140e^{-0.00586Z}$	218	0.141	0.145	0.238	

Table 3.3c. Continued

Jointing	pm I	$\alpha = 0.1145e^{0.0097Z}$	3	0.013	0.013	0.469	$\alpha = 0.1620e^{0.01195Z}$	28	0.085	0.086	0.230
	pm II	$\alpha = 0.0978e^{0.0116Z}$	45	0.003	0.017	0.941	$\alpha = 0.1980e^{0.00857Z}$	183	0.130	0.132	0.413
	pm III	$\alpha = 0.1289e^{0.0034Z}$	61	0.012	0.023	0.547	$\alpha = 0.2150e^{0.00596Z}$	166	0.141	0.145	0.253
Heading	all			-0.004	0.018	0.892			0.116	0.118	0.341
	am I	$\alpha = 0.1604e^{-0.0033Z} \dagger$	4	-0.007	0.008	0.448	$\alpha = 0.1810e^{0.01013Z}$	15	0.101	0.102	0.077
	am II	$\alpha = 0.0972e^{0.0122Z}$	30	-0.005	0.009	0.984	$\alpha = 0.2050e^{0.00711Z}$	133	0.111	0.111	0.429
	am III	$\alpha = 0.1491e^{0.0035Z}$	49	-0.002	0.022	0.531	$\alpha = 0.2140e^{0.00586Z}$	132	0.114	0.117	0.241
	pm I						$\alpha = 0.1620e^{0.01195Z}$	7	0.089	0.089	0.075
	pm II	$\alpha = 0.1011e^{0.0112Z}$	44	-0.004	0.012	0.970	$\alpha = 0.1980e^{0.00857Z}$	114	0.129	0.130	0.370
Soft Dough	pm III	$\alpha = 0.1496e^{0.0035Z}$	39	-0.003	0.022	0.554	$\alpha = 0.2150e^{0.00596Z}$	128	0.114	0.118	0.261
	all			0.009	0.014	0.938			0.125	0.126	0.365
	am I	$\alpha = 0.0992e^{0.0104Z} \dagger$	4	0.004	0.004	0.532	$\alpha = 0.1810e^{0.01013Z}$	8	0.118	0.118	0.065
	am II	$\alpha = 0.0939e^{0.0123Z} \ddagger$	17	0.004	0.010	0.978	$\alpha = 0.2050e^{0.00711Z}$	99	0.118	0.118	0.384
	am III	$\alpha = 0.1273e^{0.0059Z}$	18	0.019	0.026	0.295	$\alpha = 0.2140e^{0.00586Z}$	49	0.129	0.132	0.245
	pm I	$\alpha = 0.0975e^{0.0112Z}$	3	-0.040	0.040	0.095	$\alpha = 0.1620e^{0.01195Z}$	8	0.106	0.106	0.115
Ripe	pm II	$\alpha = 0.0949e^{0.0122Z}$	27	0.008	0.010	0.978	$\alpha = 0.1980e^{0.00857Z}$	97	0.132	0.133	0.367
	pm III	$\alpha = 0.1143e^{0.0079Z}$	9	0.004	0.006	0.984	$\alpha = 0.2150e^{0.00596Z}$	50	0.122	0.125	0.381
	all			-0.004	0.011	0.969			0.096	0.099	0.459
Ripe	am I						$\alpha = 0.1810e^{0.01013Z}$	8	0.096	0.097	0.188
	am II	$\alpha = 0.1003e^{0.0135Z}$	31	-0.001	0.006	0.990	$\alpha = 0.2050e^{0.00711Z}$	108	0.092	0.093	0.468
	am III	$\alpha = 0.1222e^{0.0096Z}$	11	-0.002	0.017	0.946	$\alpha = 0.2140e^{0.00586Z}$	44	0.083	0.087	0.514
Ripe	pm I						$\alpha = 0.1620e^{0.01195Z}$	8	0.090	0.090	0.104
	pm II	$\alpha = 0.1126e^{0.0108Z}$	27	-0.006	0.012	0.960	$\alpha = 0.1980e^{0.00857Z}$	95	0.110	0.111	0.411
	pm III	$\alpha = 0.1301e^{0.008Z}$	13	-0.009	0.013	0.890	$\alpha = 0.2150e^{0.00596Z}$	43	0.092	0.097	0.427

* Transmissivity (t) category I is 0.667 < t ≤ 1.0, category II is 0.333 < t ≤ 0.667 and category III is 0 < t ≤ 0.333

⊗ The combined results of the exponential regression equations for the phenological stage

† Due to a lack of data in this category, the equation was restricted to Z < 40°

‡ Due to a lack of data in this category, the equation was restricted to Z < 43°

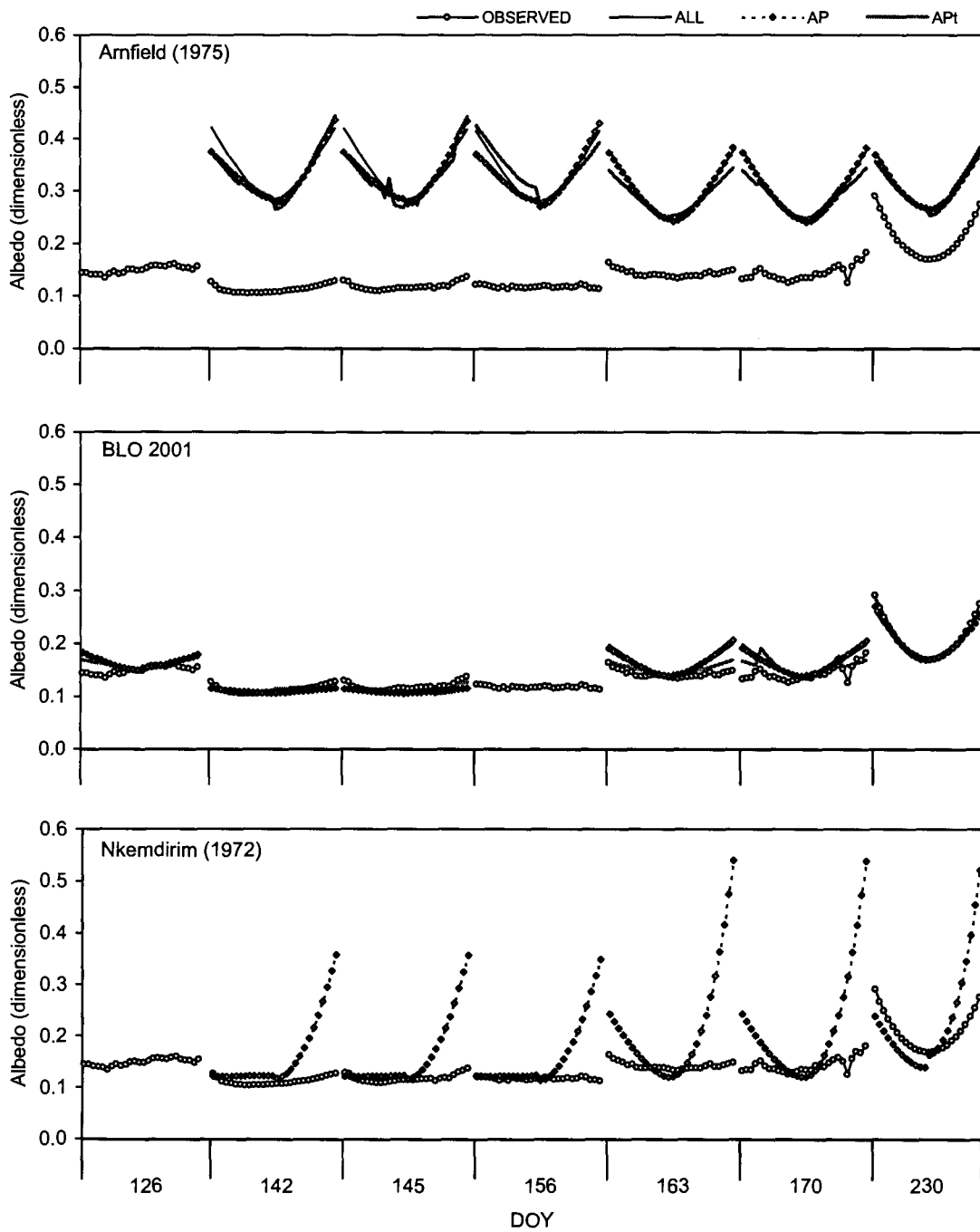


Figure 3.4. The time series of half-hour albedos on seven selected days. Data plotted are the exponential curves from Arnfield (1975), BLO 2001 and Nkemdirim (1972). Note: All refers to curves created from morning and afternoon albedos; AP refers to curves created for both the morning and afternoon; APt refers to curves created for both the morning and afternoon and for each transmissivity category (see page 52).

RMSE = 0.015 and $d = 0.355$). The equations performed unsatisfactorily because the cloudy days suppressed the zenith angle control. This resulted in the albedo being underestimated at the end of the day and overestimated on several cloudless days. Arnfield (1975) and BLO 2001's exponential regression equations also failed to mimic the asymmetry in the albedo (refer to DOY 142 in Figure 3.4). As expected, the asymmetry was not reproduced by Arnfield's (1975) equations because there was no early morning drying trend. The asymmetry was not reproduced by the BLO 2001 equations because both forenoon and afternoon albedos were used to create the equations, which masked the asymmetry.

Once vegetation dominated the surface, the overall performance of the exponential regression equations improved (Table 3.3a). Arnfield's (1975) regression equations for short grass were used to represent the albedo from joining to harvest. The equations overestimated the albedo as the short grass reflected more solar radiation than the wheat crop. On partly cloudy days, the amplitude of the regression curves were overestimated, but on cloudless days the amplitude of the regression curves were fairly good (Figure 3.4). The BLO 2001 regression equations fared better once the surface was vegetated, but the end of the day was still underestimated (Table 3.3.a and Figure 3.4). The BLO 2001 equations for the ripe stage performed the best, as there were few overcast days. When the surface was vegetated, asymmetric albedos were not reproduced by the regression equations estimated from Arnfield (1975) or BLO 2001.

It was hypothesised that an asymmetrical albedo could be reproduced by creating regression equations for the morning and afternoon. However, on all occasions, the asymmetry was inadequately reproduced (Figure 3.4). The asymmetry was incorrectly reproduced using equations from Arnfield (1975) and Nkemdirim (1972) because the cause of their asymmetry was different than that for the observed albedo at the BLO. They reported the asymmetry was from differences in sky conditions for bare

soil surfaces, and leaf wilting in the afternoon for vegetated surfaces (Arnfield, 1975; Nkemdirim, 1972). During the bare soil and emergence stages, the asymmetry was incorrectly reproduced using the BLO 2001 data because exponential functions do not produce minimum values just before the curve asymptotes. As a result, when the albedo was estimated from morning and afternoon regression equations, the difference measures illustrated no improvement when compared to the estimated albedo from a single regression equation (Table 3.3a and 3.3b).

The above results for BLO 2001 were slightly improved upon when curves were created for different cloud categories, because the estimated albedo increased when transmissivity increased (Table 3.3c). No real improvement occurred for Arnfield's (1975) estimated albedos because the albedo increased when transmissivity decreased.

3.4.3 The application of the albedo model in the Canadian Land Surface Scheme

The success of the albedo model in CLASS (α_{CLASS}) depended on the selected inputs and the phenological stage of the crop. However, two overall results were found. Figure 3.5 illustrates the relationship between the estimated and observed albedo using either estimated or observed diffused radiation. The larger scatter around the 1:1 line is all at larger zenith angles ($Z > 60^\circ$). The α_{CLASS} performed best at small zenith angles because the cosine response in α_{CLASS} did not perform well and, as a result, the albedo was underestimated at the end of the day. The other shortcoming was that when it rained, the albedo was overestimated either because of measurement errors or because α_{CLASS} could not accurately estimate the albedo when the transmissivity was low and the soil was wet. For example, in Figure 3.5, the group of outliers at $y = 0.116$ coincide with rain events during the emergence stage.

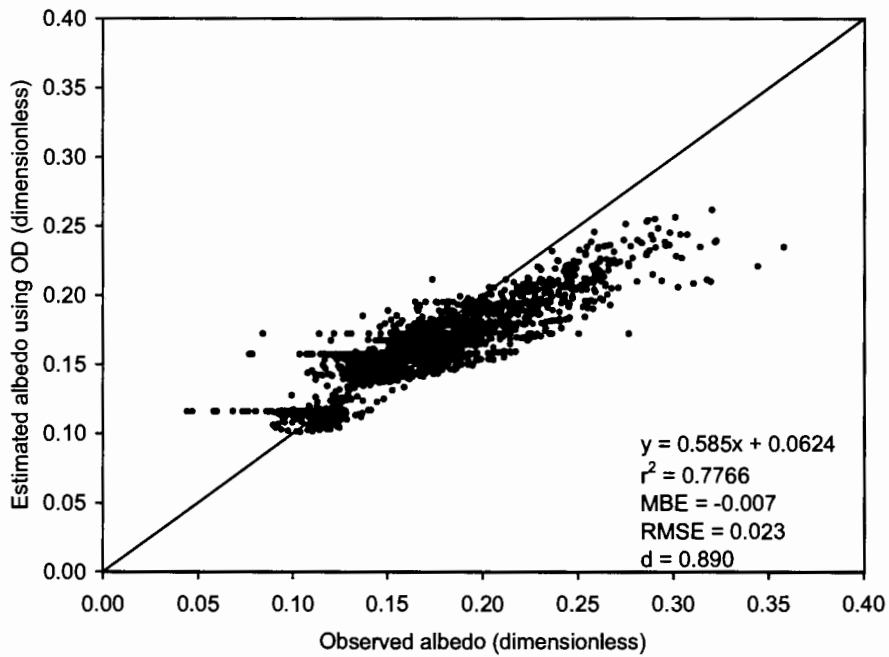
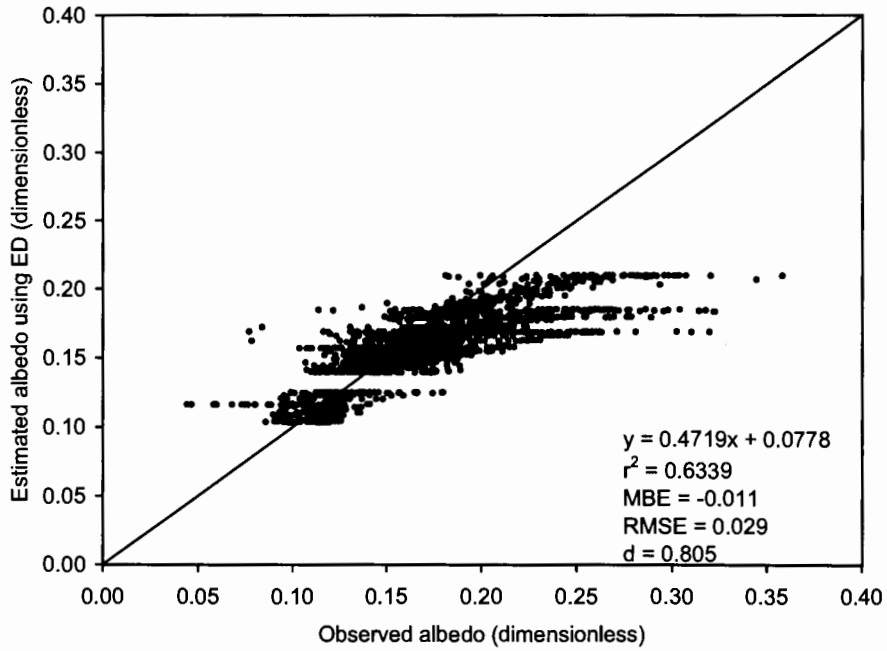


Figure 3.5. 1:1 plots of estimated (α_{CLASS}) and observed albedos. Estimated albedos were run using observed mean canopy albedos. In the upper plot, α_{CLASS} employed estimated diffuse radiation (ED), and the lower plot employed observed diffuse radiation (OD). The 1:1 line is denoted in each plot by a solid black line. The mean bias error (MBE), root mean square error (RMSE) and the index of agreement (d) are dimensionless.

Four runs were used to estimate the albedo during the bare soil and emergence stages. Runs A, B and C underestimated the albedo, while run D underestimated the albedo for 11 of the 22 days (Table 3.4). The estimated diurnal albedo trend was also very different than the observed diurnal albedo trend, as estimated albedos did not respond to atmospheric and surface controls (Figure 3.6). The estimated albedo in α_{CLASS} for bare soil was constant because it omits atmospheric controls, and a constant value for soil moisture was used. On cloudless and partly cloudy days, such as DOY 142 and 145, the observed cosine response was not simulated because the soil algorithms for α_{CLASS} did not include cosine responses for albedos when $Z \leq 80^\circ$ (Figure 3.6).

Run D performed better than runs A, B and C (Figure 3.6 and Table 3.4). The marginal success of run D is attributed to the modifications made to Verseghe's (1991) bare soil algorithm that caused run D to be more sensitive to changes in soil moisture. Run C performed better than runs A and B, but run C was expected to have the poorest performance because the limiting wet and dry soil albedos had a larger range than for a dark brown chernozemic soil (Wilson and Henderson-Sellers, 1985). Overall, run B had the weakest performance because the maximum and minimum observed albedos did not have a large enough range for the limiting dry and wet soil albedos. The accuracy of runs A, B and C suggest that the larger the range of the limiting wet and dry soil albedo, the greater its success.

When α_{CLASS} for vegetated surfaces was applied during the emergence stage, the accuracy and precision of the model measurably improved (Table 3.4). This improvement in α_{CLASS} for vegetated surfaces arose from the control for zenith angle and transmissivity. However, the accuracy of the model was limited during the emergence stage, as the estimated albedo did not reproduce asymmetric albedo trends

Table 3.4. Comparison of observed (south field) and predicted (α_{CLASS}) half-hour albedos and the difference between observed ($K\uparrow_o$) and predicted reflected solar radiation ($K\uparrow_p$). The predicted and observed albedos are compared by the mean bias error (MBE), root mean square error (RMSE) and the index of agreement (d) and units are dimensionless. The difference between the $K\uparrow_o$ and $K\uparrow_p$ for each phenological stage is expressed as a sum of the daily differences (in $MJ\ m^{-2}$) divided by the sample size (n) in days and as a maximum, minimum, mean and standard deviation (in $W\ m^{-2}$).

Phenological stage	Run*	Albedo			Reflected solar radiation				
		MBE	RMSE	d	Sum/n	Max	Min	Mean	σ
Bare Soil	A	-0.083	0.087	0.079	4.195	100.4	2.4	43.3	26.5
	B	-0.092	0.102	0.051	5.664	121.3	2.9	58.5	30.2
	C	-0.074	0.076	0.123	4.242	80.2	2.0	38.2	21.2
	D	-0.003	0.021	0.616	0.204	29.2	-23.3	-2.1	11.2
Emergence	A	-0.075	0.080	0.171	3.974	96.1	0.4	31.1	22.5
	B	-0.075	0.091	0.112	6.133	114.9	0.7	48.6	29.5
	C	-0.077	0.080	0.226	4.057	87.9	0.1	31.7	20.1
	D	-0.017	0.034	0.379	0.976	44.4	-15.3	7.6	12.7
	ED	-0.003	0.016	0.452	0.313	17.1	-14.6	2.5	5.1
	OD	0.000	0.014	0.662	0.185	17.0	-14.5	1.4	5.0
	Oke ED	0.060	0.062	0.276	-2.952	-1.9	-62.6	-23.1	13.4
	Oke OD	0.064	0.066	0.293	-3.150	-1.8	-60.9	-24.6	13.3
	lqbal ED	-0.018	0.024	0.410	1.129	28.7	-4.1	8.8	7.5
lqbal OD	-0.016	0.021	0.514	1.019	28.6	-4.1	8.0	7.5	
Jointing	ED	-0.010	0.032	0.479	0.414	28.0	-29.1	4.1	10.2
	OD	-0.006	0.028	0.667	0.719	28.9	-30.7	2.9	10.5
	Oke ED	0.013	0.033	0.560	-0.587	22.3	-48.0	-5.7	11.5
	Oke OD	0.017	0.027	0.777	-0.725	21.2	-49.2	-7.1	11.5
	lqbal ED	-0.065	0.072	0.410	2.892	65.8	-0.83	28.3	17.9
	lqbal OD	-0.062	0.069	0.427	2.815	66.9	-0.71	27.6	17.9
Heading	ED	-0.015	0.030	0.556	0.386	19.9	-16.9	3.7	6.9
	OD	-0.011	0.022	0.813	0.280	19.7	-22.7	2.7	6.3
	Oke ED	-0.007	0.027	0.605	0.045	16.3	-23.0	0.4	7.7
	Oke OD	-0.003	0.019	0.852	-0.065	15.7	-29.9	-0.6	7.0
	lqbal ED	-0.056	0.062	0.440	2.178	42.1	-0.7	20.7	10.9
	lqbal OD	-0.053	0.057	0.482	2.092	43.5	-0.5	20.0	11.1
Soft Dough	ED	-0.014	0.029	0.588	0.383	18.4	-13.8	3.7	7.1
	OD	-0.010	0.021	0.838	0.333	18.3	-11.1	3.3	6.1
	Oke ED	-0.001	0.025	0.663	-0.215	13.0	-24.0	-2.1	8.8
	Oke OD	-0.003	0.017	0.886	-0.267	12.2	-21.0	-2.6	7.3
	lqbal ED	-0.011	0.028	0.607	0.245	17.0	-16.2	2.4	7.4
	lqbal OD	-0.007	0.019	0.858	0.195	16.8	-13.4	1.9	6.3
Ripe	ED	-0.015	0.034	0.569	0.318	33.8	-31.8	3.7	9.4
	OD	-0.011	0.028	0.772	0.365	30.4	-30.4	3.3	8.2
	Oke ED	-0.030	0.043	0.558	0.985	37.7	-22.5	10.8	8.3
	Oke OD	-0.026	0.037	0.666	0.877	34.6	-21.3	10.4	7.8
	lqbal ED	0.000	0.030	0.624	-0.348	29.8	-41.1	-3.5	11.3
	lqbal OD	0.004	0.025	0.826	-0.357	26.3	-39.6	-3.9	9.6

*Summary of runs:

Bare soil surface:

A - run using limiting wet and dry soil albedos from Wilson and Henderson-Sellers (1985)

B - run using limiting wet and dry soil albedos from the maximum and minimum volumetric soil moisture measurement

C - run using minimum limiting wet and maximum limiting dry soil albedos from Wilson and Henderson-Sellers (1985)

D - run using a modified version from Mailhot *et al.* (1998)

Crop surface:

ED - run using a mean canopy albedo created from observed fluxes and estimated diffuse solar radiation

OD - run using a mean canopy albedo created from observed fluxes and observed diffuse solar radiation

Oke ED - run using a mean canopy albedo from Oke (1987) and estimated diffuse solar radiation

Oke OD - run using a mean canopy albedo from Oke (1987) and observed diffuse solar radiation

lqbal ED - run using a mean canopy albedo from lqbal (1983) and estimated diffuse solar radiation

lqbal OD - run using a mean canopy albedo from lqbal (1983) and observed diffuse solar radiation

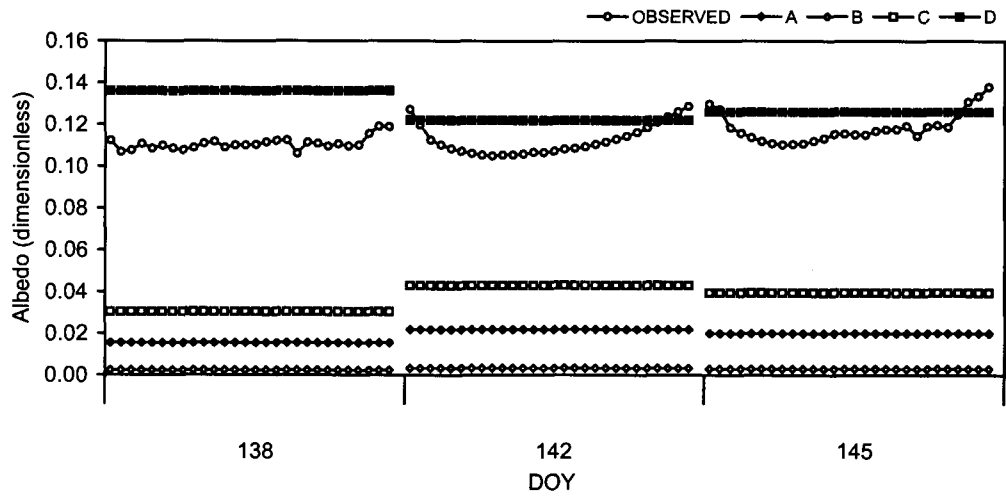


Figure 3.6 The observed and estimated albedos (A through D) on four selected days representing overcast (DOY 138), partly cloudy (DOY 142) and cloudless (DOY 145) sky conditions.

because the model includes a constant surface control (which is the mean canopy albedo).

The albedo for wheat was modelled by using both estimated and observed diffuse radiation. As expected, α_{CLASS} performed better when observed diffuse radiation was used (Figure 3.5). For example, the end of day ($\cos(Z) < 0.5$) albedo was largely underestimated when estimated diffuse radiation was used instead of observed diffuse radiation (Appendix G). Also, when estimated diffuse radiation was used in α_{CLASS} , the albedo did not respond well to changes in transmissivity (Appendix G). The α_{CLASS} did not represent the end of day and transmissivity well because estimated diffuse radiation was conservative, and tended to underestimate diffuse radiation. As a result, when observed diffuse radiation was used, α_{CLASS} responded better to changes in transmissivity over the day.

In general, when observed diffuse radiation and the observed mean canopy albedo were used, the performance of α_{CLASS} was enhanced (Table 3.4 and Figure 3.7). This is because both the albedo and α_{CLASS} are sensitive to transmissivity or the amount of direct and diffuse radiation. Hence, with more accurate diffuse and direct beam radiation inputs, the better the performance of α_{CLASS} . The difference between estimated and observed albedo was most apparent on cloudless days, as α_{CLASS} underestimated the cosine response. Overall, cloudless days had the poorest performance.

For overcast conditions, such as DOY 193, the estimated albedo was near observed values (Figure 3.7). However, when estimated diffuse radiation was used, a cosine response was present when there was none; this occurred because diffuse radiation was underestimated, and the cloud function determined that the day was partly cloudy rather than overcast.

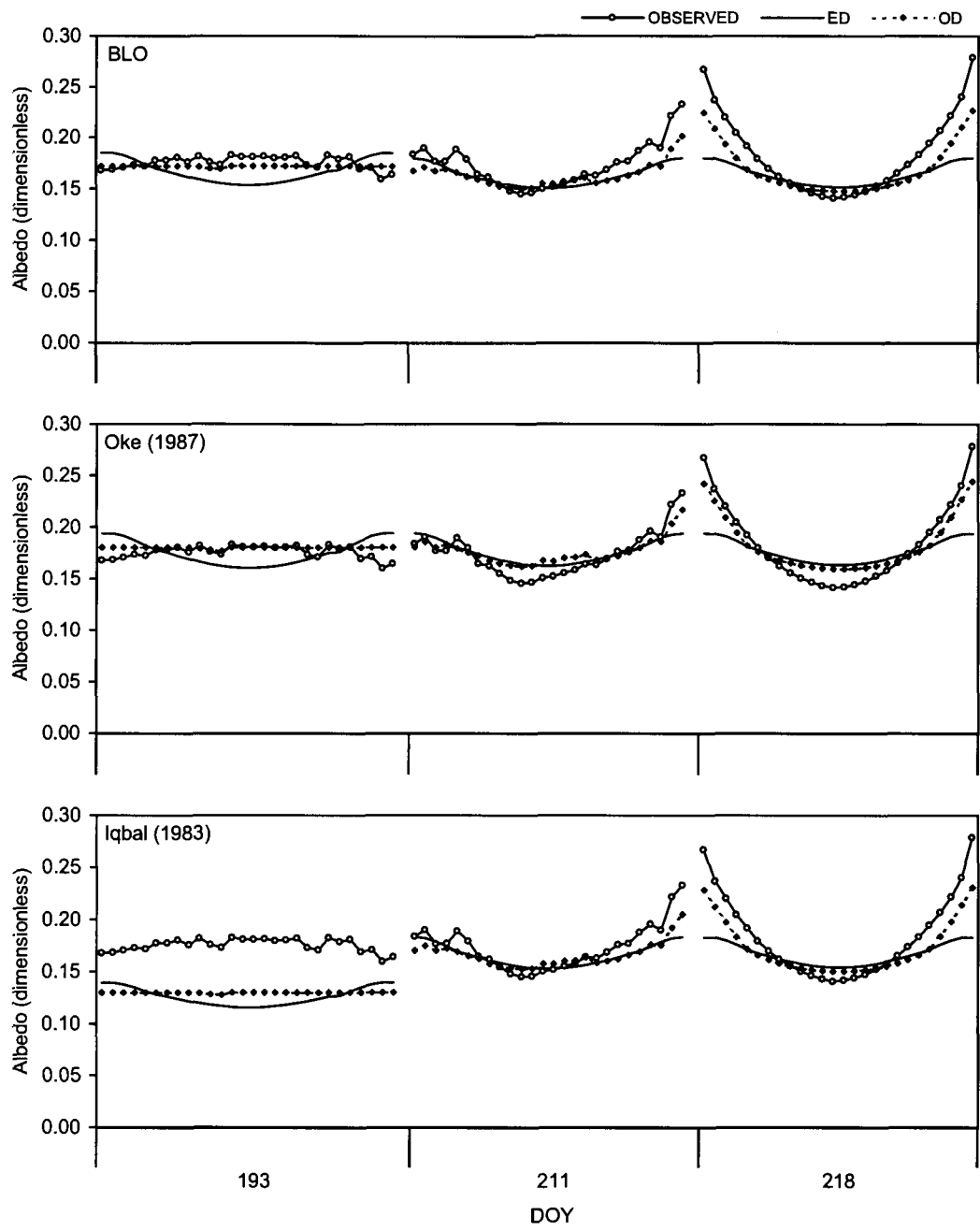


Figure 3.7. The observed and estimated crop surface albedos on three selected days representing overcast (DOY 193), partly cloudy (DOY 211) and cloudless (DOY 218) sky conditions. The albedo was determined using three mean canopy albedos: observed (BLO), a constant value from Oke (1987) and several values from Iqbal (1983). ED is estimated diffuse radiation OD and is observed diffuse radiation.

Partly cloudy days were most accurately estimated by α_{CLASS} for two reasons (Figure 3.7). First, on partly cloudy days, the diurnal amplitude of the albedo curve is less than cloudless days because more radiation is diffuse. Thus, any error arising from the cosine response is dampened. Second, partly cloudy days tend to mask errors in α_{CLASS} that arise from changes in the surface condition, because the diurnal variation of the albedo on these days is dominated by transmissivity.

The mean canopy albedo was determined from observed fluxes (the BLO mean canopy albedo), from Oke (1987) and from Iqbal (1983), and this greatly influenced the success of α_{CLASS} (Table 3.4). As hypothesised, the BLO mean canopy albedo generally produced the most accurate albedo. This run was most accurate because a mean canopy albedo was applied to each phenological stage. However, the albedo was generally underestimated (Table 3.4). When a constant mean canopy albedo was used from emergence to harvest, α_{CLASS} could not respond to changes in the surface over the season. As a result, α_{CLASS} could not accurately estimate half-hourly albedos for stages other than heading and soft dough when the mean canopy albedo was close to 0.18. During the emergence and jointing stages, the albedo was overestimated because the mean canopy albedo was lower than 0.18. During the ripe stage, the mean canopy albedo was underestimated because the albedo was greater than 0.18. Throughout the ripe stage, the constant mean canopy albedo performed better than the BLO mean canopy albedo because a few of the days had a low transmissivity, and this decreased the BLO mean canopy albedo. Hence, the accuracy of α_{CLASS} was reduced when the BLO mean canopy albedo was used during the ripe stage. The mean canopy albedos from Iqbal (1983) did not perform better than the constant albedo value (even though the wheat crop was divided into initial growth, milky light green, yellow ripeness and full ripeness stages) because they differed from the actual mean canopy albedos. As a

result, the albedo was generally underestimated. However, Iqbal's (1983) mean canopy albedo performed well during soft dough stage because the mean canopy albedo of 0.170 was close to the observed mean canopy albedo of 0.167.

As the crop matured during the jointing, soft dough and ripe stages, the accuracy of α_{CLASS} decreased because the estimated albedo did not respond to the changing surface condition (Table 3.4). During the jointing stage, the albedo increased as the canopy matured. When α_{CLASS} was run using the BLO mean canopy albedo, the estimated albedo was only accurate at the mid-point of the jointing stage. As a result, when the BLO mean canopy albedo was used, the accuracy of the estimated albedo decreased before and after DOY 168 - 177, where both the RMSE (0.015 - 0.046) and the d (0.214 - 0.874) often performed weakly. However, the estimated albedo improved from DOY 168 - 177, where the RMSE was between 0.013 and 0.022 and the d was between 0.650 and 0.895. For the soft dough stage, the albedo decreased until DOY 213 and then increased (Figure 2.7). As a result, the accuracy of α_{CLASS} was lower at the beginning and end of the stage. Finally, during the ripe stage, the albedo increased and the estimated albedo was most accurate at the mid-point of this stage.

3.5 Conclusions

This chapter has demonstrated that the diurnal albedo is dependent on atmospheric controls (such as zenith angle and transmissivity) and surface controls (such as soil moisture). As only a handful of published studies have examined the asymmetry of diurnal albedos (Grant *et al.*, 2000; Minnis *et al.*, 1997; Nkemdirim, 1972; Song, 1998), this chapter has provided a more comprehensive examination of the symmetry of the albedo throughout the day. It also examined the application of exponential regression equations to estimate half-hourly albedos. Finally, the

performance of α_{CLASS} for bare soil and crop surfaces was compared to observed albedos throughout a growing season.

A number of studies have only examined the albedo on cloudless days, which are usually symmetrical around solar noon. However, most days are partly cloudy in character. This research has extended the finding of many studies found in the literature because it has characterized the symmetry of the albedo for various atmospheric conditions. The diurnal symmetry in the albedo was sensitive to changes in transmissivity and surface condition. From the pre-seeding stage to the end of the emergence stage, the albedo was primarily controlled by the zenith angle, transmissivity and soil moisture. When the surface was vegetated, the albedo was primarily controlled by the zenith angle and transmissivity. In terms of atmospheric controls, the albedo was symmetrical for cloudless, near cloudless days, overcast and nearly overcast days. Conversely, the albedo was asymmetrical for partly cloudy days. During bare soil conditions, the diurnal asymmetry of the albedo was controlled by changes in surface soil moisture where the forenoon albedo was lower than the afternoon albedo because the surface was moist from dew in the morning. This has also been observed by other authors (Grant *et al.*, 2000; Song, 1998).

Arnfield (1975) and Nkemdirim (1972) accurately estimated half-hourly albedos using exponential regression equations. Unfortunately, when exponential regression equations were employed in this study, a number of limitations were discovered. When exponential regression equations were produced from 70 percent of the observed data and applied to the remaining data, the regression curves did not accurately reproduce diurnal albedo trends. Arnfield (1975) and Nkemdirim's (1972) regression equations were expected to perform poorly because they were created from different surface types. Their equations grossly overestimated the albedo and inaccurately simulated the

albedo's asymmetry. In light of the above, the use of regression analysis for half-hourly albedos should be cautiously employed. Exponential regression equations should only be created from cloudless data with a constant surface condition. The equations can then be employed to estimate half-hour albedo for cloudless skies with the same surface type and condition as the original dataset.

The BLO 2001 exponential regression equations performed better than α_{CLASS} . The performance of α_{CLASS} was dependent on surface type (i.e. bare soil or wheat crop) and the phenological stage of the wheat crop. For example, α_{CLASS} for bare soils did not accurately estimate the albedo. Three shortcomings of the experiment and α_{CLASS} for bare soils were identified. Firstly, volumetric soil moisture was measured once a day and, as a result, the estimated albedo was constant throughout the day. Although this is not a deficiency in α_{CLASS} , this issue is difficult to overcome since surface soil moisture sampling would need to be conducted on a half-hourly basis and most surface climate studies do not have the labour or resources to undertake such an intense sampling scheme. Second, the observed bare soil albedo showed a cosine response, but the estimated albedo was constant over the day because α_{CLASS} does not contain a zenith angle control. Third, estimated bare soil albedos were erroneous. Mailhot *et al.* (1998) improved α_{CLASS} for bare soil surfaces, but the results were still limited as the albedo was constant over the day.

When the surface was vegetated, the performance of α_{CLASS} improved. The estimated albedo performed well when $\cos(Z) < 0.5$, but when $\cos(Z) \geq 0.5$ the albedo was underestimated. The results of α_{CLASS} also markedly improved when measured direct beam and diffuse radiation were used instead of estimated fluxes. For the growing season, the accuracy of estimated reflected solar radiation increased between

0.0002 and 0.47 MJ m⁻² d⁻¹ with an average of 0.13 MJ m⁻² d⁻¹. This result is an average 79.6 percent improvement. Estimated diffuse radiation had a very low correlation with observed diffuse radiation. As a result, when estimated diffuse radiation was used in α_{CLASS} , the estimated albedo did not change in accordance with transmissivity and, on occasion, the cloud function inaccurately determined the sky condition.

The cloud function in α_{CLASS} always categorised cloudless conditions as partly cloudy because the cloud function assumes that no diffuse solar radiation occurs during cloudless conditions. However, during cloudless days, approximately 9 percent of global solar radiation was diffuse. Nonetheless, when cloudless days were categorised as partly cloudy, the accuracy and precision of the estimated albedo was not compromised since α_{CLASS} for partly cloudy conditions includes direct beam and diffuse solar radiation.

The accuracy of the estimated albedo was also related to the mean canopy albedo. When a mean canopy albedo was created for each phenological stage, the albedo was estimated well. However, α_{CLASS} failed to represent the growth aspect of the crop during the jointing stage and the loss of plant internal water content and chlorophyll during the ripe stage because the mean canopy albedo was constant. The success of α_{CLASS} decreased further when only a single mean canopy albedo was applied throughout the growing season as the estimated albedo failed to represent the maturing crop.

The difference between using a mean canopy albedo for each phenological stage and a single mean canopy albedo throughout the season is substantial, where the sum of the daily differences for reflected solar radiation is -61 MJ m⁻² or a difference of 34 percent. The runs using a mean canopy albedo from observed fluxes, Oke (1987) and Iqbal (1983) suggest that a single mean canopy albedo cannot be used in α_{CLASS}

throughout a growing season. At the very least, a mean canopy albedo for each phenological stage should be employed when considering the albedo over a growing season.

The results contained in this chapter demonstrate that the diurnal albedo is sensitive to the zenith angle, atmospheric transmissivity, and surface type and condition. The albedo will only be symmetrical around solar noon when both the sky and surface conditions are constant. When estimating the albedo of a bare soil, the zenith angle, transmissivity and surface soil moisture should be considered, and when estimating the albedo of a crop, the zenith angle, transmissivity and phenological stage of the crop should be considered. Regression analysis cannot include all of these factors unless equations are produced for all sky and surface conditions. Regression analysis is also restrictive because it is specific to the site and conditions. Conversely, albedo models, such as α_{CLASS} that are functions of both atmospheric and surface controls can be used in a variety of locations and can be more readily modified to improve performance.

CHAPTER 4

CONCLUSIONS

The diurnal and seasonal progression of the albedo for a wheat crop was documented. Research was conducted at the Meteorological Service of Canada's Bratt's Lake Observatory, located in southern Saskatchewan. One minute averages of global and reflected solar radiation were observed throughout the growing season and compiled into half-hourly and daily albedos. Unlike most albedo studies found in the literature, half-hour albedos for all observed atmospheric conditions were analysed and described. This allowed for a detailed description of the albedo and its controls.

One of the primary objectives of this thesis was to investigate atmospheric and surface controls on half-hour and daily albedos throughout the growing season by comparing and correlating the albedo to atmospheric and surface controls. The daily albedo was virtually unaffected by changes in transmissivity from one day to the next, but half-hourly albedos were greatly affected. Numerous authors (e.g. Ahmad and Lockwood, 1979; Nkemdirim, 1972) have reported that the albedo will decrease with decreasing transmissivity, and this study found a direct relationship between half-hourly albedos and transmissivity.

The albedo was compared to the surface condition throughout the growing season, which included the organic litter layer at pre-seeding and the five phenological stages of the wheat crop. During the pre-seeding stage, the albedo was influenced by the amount of organic litter layer on the surface. Following cultivation, the albedo decreased by approximately 9.0 and 6.6 percent in the north and south fields respectively. Throughout the pre-seeding, bare soil and emergence stages, the albedo was primarily controlled by the amount of surface soil moisture. Approximately 10 days after plant emergence (plant extended height of 0.12 m), biomass increased

dramatically, and the plants became the prevalent control on albedo. The albedo reached a plateau at approximately 0.17, and was related to the peak in plant height and the emergence of the wheat heads (DOY 189). The wheat began to senesce during the week of DOY 213. Consequently, the albedo began to increase and, by harvest, the albedo was 0.22. The above albedo trends confirm observations presented in other studies (Ahmad and Lockwood, 1979; Al-Yemeni and Grace, 1995; Song, 1999; Walter-Shea *et al.*, 1992).

Daily and diurnal albedo trends were correlated to daily volumetric soil moisture, plant height, plant weights and leaf area index (LAI) measurements. The albedo trends during the season were also related to visual observations of the surface, to each surface type and to the five phenological stages of wheat. The division of the season into seven stages enhanced the description of the surface because, for each phenological stage, a numerical summary of the dominant albedo control could be assessed. However, the soft dough stage could not be readily summarized by a single numerical expression because the first half of this stage was controlled by a decline in LAI, and the second half was controlled by the dry to fresh weight plant ratio.

Daily and half-hourly albedos for the north and south fields were compared and contrasted. For the most part, it was observed that the trends in the albedos were identical, but the absolute albedo values were not identical. During the pre-seeding stage, the albedo was different because the amount and type of organic litter on the surface was dissimilar. During the bare soil stage, the albedo was different because the organic matter content of the soils was probably different. Throughout the jointing stage, the albedo in the north field was lower than the south field because the plant development in the north field lagged behind the south field. Once the heads emerged, the albedos of the two fields were similar.

Increasingly, diurnal albedo trends are being examined. A few studies have recently compared forenoon and afternoon albedos, but they do not include all sky conditions (Grant *et al.*, 2000; Minnis *et al.*, 1997; Song, 1998). An objective of this thesis was to document and explain the diurnal symmetry and asymmetry of the albedo from pre-seeding to harvest for all sky conditions. This objective was met by examining the diurnal trends as the percent difference between forenoon and afternoon albedos at the same zenith angle. Throughout the growing season, the albedo was symmetrical around solar noon when the sky and surface conditions remained nearly constant over the day. The diurnal albedo was primarily asymmetrical because atmospheric transmissivity fluctuated during the day. There is very little in the literature that characterizes the albedo during partly cloudy conditions, even though many days at many locations are partly cloudy. This study has gone beyond most other studies as it characterized the asymmetry of the albedo on partly cloudy days. From pre-seeding to the end of the emergence stage (DOY 120 to 160), the albedo was also asymmetrical, where the forenoon albedo was lower than the afternoon albedo. The primary cause is suggested to be the observed surface moistening from dew.

Once the daily and half-hourly albedos were described, regression analysis was used to estimate diurnal albedo trends. It was expected that exponential regression equations would adequately reproduce the range of diurnal albedo trends observed throughout the season. However, the regression equations produced from the observed data often overestimated the albedo towards the end of the day. Further, when the albedo was asymmetrical, the exponential regression equations could not correctly reproduce the asymmetry in the albedo.

The final objective of this thesis was to assess the performance of the albedo model in the Canadian Land Surface Scheme (α_{CLASS}) for bare soil and crop surfaces.

This objective was met by producing several runs of α_{CLASS} . Four runs were produced for the bare soil algorithms. In all four runs, the α_{CLASS} did not successfully estimate the amplitude and magnitude of the albedo because a constant soil moisture value for each day was used and the α_{CLASS} for bare soil excludes a cosine response. The α_{CLASS} for vegetated surfaces yielded better albedo estimates. The estimated albedo was most accurate at lower zenith angles on cloudless and partly cloudy days, and its accuracy remained constant on overcast days. The best results were obtained on overcast and partly cloudy days because α_{CLASS} underestimated the cosine response when $\cos(Z) < 0.5$. The diffuse function in α_{CLASS} also had a very low correlation with observed diffuse radiation. As a result, the estimated albedo inaccurately responded to changes in transmissivity, and on occasion, the cloud function inaccurately determined the sky condition.

The application of CLASS requires mean canopy albedos and these were determined from Iqbal (1983), Oke (1987) and the observed fluxes. The modelling results showed that a single mean canopy albedo is insufficient to predict the albedo throughout the growing season because the albedo responds to changes in canopy cover and crop structure. Therefore, a mean canopy albedo for each phenological stage should be employed when considering the albedo throughout a growing season. In the case of a wheat crop, it would be more appropriate to alter the mean canopy albedo during the jointing stage when the albedo increases as crop height increases and during senescence when the albedo decreases as plant water content decreases. In this study, the mean canopy albedos during these stages could be produced from equation 2.7 for the jointing stage and equation 2.10 for senescence.

Although this thesis met all of its objectives, a number of improvements can be suggested. A more thorough analysis during the pre-seeding, bare soil and emergence

stages could have been achieved if surface soil moisture was measured more than once a day as diurnal changes in the albedo could have been directly related to surface soil moisture. Also, plant turgidity is known to affect the albedo (Al-Yemeni and Grace, 1995; Jacobs and Van Pul, 1990; Song, 1999). If leaf water potentials were measured throughout the growing season, improved insight into how the albedo responds to plant water stress could have been made. For example, the crop was visibly water stressed during parts of the growing season, and this potentially affected the albedo. However, plant water content was not measured; hence, no relationship could be established.

There is still a paucity of information on how the albedo changes over a day and throughout a growing season. In the last few years, several researchers have been exploring the symmetry or asymmetry of diurnal albedos (Al-Yemeni and Grace, 1995; Arnfield, 1975; Grant *et al.*, 2000; Minnis *et al.*, 1997; Nkemdirim, 1972; Song, 1998), and more studies are needed to confirm the findings in these studies. Research on the seasonal variation of the albedo is primarily on crops. The seasonal and annual variation of the albedo needs to be examined over many different types of surfaces. Such efforts would provide a better understanding of regional climates, would serve to confirm satellite measurements, and would improve climate modelling over a range of spatial and temporal scales.

Appendices

APPENDIX A

LIST OF SYMBOLS AND UNITS

Roman upper case

D	Diffuse radiation (W m^{-2})
DOY	Day of year (1 to 365)
ED	Estimated diffuse solar radiation (W m^{-2})
ES	Estimated direct beam solar radiation (W m^{-2})
F	Flux density (W m^{-2})
FCloud	Cloud function (dimensionless)
I_0	Solar constant (1366.1 W m^{-2}); source: ASTM E490
$K \downarrow$	Global solar radiation (W m^{-2})
$K \uparrow$	Reflected solar radiation (W m^{-2})
$K \uparrow_0$	Observed reflected solar radiation (W m^{-2})
$K \uparrow_p$	Predicted reflected solar radiation (W m^{-2})
K_{ex}	Extraterrestrial solar radiation (W m^{-2})
K_{vis}	Estimated visible solar radiation (W m^{-2})
K_{NIR}	Estimated near infrared solar radiation (W m^{-2})
LA	Leaf area (m^2)
LAI	Leaf area index (dimensionless)
LAT	Local apparent time (hours)
MBE	Mean bias error
S	Direct beam irradiance (W m^{-2})
RMSE	Root mean square error
RV	Radius vector (degrees)
Z	Zenith angle (degrees)

Roman lower case

b	Regression coefficient that describes the rate of change in the albedo with respect to the zenith angle (degrees ⁻¹)
c	calibration constant of a sensor
d	Index of agreement
dw	Dry weight of the plant sample (kg m ⁻²)
dfw	Dry to fresh weight ratio (dimensionless)
e	Vapour pressure (hPa)
e _s (T)	Saturation vapour pressure (hPa)
h	Solar hour angle (degrees); Plant height (m)
ldw	Leaf dry weight of a sample (kg m ⁻²)
m	Electromotive output from a record apparatus
max	Maximum value in a sample
min	Minimum value in a sample
n	Sample size
r	Pearson product-moment coefficient of correlation
t	Transmissivity (dimensionless)
vpd	Vapour pressure deficit (hPa)
xdiffuse	Factor to estimate diffuse solar radiation

Greek

α	Albedo (dimensionless)
α_0	Regression coefficient - an estimate of the albedo at $Z = 0^\circ$ (dimensionless)
α_{AM}	Forenoon albedo (dimensionless)
α_b	Bare soil albedo (dimensionless)

$\bar{\alpha}_b$	Average albedo for the bare soil stage (dimensionless)
$\bar{\alpha}_c$	Mean canopy albedo (dimensionless)
α_{cc}	Albedo during cloudless conditions (dimensionless)
α_{CLASS}	The albedo model employed in the Canadian Land Surface Scheme
α_{oc}	Albedo during overcast conditions (dimensionless)
α_{diff}	The percent difference between the albedos of the north and south fields (dimensionless)
α_{dry}	Limiting dry soil albedo (dimensionless)
$\bar{\alpha}_e$	Average albedo for the emergence stage (dimensionless)
$\bar{\alpha}_{hs}$	Average albedo from DOY 189 to 215 (dimensionless)
α_{jN}	Daily albedo during the jointing stage in the north field (dimensionless)
α_{jS}	Daily albedo during the jointing stage in the south field (dimensionless)
α_N	North field albedo (dimensionless)
α_{pc}	Albedo during partly cloudy conditions (dimensionless)
α_{PM}	Afternoon albedo (dimensionless)
$\bar{\alpha}_p$	Average albedo for the pre-seeding stage (dimensionless)
α_S	South field albedo (dimensionless)
α_{sat}	Limiting wet soil albedo (dimensionless)
α_{sN}	Daily albedo of a senesced wheat crop in the north field (DOY 216 to 236) (dimensionless)
α_{sS}	Daily albedo of a senesced wheat crop in the south field (DOY 216 to 236) (dimensionless)
$\Delta\alpha$	The difference between estimated and observed albedos (dimensionless)

$\Delta\bar{\alpha}_{PS}$	The difference between two mean albedos at different phenological stages (dimensionless)
$\Delta\alpha_z$	Percent difference between the morning and afternoon albedo at a particular zenith angle (dimensionless)
δ	Solar declination (degrees)
$\delta\alpha_{rms}$	Probable absolute error in the albedo
δF_{rms}	Probable absolute error in the flux density
δY_{rms}	Probable absolute error
ϕ	Latitude (degrees)
θ	Volumetric soil moisture ($\text{mm}^3 \text{H}_2\text{O}/\text{mm}^3 \text{soil}$)
σ	Standard deviation

APPENDIX B

MISSING DATA

Table B.1 Missing data from the Kipp and Zonen CM21 pyranometer measuring global solar radiation at the meteorological compound, and from the inverted Kipp and Zonen CM21 and CM11 pyranometers measuring reflected solar radiation over the north and south fields respectively.

DATE AND TIME (CST)	INSTRUMENT AND LOCATION	REASON AND ACTION
April 30 (12:00 to 15:00)	CM21 pyranometer at the meteorological compound	Instrument failed; used CM21 pyranometer located at the tower
May 1	CM21 pyranometer at the meteorological compound	Instrument failed; used CM21 pyranometer located at the tower
May 3 (9:00 to 13:00)	Inverted CM21 and CM11 pyranometers, north and south fields	Human error - data erased
May 5 (12:00) to May 8 (8:00)	Inverted CM21 pyranometer, north field	Inverted pyranometer stand fell due to high winds
May 12 to 14	Inverted CM21 and CM11 pyranometers, north and south fields	Fields seeded and harrowed
June 15 (12:00 to 14:00)	Inverted CM21 and CM11 pyranometers, north and south fields	Fields were treated with a herbicide and the pyranometers were shielded from the chemicals being sprayed
June 16	CM21 pyranometer at the meteorological compound	Instrument failed; used CM21 pyranometer located at the tower
June 26 (17:00 to 21:57)	CM21 pyranometer at the meteorological compound	Instrument failed; used CM21 pyranometer located at the tower
June 28 (20:00 to 21:33)	CM21 pyranometer at the meteorological compound	Instrument failed; used CM21 pyranometer located at the tower

APPENDIX C

DOMINANT WEED SPECIES

Table C.1. Dominant weed species in the north and south fields during the 2001 growing season.

Species	Location	Date
Canada thistle (<i>Cirsium arvense</i> (L.) Scop.)	Both fields*	July and August
Curled dock (<i>Remex crispus</i> L.)	Mainly in the south field	April to the end of August
Dandelion (<i>Taraxacum officinale</i> Weber)	Both fields*	May to the end of August
Fox tail barley (<i>Hordeum jubatum</i> L.)	Both fields	May and June
Perennial sow thistle (<i>Sonchus arvensis</i> L.)	North field*	Mid-July to the end of August
	South field*	
Wild oat (<i>Avena fatua</i> L.)		Mid-July to the end of August
	Both fields*	August
Wild mustard (<i>Brassica Kaber</i> (DC) L.C. Wheeler)		Late June to the end of July

* Found under or close to the inverted pyranometer stand

APPENDIX D

A COMPARISON OF ESTIMATED REFLECTED SOLAR RADIATION FROM REGRESSION EQUATIONS AND OBSERVED REFLECTED SOLAR RADIATION

Table D.1. Comparison of estimated reflected solar radiation ($K\hat{\uparrow}_p$) from regression equations and observed reflected solar radiation ($K\hat{\uparrow}_o$). The difference between the $K\hat{\uparrow}_o$ and $K\hat{\uparrow}_p$ for each phenological stage is expressed as a sum of the daily differences (in MJ m^{-2}) and the half-hour maximum, minimum, mean and standard deviation (in W m^{-2}) for each phenological stage is also provided.

Phenological Stage	$K\hat{\uparrow}_o - K\hat{\uparrow}_p$	BLO 2001			Arnfield			Nkemdirim
		(all*)	(ap [†])	(ap [*])	(all)	(ap)	(ap _i)	(ap)
Pre-seeding	sum	1.22	1.21	1.40				
	mean	0.6	0.6	0.6				
	max	17.7	15.8	15.5				
	min	-20.8	-22.3	-13.2				
	σ	4.9	4.9	5.0				
	n	78	78	78				
Bare soil	sum	0.71	4.94	0.10	-120.89	-116.88	-116.59	7.34
	mean	0.6	4.3	0.1	-103.6	-100.2	-102.8	6.3
	max	11.2	15.7	11.5	-9.8	-10.3	-14.4	41.2
	min	-13.5	-8.3	-11.3	-180.6	-179.1	-205.2	-25.4
	σ	4.6	5.3	4.3	48.4	47.2	46.4	17.8
	n	84	84	84	320	320	320	320
Emergence	sum	-0.95	2.47	1.93	-120.38	-116.30	-118.81	-17.17
	mean	-0.7	1.8	1.4	-85.5	-82.6	-85.7	-12.2
	max	14.4	15.0	15.0	-5.3	-5.4	-8.8	11.8
	min	-23.7	17.1	-16.4	-181.5	-178.0	-182.5	-53.7
	σ	6.2	4.9	4.7	45.7	44.7	43.3	14.3
	n	112	112	101	391	391	391	391
Jointing	sum	1.62	1.68	-1.23	-153.29	-153.41	-152.63	-27.85
	mean	0.6	0.6	-0.4	-55.6	-55.6	-55.3	-10.1
	max	24.3	23.8	26.3	-0.8	-0.8	0.3	34.9
	min	-33.8	-32.3	-31.1	-138.2	-139.5	-139.5	-81.7
	σ	9.2	9.1	8.1	30.7	30.7	31.9	22.1
	n	221	221	221	765	765	765	765
Heading	sum	0.49	0.98	1.08	-106.77	-107.00	-100.34	-16.34
	mean	0.2	0.4	0.5	-48.3	-48.4	-48.6	-7.4
	max	12.4	13.6	20.5	-2.2	-2.3	-1.8	30.6
	min	-18.4	-18.9	-16.0	-107.4	-107.3	-113.4	-83.4
	σ	5.2	5.2	4.2	30.8	30.8	32	23.8
	n	168	168	166	613	613	613	613
Soft Dough	sum	-0.16	-0.16	-0.44	-64.52	-64.64	-64.49	-14.54
	mean	-0.1	-0.1	-0.4	-57.4	-57.5	-57.4	-12.9
	max	8.0	8.5	10.1	-2.3	-2.4	2	17.3
	min	-17.7	-17.9	-18.7	-104.7	-105.9	106.7	-63.4
	σ	4.2	4.2	3.9	30.8	30.9	32	22.8
	n	78	78	78	312	312	312	312

Table D.1 Continued

Phenological		BLO 2001			Arnfield			Nkemdirim
Stage	$K\uparrow_o - K\uparrow_p$	(all*)	(ap [†])	(ap _t *)	(all)	(ap)	(ap _t)	(ap)
Ripe	mean	1.2	1.1	0.8	-49.2	-49.2	-47.9	-2.5
	max	24.8	26.8	28.1	-1.9	-2.6	3.8	35.1
	min	-33.8	-34.7	-35.5	-100.4	-99.6	97.7	-58.3
	σ	6.0	5.9	6.1	23	23.1	25.1	24.6
	n	96	96	82	355	355	355	355

*all - regression equations were produced when $Z \leq 80^\circ$

†ap - separate forenoon and afternoon regression equations were produced to estimate the albedo during the day

*ap_t - separate forenoon and afternoon regression equations were produced for each cloud cover category to estimate the albedo during the day

APPENDIX E

DAY OF YEAR CONVERSION CALENDAR

Day	Month				
	April	May	June	July	August
1	91	121	152	182	213
2	92	122	153	183	214
3	93	123	154	184	215
4	94	124	155	185	216
5	95	125	156	186	217
6	96	126	157	187	218
7	97	127	158	188	219
8	98	128	159	189	220
9	99	129	160	190	221
10	100	130	161	191	222
11	101	131	162	192	223
12	102	132	163	193	224
13	103	133	164	194	225
14	104	134	165	195	226
15	105	135	166	196	227
16	106	136	167	197	228
17	107	137	168	198	229
18	108	138	169	199	230
19	109	139	170	200	231
20	110	140	171	201	232
21	111	141	172	202	233
22	112	142	173	203	234
23	113	143	174	204	235
24	114	144	175	205	236
25	115	145	176	206	237
26	116	146	177	207	238
27	117	147	178	208	239
28	118	148	179	209	240
29	119	149	180	210	241
30	120	150	181	211	242
31		151		212	243

APPENDIX F

POST-SEASON PYRANOMETER INTERCOMPARISON

At the end of the 2001 growing season, the Kipp and Zonen CM11 pyranometer employed in the south field and the Kipp and Zonen CM21 pyranometer from the north were compared for 10 days. Incoming fluxes were collected and stored by a Campbell Scientific 21X datalogger that measured sensor outputs every second, and every minute a mean, maximum, minimum and standard deviation was recorded.

The fluxes from both pyranometers were compared at the 1-minute timescale for all ten days. The pyranometers demonstrated very good agreements during cloudless and overcast conditions. The performance of the sensors slightly decreased during partly cloudy conditions, but the absolute difference of the sensors was under 27 W m^{-2} (Table F.1). Overall, 49 percent of the observed absolute difference between the pyranometers was $\leq 1 \text{ W m}^{-2}$, 76 percent of the absolute difference was $< 5 \text{ W m}^{-2}$, and 96 percent of the absolute difference $< 10 \text{ W m}^{-2}$ (Table F.2.).

Table F.1. Results of a ten day intercomparison of the pyranometers. The absolute difference in global solar radiation between the north and south fields, root mean square error (RMSE), mean bias error (MBE), and the index of agreement (d) are provided. Average, maximum, minimum, RMSE and MBE units are in W m^{-2} and d is dimensionless.

Number of minutes	Absolute average difference	Absolute maximum difference	Absolute minimum difference	RMSE	MBE	d
12719	2.7	26.9	0	4.4	-2.3	0.99992

Table F.2. The frequency of the absolute difference in global solar radiation between the pyranometers. Note that the first class interval is 0 - 1 W m^{-2} , and the remaining class intervals are in 5 W m^{-2} intervals beginning with 0 - 4.9 W m^{-2} .

	Absolute difference						
	0-1	0-4.9	5-9.9	10-14.9	15-19.9	20-24.9	25-26.9
Frequency (n)	6219	9709	2476	426	57	46	5

APPENDIX G

THE DIFFERENCE BETWEEN OBSERVED AND ESTIMATED CROP SURFACE ALBEDOS

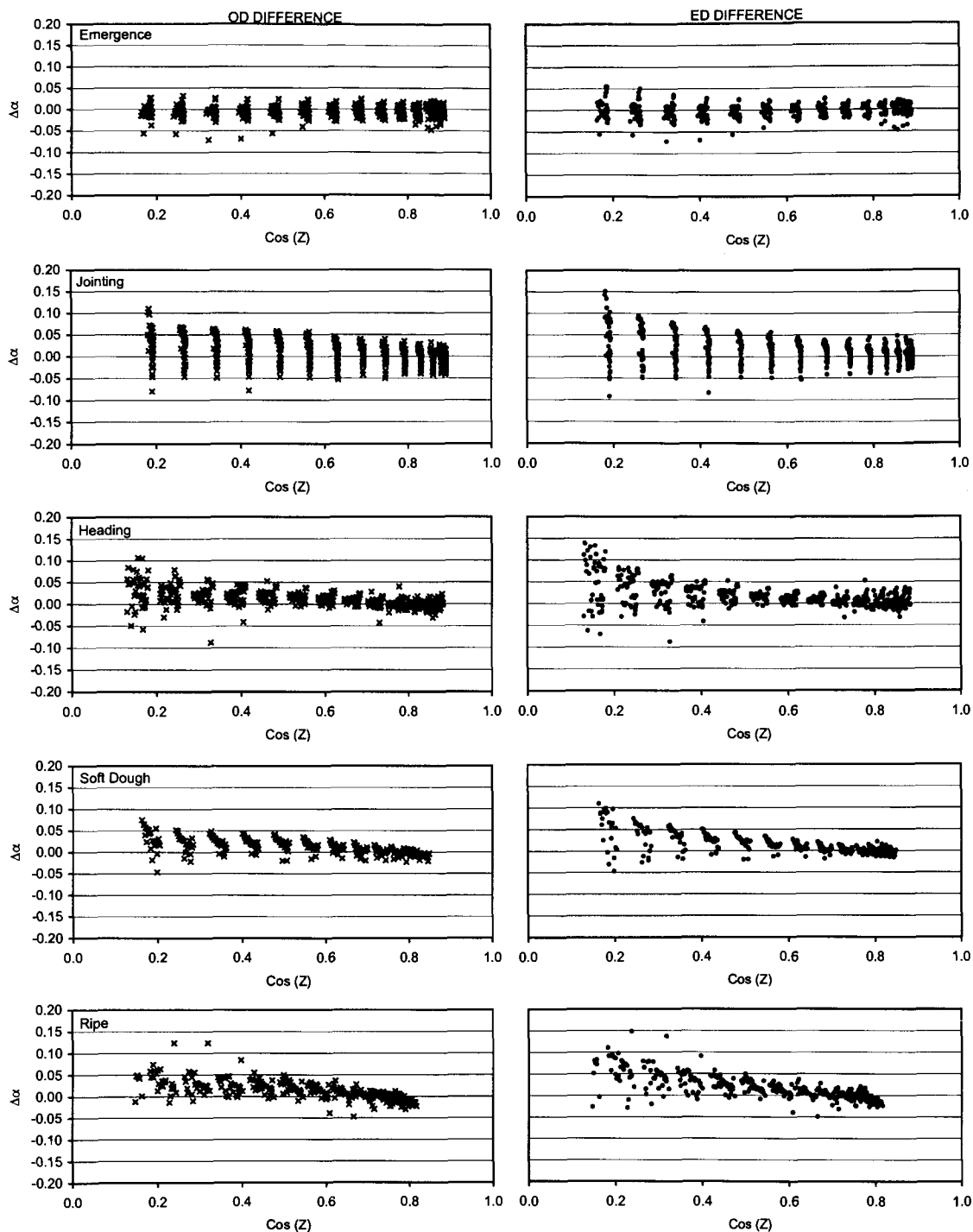


Figure G.1. The difference ($\Delta\alpha$) between observed and estimated (α_{CLASS}) albedos plotted against the cosine of the zenith angle ($\cos(Z)$). The OD difference is the difference between the estimated albedo, using observed diffuse radiation and the observed albedo. The ED difference is the difference between the estimated albedo, using estimated diffuse radiation and the observed albedo.

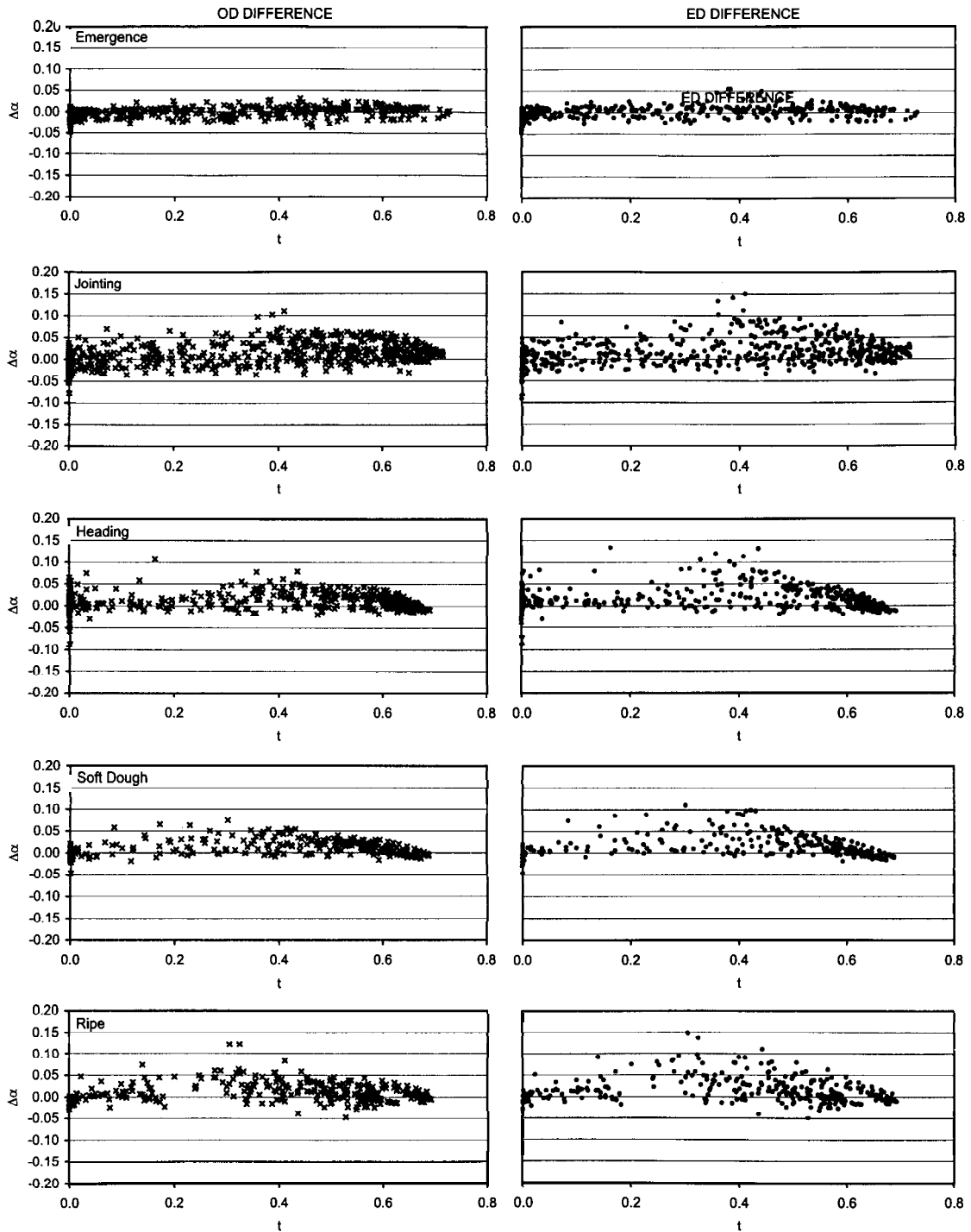


Figure G.2. The difference ($\Delta\alpha$) between observed and estimated (α_{CLASS}) albedos plotted against transmissivity (t). The OD difference is the difference between the estimated albedo, using observed diffuse radiation and the observed albedo. The ED difference is the difference between the estimated albedo, using estimated diffuse radiation, and the observed albedo.

APPENDIX H

ERROR ANALYSIS

The error in measured fluxes and albedos were estimated by the probable absolute error. A value (Y) can be expressed as a function of a set of measurements $X_1, X_2 \dots X_n$, which have associated errors (δX), thus

$$Y = f(X_1 \pm \delta X_1, X_2 \pm \delta X_2 \dots X_n \pm \delta X_n). \quad (H.1)$$

The total error of a value (δY), is given by

$$\delta Y = \frac{\partial Y}{\partial X_1} \delta X_1 + \frac{\partial Y}{\partial X_2} \delta X_2 + \dots + \frac{\partial Y}{\partial X_n} \delta X_n. \quad (H.2)$$

The probable absolute error (δY_{rms}) will be less than the total error, and is found by taking the root mean square of equation H.2, so that

$$\delta Y_{rms} = \left[\left(\frac{\partial Y}{\partial X_1} \delta X_1 \right)^2 + \left(\frac{\partial Y}{\partial X_2} \delta X_2 \right)^2 + \dots + \left(\frac{\partial Y}{\partial X_n} \delta X_n \right)^2 \right]^{0.5}. \quad (H.3)$$

The relative error is $\frac{\delta Y_{rms}}{Y}$ and is expressed as a percentage.

The above can be applied to both global ($K\downarrow$) and reflected ($K\uparrow$) solar radiation, and the flux density (F) is determined by

$$F = c m \quad (H.4)$$

where c is the sensor calibration constant and m is the electromotive output from the record apparatus. The probable absolute error in the measured flux density therefore is

$$\delta F_{rms} = \left[(c\delta m)^2 + (m\delta c)^2 \right]^{0.5} \quad (H.5)$$

where δm is assumed to be $\pm 1\%$ of the electromotive output (mV). Table H.1 provides the probable absolute error and relative error for the pyranometers used to determine the albedo in the south field. The error for both sensors is low and the relative error is near constant at 2.24 and 3.16 for the global (Kipp and Zonen CM21) and reflected solar

radiation (Kipp and Zonen CM11) pyranometers respectively. The Kipp and Zonen CM21 performed better than the Kipp and Zonen CM11 by 0.88 percent.

The albedo is the ratio of reflected to global solar radiation. The probable absolute error in the albedo (α) is

$$\delta\alpha_{\text{rms}} = \left[\left(\frac{\partial\alpha}{\partial K \uparrow} \delta K \uparrow \right)^2 + \left(\frac{\partial\alpha}{\partial K \downarrow} \delta K \downarrow \right)^2 \right]^{0.5} \quad (\text{H.6})$$

which reduces to

$$\delta\alpha_{\text{rms}} = \left[\left(\frac{1}{K \downarrow} \delta K \uparrow \right)^2 + \left(\frac{-K \uparrow}{K \downarrow^2} \delta K \downarrow \right)^2 \right]^{0.5} \quad (\text{H.7})$$

The calculated probable absolute error and relative errors for the albedo are provided in Table H.2. The probable absolute error of the albedo directly increased with the albedo, whereas the relative decreased. In summary, the albedo can be assessed with confidence to two decimal places, and caution should be employed when comparing albedos to three decimal places.

Table H.1. Error Analysis results for global ($K \downarrow$) and reflected solar radiation ($K \uparrow$) for the south field.

Flux Density (W m^{-2})	Kipp and Zonen CM21			Kipp and Zonen CM11		
	mV	$\delta K \downarrow$ (W m^{-2})	$\frac{\delta K \downarrow}{K \downarrow}$ (%)	mV	$\delta K \uparrow$ (W m^{-2})	$\frac{\delta K \uparrow}{K \uparrow}$ (%)
50	0.84	1.1	2.24	0.17	1.56	3.16
100	1.67	2.2	2.24	0.34	3.10	3.16
250	4.18	5.6	2.24	0.86	7.90	3.16
500	8.35	11.2	2.24	1.72	15.8	3.16
1000	16.74	22.4	2.24	3.45	31.6	3.16

Table H.2. Error Analysis results for the albedo (α)

α (dimensionless)	$\delta\alpha$ (W m^{-2})	$\frac{\delta\alpha}{\alpha}$ (%)
0.01	0.0039	3.9
0.02	0.0077	3.9
0.03	0.0097	3.2

REFERENCES

- Aase, J.K. and Tanaka, D.L. 1991. Reflectances from four wheat residue cover densities and influenced by three soil backgrounds. *Agronomy Journal* 83: 753-757.
- ACE, 2002. How do these maps relate to crop growth conditions, <http://www.aceweather.ca/generalinfo.htm>. Agrometeorological Centre of Excellence.
- Ahmad, S.B. and Lockwood, J.G. 1979. Albedo. *Progress in Physical Geography* 3: 510-543.
- Al-Yemeni, M. and Grace, J. 1995. Radiation balance of an alfalfa crop in Saudi Arabia. *Journal of Arid Environments* 29: 447-454.
- Angle, R.P., Brennand, M. and Sandhu, H.S. 1992. Surface albedo measurements at 53°N latitude. *Atmospheric Environment* 26: 1545-1547.
- Arnfield, A.J. 1975. A note on the diurnal, latitudinal and seasonal variation of the surface reflection coefficient. *Journal of Applied Meteorology* 14: 1603-1608.
- Bailey, W.G. and Dexter, R.H. 2003. Soil Moisture and Vegetation Regimes during the 2002 Growing Season at the Bratt's Lake Observatory, Saskatchewan Volume A: Summary of Field Research Programs and Overview of the Observational Findings. SFU Climatology Report 03-01, Simon Fraser University, Burnaby, 41 pp.
- Bailey, W.G. and Stewart, R.B., 1982. A method for assessing leaf area. *Canadian Journal of Plant Science* 62: 211-214.
- Bauer, A., Frank, A.B. and Black, A.L. 1987. Aerial parts of hard red spring wheat. I. Dry matter distribution by plant development stage. *Agronomy Journal* 79: 845-852.
- Baumgardner, M.F., Silva, L.F., Biehl, L.L. and Stoner, E.R. 1985. Reflectance properties of soils. *Advances in Agronomy* 38: 1-40.
- Depauw, R.M., McCaig, T.N., Clarke, J.M., McLeod, J.G., Fernandez, M.R. and Knox, R.E. 1997. Registration of 'AC Barrie' wheat. *Crop Science* 37: 289.
- Dixon, R.E. 1983. Land surface processes and climate - surface albedos and energy balance. In: B. Saltzman (Editor), *Theory of Climate*. *Advances in Geophysics*. Academic Press, New York, 305-334.
- Duchon, C.E. 1997. A time series of daily surface albedo in central Oklahoma. 10th Conference on Applied Climatology. American Meteorological Society, 163-166.
- Fung, K.I. (Editor). 1999. *Atlas of Saskatchewan*. PrintWest, Saskatoon, 293 pp.
- Grant, I.F., Prata, A.J. and Cechet, R.P. 2000. The impact of the diurnal variation of albedo on the remote sensing of the daily mean albedo of grassland. *Journal of Applied Meteorology* 39: 231-243.

- Hasson, A.M. 1990. Radiation components over bare and planted soils in a greenhouse. *Solar Energy* 44: 1-6.
- Hucl, P. 1995. Growth response of four hard red spring wheat cultivars to date of seeding. *Canadian Journal of Plant Science* 75: 75-80.
- Hummel, J.R. and Reck, R.A. 1979. A global surface albedo model. *Journal of Applied Meteorology* 18: 239-253.
- Idso, S.B., Jackson, R.D., Reginato, R.J., Kimball, B.A. and Nakayama, F.S. 1975. The dependence of bare soil albedo on soil water content. *Journal of Applied Meteorology* 14: 109-113.
- Iqbal, M. 1983. *An Introduction to Solar Radiation*. Academic Press, Don Mills, 390 pp.
- Jacobs, A.F.G. and Van Pul, W.A.J. 1990. Seasonal changes in the albedo of a maize crop during two seasons. *Agricultural and Forest Meteorology* 49: 351-360.
- Joel, A.H., Mitchell, J., Edmunds, F.H. and Moss, H.C. 1936. *Reconnaissance Soil Survey of Saskatchewan for the International Boundary on the South to the Top of Township 48 on the North, No.10*, University of Saskatchewan, College of Agriculture, Saskatoon, 120 pp.
- Kondratyev, K.Y., Korzov, V.I., Mukhenberg, V.V. and Dyachenko, L.N. 1981. The shortwave albedo and the surface emissivity. In: P.S. Eagleson (Editor), *Land Surface Processes in Atmospheric General Circulation Models*. Cambridge University Press, New York, 463-514.
- Kukla, G. and Robinson, D. 1980. Annual cycle of surface albedo. *Monthly Weather Review* 108: 56-68.
- Kung, E.C., Bryson, R.A. and Lenschow, D.H. 1964. Study of a continental surface albedo on the basis of flight measurements and structure of the earth's surface cover over North America. *Monthly Weather Review* 92: 543-563.
- Mailhot, J., Stéphane, B., Benoit, R., Bilodeau, B., Delage, Y., Fillion, L., Garand, L., Girard, C. and Tremblay, A. 1998. Scientific description of RPN physics library (version 3.6), *Recherche En Prévision Numérique Atmospheric Environmental Service*, Dorval.
- Major, D.J., Janzen, H.H., Olson, B.M. and McGinn, S.M. 1992. Reflectance characteristics of southern Alberta soils. *Canadian Journal of Soil Science* 72: 611-615.
- Maas, S.J. 1993. Agroclimatology and modeling parameterized model of gramineous crop growth: I. Leaf area and dry mass simulation. *Agronomy Journal* 85: 348-353.

- Matthias, A.D., Fimbres, A., Sano, E.E., Post, D.F., Accioly, L., Batchily, A.K. and Ferreira, L.G. 2000. Surface roughness effects on soil albedo. *Soil Science Society of America Journal* 64: 1035-1041.
- McArthur, L.J.B. 1998. *Baseline Surface Radiation Network (BSRN) Operations Manual (Version 1.0)*. WMO/TD-No. 879, World Climate Programme, North York, 64 pp.
- Meek, D.W. and Hatfield, J.L. 2001. Iowa's surface albedo variability in space and time throughout the 1990 growing season, *Remote Sensing and Hydrology*. IAHS AISH Publication, Santa Fe, New Mexico, 225-227.
- Minnis, P., Mayor, S., Smith, W.L., Jr. and Young, D.F. 1997. Asymmetry in the diurnal variation of surface albedo. *IEEE Transactions on Geoscience Remote Sensing* 35: 879-891.
- Morozova, I.V. 1994. On the calculation of monthly values of underlying surface albedo. *Atmospheric and Oceanic Physics* 30: 379-381.
- Myhre, G. and Myhre, A. 2003. Uncertainties in radiative forcing due to surface albedo changes caused by land-use changes. *Journal of Climate* 16: 1511-1524.
- Nkemdirim, L.C. 1972. A note on the albedo of surfaces. *Journal of Applied Meteorology* 11: 867-874.
- Oke, T. R. 1987. *Boundary Layer Climates* 2nd Edition. Methuen, New York, 435 pp.
- Phillips, D. 1990. *The Climates of Canada*. En56-1/1990E, Canadian Government Publishing Centre, Ottawa, 176 pp.
- Piggin, I. and Schwerdtfeger, S. 1973. Variations in the albedo of wheat and barley crops. *Archiv fur Meteorologie, Geophysik und Bioklimatologie Series B* 21: 365-91.
- Policy Branch. 2003. *Agricultural Statistics 2001*. 2M ISSN 0702-7389 POL93, Saskatchewan Agriculture, Food and Rural Revitalization, Regina, 150 pp.
- Post, D.F., Fimbres, A., Matthias, A.D., Sano, E.E., Accioly, L., Batchily, A.K. and Ferreira, L.G. 2000. Predicting soil albedo from soil color and spectral reflectance Data. *Soil Science Society of America Journal* 64: 1027-1034.
- Potter, K.N., Horton, R. and Cruse, R.M. 1987. Soil surface roughness effects on radiation reflectance and soil heat flux. *Soil Science Society of America Journal* 51: 855-860.
- Prata, A.J., Grant, I.F., Cechet, R.P. and Rutter, G.F. 1998. Five years of shortwave radiation budget measurements at continental land site in southeastern Australia. *Journal of Geophysical Research* 103: 26093-26106.
- Proctor, J.T.A. and Blackburn, W.J. 1983. Albedo characteristics of a strawberry planting. *HortScience* 18: 233-235.

- Randall, D.A. 1991. Global climate models: what and how. In: B.G. Levi, D. Hafemeister and R. Scribner (Editors), *Global Warming: Physics and Facts*. American Institute of Physics, Washington, D.C., 24-45.
- Robertson, G.W. 1968. A biometeorological time scale for a cereal crop involving day and night temperatures and photoperiod. *International Journal of Biometeorology* 12: 191-223.
- Song, J. 1998. Diurnal asymmetry in surface albedo. *Agricultural and Forest Meteorology* 92: 181-189.
- Song, J. 1999. Phenological influences on the albedo of prairie grassland and crop fields. *International Journal of Biometeorology* 42: 153-157.
- Twomey, S.A., Bohren, C.F. and Mergenthaler, J.L. 1986. Reflectance and albedo differences between wet and dry surfaces. *Applied Optics* 25: 431-437.
- Verseghy, D.L. 1991. CLASS - A Canadian Land Surface Scheme for GCMs. I. Soil model. *International Journal of Climatology* 11: 111-133.
- Verseghy, D.L. 2000. The Canadian Land Surface Scheme (CLASS): Its history and future. *Atmosphere-Ocean* 38: 1-13.
- Verseghy, D.L., McFarlane, N.A. and Lazare, M. 1993. CLASS - A Canadian Land Surface Scheme for GCMs, II. Vegetation model and coupled runs. *International Journal of Climatology* 13: 347-370.
- Walter-Shea, E.A., Blad, B.L., Hays, C.J., Mesarch, M.A., Deering, D.W. and Middleton, E.M. 1992. Biophysical properties affecting vegetative canopy reflectance and absorbed photosynthetically active radiation at FIFE site. *Journal of Geophysical Research* 97: 18925-18934.
- Wanjura, D.F. and Hatfield, J.L. 1986. PAR and IR reflectance, transmittance, and absorptance of four crop canopies. *Transactions of the ASAE* 29: 143-150.
- Weiss, A. 1982. An experimental study of net radiation, its components and prediction. *Agronomy Journal* 74: 871-874.
- Wilson, M.F. and Henderson Sellers, A. 1985. A global archive of land cover and soils data for use in general circulation climate models. *Journal of Climatology* 5: 119-143.
- Willmott, C.J. 1982. Some comments on the evaluation of model performance. *Bulletin of the American Meteorological Society* 63: 1309-1313.
- Wittrock, V. 2002. Preliminary Description of the 2001 Drought in Saskatchewan. SRC Publication No. 11501-1E02, Minister of Agriculture and Agri-Food, Saskatoon, 166 pp.
- Yin, X. 1998. The albedo of vegetated land surfaces: systems analysis and mathematical modeling. *Theoretical and Applied Climatology* 60: 121-140.